MOLECULAR VISUALIZATION OF INDIVIDUAL MOLECULES DURING FLOW

Michael John Barrett

A dissertation submitted to the faculty of the University of North Carolina at Chapel Hill in partial fulfillment of the requirements for the degree of Doctor of Philosophy in the Department of Chemistry.

Chapel Hill
2009

Approved by:

Professor Tomas Baer

Professor Dorothy Erie

Professor John Papanikolas (chair)

Professor Sergei Sheiko

Professor Mark Schoenfisch

Abstract

MOLECULAR VISUALIZATION OF INDIVIDUAL MOLECULES DURING FLOW
(under the direction of Sergei Sheiko)

Wetting and flow properties of molecularly thin polymer films are at the heart of many practical applications such as coatings, composites, microfluidics, and lubrication In some applications, these properties ensure even surface coverage; while in others, molecular flows act as new tools for surface patterning and performing biochemical assays on microchips. Further advances in these fields depend on our understanding (i) the mechanisms controlling the kinetics of flow and (ii) molecular organization of thin polymer films. In thin films polymers can adopt a wide range of conformations, topologies, and packing arrangements. Most of the structures correspond to metastable states that, however, are practically relevant due to extremely slow equilibration of the spatially constrained systems. Equilibration rates depend on the film formation process, which involves spreading of long and flexible macromolecules on a substrate. As such, the goal of this paper is (i) to examine molecular organization of thin polymer films and (ii) to study molecular mechanism of spreading of thin films on a solid substrate.

Traditional techniques lack the resolution to completely map out the conformation of each and every individual molecule in these films, thus our knowledge of the relative shape of neighboring molecules is incomplete.

Because of this we turn to polymer bottle brush molecules, with the ability to be visualized using atomic force microscopy, to model linear polymer systems in thin films. We have shown that polymer films are largely composed of two distinct conformations (coiled chain and folded chain) whose relative contribution varies depending on film preparation and spreading coordinate. Although it is known that polymer molecules typically undergo a plug flow, we have discovered and modeled an unusual fractionation when we mix chemically similar linear polymer with brush polymer. *In situ* studies were also conducted and for the first time we were able to directly observe molecular slip, dissociation and scission during the spreading process. Finally we introduce preliminary studies concerning the control of the molecular properties in these films. In doing so we explore the role of confinement on these polymer films as well as the effects electric fields have when manipulating these flows.

For Stephanie
and my friends and family

Acknowledgements

Most importantly I would like to thank my advisor Dr. Sergei Sheiko for the opportunity to conduct research in his lab. I will be forever indebted to him for the time he has given me to help shape me into the scientist I have become today. I am equally grateful to the late Dr. Roger Miller who supplied me with the confidence to undertake any scientific task no matter how challenging.

I would like to thank every member of the Miller and Sheiko groups who have helped me along the way. Thank you Sherryl (hands down the best proof reader I have ever known), Frank, Jamie, Isaac, for showing me the ropes and thoughtful discussions to bounce ideas off of and thanks to Ping, Jing, and Yuan Chao for the opportunity to pass what I have learned along. Alper Nese from Carnegie Mellon for his wonderful synthetic work and his always eager to help attitude. David Shirvanyants for his work with the Pen program and making data analysis orders of magnitude easier. I would also like to thank Professor Michael Rubinstein for his thought provoking discussions during our polymer physics group seminars. Finally I would like to thank my graduate committee for their advice, time and discussions.

I would like to thank all my family. My wife Stephanie for her love and support throughout this whole process (and her overall patients in general). My parents Jeanne and John, for the sacrifices they have made over the years on

my behalf and values they have instilled upon me and my siblings Jamie and Matthew for putting up with me over the years. I would also like to thank my grandparents, Jack, Nancy, John, and Janet for everything they have done for me throughout my life. Finally I would like to thank all of my friends, Stephanie (again), Dave, Matthew, Miranda, Stef, Joe, and others who I may have missed, who have helped me get to this point in one piece. I couldn't have made it this far without any of your help.

TABLE OF CONTENTS

LIST OF TABLES

LIST OF FIGURES

Figure

LIST OF ABBREVIATIONS AND SYMBOLS

2D	two dimensional
3D	three dimensional
A	area of a section of the fluid
a	monomer size
AFM	atomic force microscopy
ATRP	atom transfer radical polymerization
b	kuhn monomer size
brush	cylindrical polymer brush
C	capacitance
D	dimensionality
D	spreading rate
d	distance between electrodes
DP	degree of polymerization
ε	energy of adsorption
E_c	energy of a capacitor
ϕ_0	coverage of all length
FENE	Finitely Extensible Nonlinear Elastic
ϕ_N	coverage of degree of polymerization N
f_t	tensile force
γ	surface energy
g	number of monomers in adsorption blob

$\gamma_{l\text{-}v}$	surface energy at the liquid-vapor interface
$\gamma_{s\text{-}l}$	surface energy at the solid-liquid interface
$\gamma_{v\text{-}s}$	surface energy at the vapor-solid interface
H	Hamaker constant
h	equilibrium film thickness
HOPG	highly ordered pyrolytic graphite
hr	hour
j	grafting density
k	rate constant
kHz	kiloHertz
l	bond distance
L	molecular length
λ	wavelength of light
L_0	initial contour length
L_∞	final contour length after scission
LB	Langmuir-Blodgett
λ_b	persistance length of ungrafted backbones
L_e	entanglement length
L_n	number averaged length
l_p	persistance length
λ_s	persistance length of side chains
L_w	weigth averaged length
m	meter

m	linear polymer degree of polymerization
m	mass
M_e	entanglement mass
min	minute
mN	milli Newton
N	backbone degree of polymerization
n	side chain degree of polymerization
N	Newton
N_e	monomers per entanglement
nm	nanometer
O.P.	Order parameter
PBA	poly n-butyl acrylate
PBPEM	poly (2-(2-bromopropionyloxy) ethyl methacrylate)
PDI	polydispersity index
PDMS	poly(dimethylsiloxane)
P_e	entanglement strands
R	film length
r	distance along the film
R	Spreading coordinate
R_0	drop radius
R_{edge}	radius of precursor film
R_g	Radius of gyration

RH	relative humidity
s	second
S	spreading coefficient
SEM	scanning electron microscopy
STM	scanning tunneling microscopy
t	time
T_g	glass transition temperature
U	Lenard-Jones potential energy
U	electric potential
U	electric potential
V	velocity of fluid
V	velocity of brush
V	volt
V_0	velocity of matrix
v_0	monomer volume
V_{slip}	slip velocity
w	brush width
ξ	adsorption blob size
x	distance along the film
β	fitting parameter
γ_{slip}	fitting parameter
ε	Lenard-Jones interaction parameter
ε_0	permittivity of free space

η	viscosity
θ	bond angle
θ_c	contact angle
κ	dielectric constant
μm	micrometer
ξ	friction coefficient of the fluid-surface interface
ξ	friction coefficient of the brush-surface interface
ξ	polymer-surface friction
ξ_0	friction coefficient of the matrix-surface interface
ξ_{bm}	brush matrix friction
Π	surface pressure
ρ	density
σ	Lenard-Jones particle diameter
σ_{ij}	energy of an interface
φ	fitting parameter

Chapter 1

Introduction

1.1 Preamble Understanding the structure and spreading behavior of thin polymer films is vital for the advancement of many applications, such as lithography,[1-4] coatings,[5,6] microfluidics,[7] lubrication,[8] and printing.[9] It is important to understand (i) the packing of large macromolecules within films that are thinner than the macromolecular dimensions and (ii) the kinetics of the spreading process. Both the thermodynamic (driving forces) and kinetic (dissipation mechanisms) properties of thin films are largely controlled by molecular interactions between the adsorbed macromolecules and the substrate. The interaction affects conformation,[10,11] ordering,[12] and even chemical structure[13] of the adsorbed macromolecules. Furthermore, the short-range molecular interactions also have an effect on the sliding friction and thus the dynamics of the molecules on the surface. The friction coefficient depends on the chemical structure, conformation, and orientation of the adsorbed macromolecules and may also exhibit minute variations due to the intrinsically heterogeneous structure of the substrate's surface. These variations provide an opportunity to induce diffusion within a plug flow, enhance the mixing of spreading macromolecules, facilitate their ordering, and perform molecular fractionation.

A lot of studies have been conducted in the past 2 decades to understand the packing and spreading of polymer chains. Yet, the current level of understanding lacks molecular information, including conformation and motion of individual molecules within thin films. This information has been largely inaccessible due to a limited number of techniques that have enough resolution and sensitivity for molecularly thin films. Figure 1.1 illustrates these limitations. The image on the left consists of single linear polymer molecules that are clearly resolved enabling conformational analysis using atomic force microscopy (AFM). When polymer molecules are densely packed into a solid film, their individual structure is no longer visible (Figure 1.1 center). The experimental challenge of this work is to apply molecular imaging techniques to monitor individual polymer molecules as they move and arrange themselves on a substrate. We accomplish this using a model polymer system that enables both imaging of individual molecules and synthetic control of their characteristic properties (size, shape, flexibility) (Figure 1.1 right). We are interested in monomolecular layers of these molecules and their conformational and topological properties in both static and flowing films. For static films we investigate the effects the preparation method on their structure and for flowing films, we are interested in their structure while spreading by both spontaneous (thermodynamically controlled) and directed phenomena (electric field).

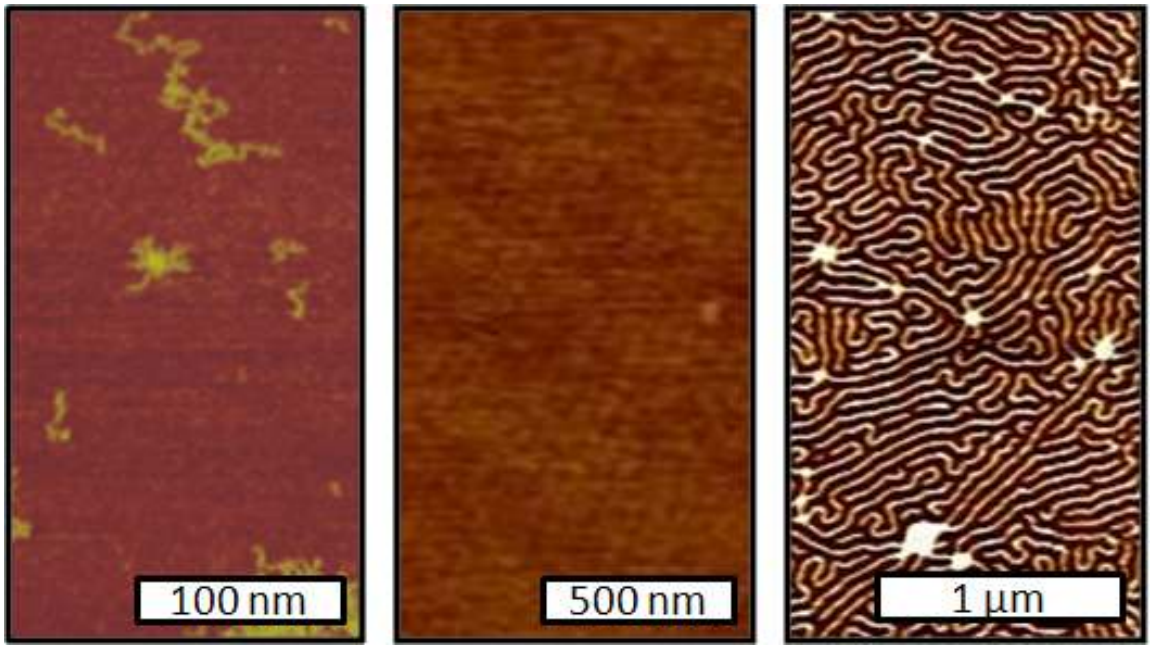

Figure 1.1 Images of various polymer configurations. Lone molecules (left), a dense linear film (center), and a dense film of model polymers (right).

1.2 Molecular structure in thin films. The physical properties of polymer films depend greatly on their molecular structure. To explain the observation of the depressed glass transition temperature at the interfaces of polystyrene films,[14,15] it has been theorized that the orientation of the chain ends at the film interface inhibit the polymers solidification.[16,17] As films become thinner the properties of their molecular structures become critical to certain applications. For example, liquid crystals rely on a highly ordered film to transmit and block light in a controllable manner.[18] This approach depends directly on the relative alignment and packing relationships of individual molecules. In ultra thin films, surface tension may be dependent on the structure, composition, or topology of the individual molecules.[19]

Theoretical scaling analysis predicts the structure of individual polymer molecules adsorbed to the substrate in the absence of additional molecules. An adsorbed polymer chain can be modeled as a string of adsorption blobs. The size of these adsorption blobs (ξ) corresponds to the thickness of the film and is determined by balancing the energy of adsorption (ε) of the small section of chain with its entropy as $\xi \sim b/\varepsilon$, where b is the length of the Kuhn monomer. Inside each blob, the chain adopts unperturbed conformation which scales as if it were in a bulk melt ($\xi \sim g^{1/2}$, where g is the number of monomers in the adsorption blob), while outside the adsorption, blobs line up to form an extended chain (the size of the molecule is proportional to the number of monomers R~N). These are predictions for a single chain. Even less information is available about the conformation of individual chains within dense monolayers. It is unknown whether or not these chains overlap and form crosses or networks when they are adsorbed onto a surface. It is unresolved as to what conformation, alignment, and packing these chains really undergo when they are confined to thin films (Figure 1.2). It remains largely unknown how the molecular conformation and alignment change during spreading.

Figure 1.2 Different packing arrangements and conformations of polymer molecules. Collapsed and separated (left), coiled and blended (center), and extended and aligned (right).

Past studies have focused on the behavior of thin films by treating them as macroscopic continuum objects. Ellipsometry studies of these films yield information about their bulk properties[20,21] including the thickness of the film as well as optical properties (such as index of refraction). These properties are sensitive to various film parameters such as phase transitions and crystallization and the monitoring of the optical properties allow for the determination of these transitions. The spatial resolution of the imaging ellipsometry is at best 10 μm, meaning that any information about the individual polymer molecules is lacking. We must turn to techniques with the ability to resolve molecules if we are to obtain information about the molecular structures.

Fluorescence studies have also been conducted to measure an individual polymer's mobility within a thin film.[22] These are conducted by labeling probe molecules in the film and measuring their motion. The resolution of optical techniques is limited by the Bragg diffraction limit ($\lambda/2 \sim 200$ nm), where λ is the wavelength of light. The technique is unable to resolve structure and curvature under 200 nm and molecular resolution is gradually lost as higher fractions of

molecules are fluorescently labeled, making it impossible to study these molecules in relation to the shape, structure, and entanglements of their closest neighbors.

The fluorescence studies indicate that there is a substantial decrease in the lateral mobility of polymers in films thinner than 150 nm. This indicates that as films become thinner there motion becomes slower and thus they require more time to reach an equilibrium conformation. If films are a monolayer in thickness their equilibration processes can be very prohibitively slow. Due to the slow equilibration process, long chains may assume different metastable, yet practically relevant, structures. As such, one of the goals in this work is to study polymer films prepared by different techniques to explore the equilibrium state (if it exists) of polymer conformation in thin films. In this work we will use a model polymer system along with force microscopy imaging techniques to investigate the nature of individual molecules confined to thin films and answer the following questions:

- What differences are present when films of polymers are prepared using the Langmuir-Blodgett trough as opposed to being prepared from spreading?
- What is the conformation of adsorbed macromolecules and how does it depend on the preparation technique? We will determine the characteristic scaling dimensionality and examine its spatial variations both within the same film and between different films. We will measure the characteristic persistence length and its dependence on the chemical structure.

- How do long and flexible polymer molecules pack within thin films? Do they form a homogeneous or domain-like structure? We will measure the overlap parameter as a function of the persistence length and examine its dependence on the preparation technique. Is there any order along the domains?
- What does the topology of the adsorbed macromolecules look like within dense monolayers? We will examine the formation and dissociation of crosses and networks as a function of molecular size and stiffness.

1.3 Polymer spreading. The spreading of polymers is vital to both macroscopic and microscopic systems and applications. We define macroscopic spreading as the spreading of bulk films and fluids on a scale greater than the molecular size (>1 μm). This spreading is affected by the forces which govern the energy of the bulk system, such as surface energies and van der Waals forces and is important to industries such as oil recovery[23] and crop dusting.[24] As we scale down the size of the polymer, spreading application or phenomena, the size of the application begins to intersect the size of the polymer. For example, it is possible to fabricate microfluidic channels[25] on size scales smaller that 1 μm which is approaching the dimensions of individual polymer molecules. It becomes critical to understand the effect of the geometrical confinement both on the molecular conformation and on their flow properties.

The spreading of fluids is governed by spontaneous forces described in detail in Section 1.3.1. These forces control whether or not the polymers will

spread (thermodynamics) as well as their spreading rate (kinetics). This spontaneous spreading enables a flow induced diffusion of the polymers[26] which allows for the individual molecules to undergo a rearrangement as they flow. As the conformations and arrangements of the individual molecules change as they flow, so can the properties controlled by the order and topology of the molecules. We can then use techniques to control the flow of the molecules. Two methods used to control these films are their confinement to channels and exposure to electric fields. Their confinement to channels on the order of their molecular size can influence the behavior of the films and can alter it compared to the bulk. For example, confinement can enhance miscibility of separate polymers[27] and alter their molecular dynamics.[28] We can also use electric fields to control the orientation and spreading dynamics of these films. We know that fluids can rearrange themselves to maximize their stored electrical energy when an electric potential is applied to electrode systems using electrowetting[29] and dielectrophoresis.[30] This control of these films can be used to direct the spreading of the bulk films as well as affect the alignment of the individual molecules.[31]

This text focuses on the spreading of polymer films, both spontaneous and controlled. We study polymer films as they spontaneously flow and rearrange (*equilibrium*), separate and fractionate in mixtures (*molecular mixing*) and study these films in situ and monitor the affects of real substrates (*real substrates*) have on these films. We also attempt to control these films using confinement to channels (*channels*) and manipulation using electric fields (*electric fields*).

1.3.1 Spreading physics. When a fluid is placed onto a surface it creates three separate interfaces with their corresponding surface energies: solid-liquid ($\gamma_{s\text{-}l}$), liquid-vapor ($\gamma_{l\text{-}v}$), and vapor-solid ($\gamma_{v\text{-}s}$). If the surface energy of the original interface, $\gamma_{v\text{-}s}$, is less than the surface energy of the two new interfaces, $\gamma_{l\text{-}v} + \gamma_{s\text{-}l}$, then the drop will spread. To describe this process we define the so-called spreading coefficient, S, as the differences between these energies ($S = \gamma_{v\text{-}s} - \gamma_{l\text{-}v} + \gamma_{s\text{-}l}$). If $S < 0$ then the drop will only partially wet the surface and long range interactions with the surface will cause the drop to form a cap with a contact angle of the form $\cos\theta_c = S/\gamma_{l,g}+1$. However, if $S > 0$ the drop will completely wet the surface and spread.[32] This process can happen in either one of two ways: the bulk drop can expand or a precursor layer can spread ahead of the drop as shown in Figure 1.3.

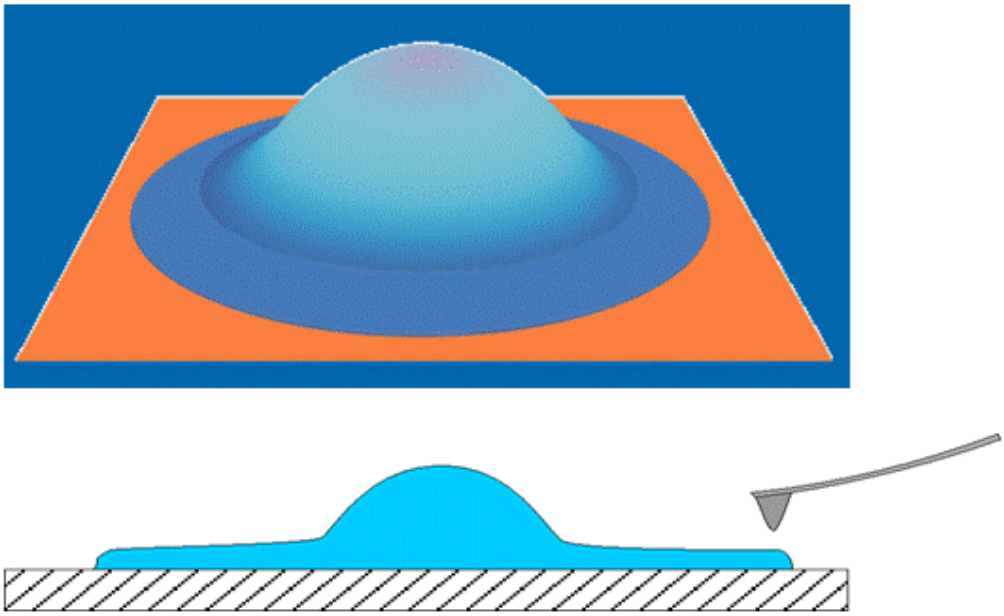

Figure 1.3. Diagrams of a spreading drop. (top) A three dimensional rendering of a polymer drop spreading on a substrate. The precursor layer can be seen spreading ahead of the drop. (bottom) A profile of a spreading drop with an AFM probe imaging its height.

The wetting behavior of a film is more complicated than just the spreading coefficient, which is largely controlled by short-range interactions. We must also consider 'long range' forces that act on the systems such as van der Waals forces. We use the Hamaker constant, H_{slg}, which account for the van der Waals forces of the solid and gas interacting through the liquid. If $H < 0$ then there will be a repulsive force between the solid and gas allowing the drop to spread, however if $H > 0$ there will be attractive forces between the two which can prevent the precursor film from spreading.[33] When considering the wetting behavior of a spreading drop there are two important terms to consider: S and H, i.e. short range and long range molecular interactions. If H is negative (net attraction) and S is positive the drop will spread. This spreading dependence

allows us to calculate the equilibrium film height by minimizing the free energy of the equilibrium film to get its thickness, $h = \sqrt{(-H/4\pi S)}$.

These terms affect only the thermodynamics of the film and provide little information about the spreading kinetics and formation of the precursor film represented in Figure 1.4. To understand the dynamics of these spreading films, we should understand the forces that act on them. We first consider the force that drives the flow of all fluids: pressure gradient. When a liquid film covers the surface to minimize its surface energy, it is left with a zero pressure at the free edge of the film and a high pressure at the drop reservoir. The fluid will move from the high to low pressure area with a force of $\vec{F}_p \approx -\frac{\partial \Pi}{\partial r} A$, where r is the distance along the film, A is the area of a section of the film, and Π is the linear pressure of the film. The pressure gradient is balanced by sliding friction $\vec{F}_{sf} = -\xi \vec{V} A$, where V is the velocity of the film, and ξ is the friction coefficient of the polymer surface. Since our flows are assumed to be in equilibrium we solve for an equation of motion to be $\frac{d\Pi}{dr} A = -\xi \vec{V} A$. We can then proceed to solve this equation for $S=\Pi_{drop}-\Pi_{edge}$ by integrating the energy gains and loses over the total film length R. The integration of the above equation over r gives $S = -\xi \vec{V} R$. We then can run the second integration over time (V=dR/dt) to obtain an equation for the spreading rate $D=S/\xi$: $(R-R_0)^2=L^2 = 2Dt$, where t is the time of spreading.

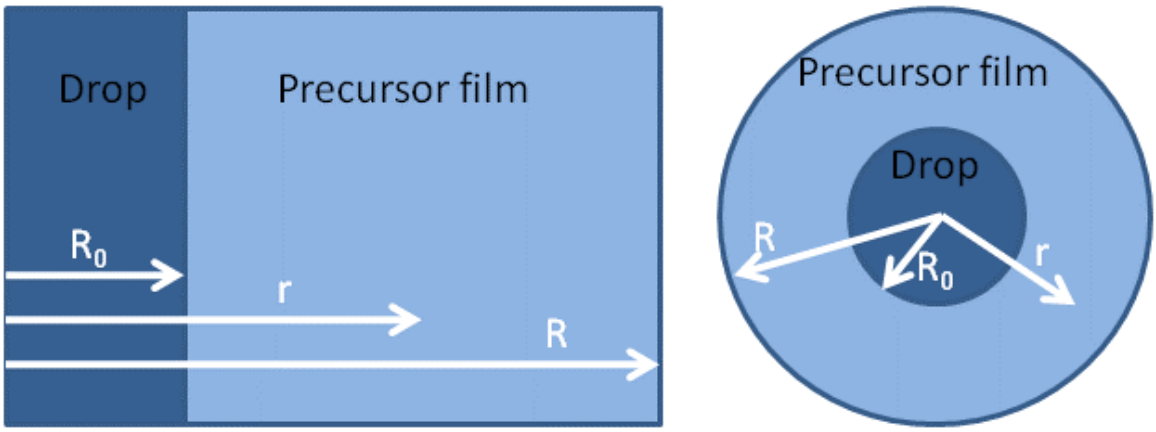

Figure 1.4 Diagrams of spreading films. A one dimensional (left) and two dimensional (right) spreading film showing the length of the bulk drop reservoir (R_0), the length of the precursor film (R), and an arbitrary distance along the film (r).

The equations previously derived were for that of a linear spreading film. In the case of our experiments we place a circular drop onto the surface and allow it to spread. To take into account this radial spreading we must re-derive the above equations (present in Table 1.1). The table shows the properties each equation is typically used to compute.

Table 1.1 Equations of motion for linear and radial spreading films.

	Linear spreading (short radial film approximation $R-R_0<<R_0$)	Radial spreading ($R>>R_0$)
Flow velocity	$V(r)=\dot{R}$	$V(r)=\frac{R\cdot\dot{R}}{r}$
Pressure gradient	$\frac{\partial\Pi}{\partial x}=\dot{R}\cdot\zeta$	$\frac{\partial\Pi}{\partial x}=\zeta\cdot\frac{R\cdot\dot{R}}{r}$
Front velocity	$\dot{R}=\frac{S}{\zeta(R-R_0)}$	$\dot{R}=\frac{S}{\zeta\cdot R\,ln\frac{R}{R_0}}$
Film radius	$(R-R_0)^2=2Dt$	$R^2(2\,ln\frac{R}{R_0}-1)+R_0^2=2Dt$

1.3.2 Spontaneous spreading. *Equilibrium.* When a drop of polymers is deposited on a surface its spreading is governed by spontaneous forces described above. The nature and structure of the precursor layer has been studied in depth. Leger *et. al*. used ellipsometry to characterize the precursor films precise profile as it spreads.[34] Also using ellipsometry Heslot *et. al*. studied the films dynamics.[35] Due to the resolution of the techniques used (>10 μm), the researchers were only able to study the spreading film as a continuum of polymer. However, as the molecules spread away from the drop, the film undergoes physical changes, such as a pressure drop,[36] as well as the molecular rearrangement but the conformations and topologies of the individual molecules are unknown. It is of particular interest of the authors to study these spreading processes on the molecular scale. This allows direct and quantitative monitoring of the velocity field (relative molecular displacement) along with molecular

dynamics (rotation and bending).[37] Chapter 4 will answer the following questions about molecules under flow.

- Do polymer molecules leave the drop reservoir at the same rate or is there size dependence?
- Do all molecules move with the same velocity (plug flow) or undergo diffusive motion?
- Does the conformation of the molecules change as they flow?
- Do polymer molecules align during flow?

Molecular mixing. Flow and mixing of molecules is critical in the field of microfluidics. In both open and closed channel microfluidics (Fig. 1.5), a major goal is to push the lower limit to the size of these devices. As strides are made toward this goal the surface area to volume ratio of these devices is drastically increasing, making the short range interactions between the surface and fluid more and more important. To understand how molecules, fluids, and polymers are going to respond to these constraints we must first understand their behavior as they flow on surfaces in single monolayers. In systematic studies of the relationship between the spreading diffusion coefficient, D, and molecular weight of unentangled polymer chains, a dependence on the relative humidity of the atmosphere above the substrate was determined.[38] These studies are conducted as one component systems. Again, these studies were conducted using ellipsometry with no molecular resolution. It is our goal to use model polymer systems with atomic force microscopy to study these phenomena with

molecular detail. Contrary to this study, we have observed polymer brush molecules under flow and have seen no difference in velocities of these molecules regardless of molecular weight. In other words, we observe a plug flow when spreading molecular brushes of different lengths. However when we mix two separate architectures of molecules with the same chemical makeup (linear polymer and polymer brushes with side chains constituted of the same linear polymer) we are able to separate brushes according to their molecular weight. This leads us to ask the following questions:

- How do single molecules fractionate under flow?
- How do they interact with the surrounding solvent (matrix of small linear chains)?
- What role does friction play in the fractionation of the molecules?

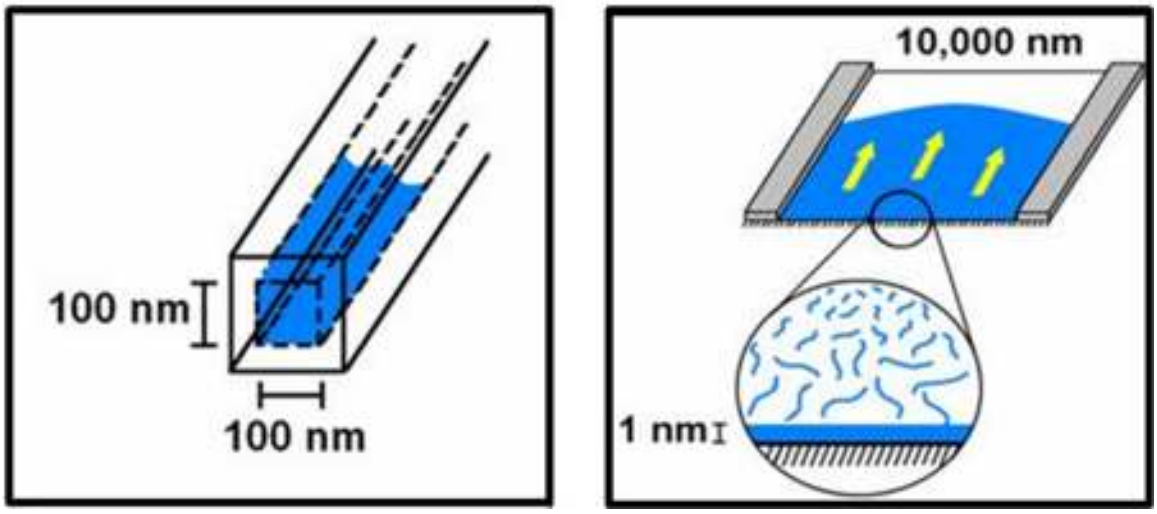

Figure 1.5 Types of microfluidic channels. Closed channel (left) and open channel (right).

Real substrates. The surfaces in real world spreading applications like those on metal, plastics, and other rough substrates are by no means perfect. The surfaces are rough and have heterogeneities which have effects on the friction, absorption, and short range interactions that molecular flows have with the surface. The most typical heterogeneities include impurities, roughness, grain boundaries, dislocations, and terraces. These can change conformation, orientation, and even chemical structure of adsorbed macromolecules, which all in turn have crucial effects on molecular mixing and reactivity. There is a growing body of work which examines these flows in the bulk, on both rough and smooth surfaces as well as studies that emphasize these flows in molecularly thin films at bulk flows on both ideal and rough substrates. The contact line of drops were studied in the case of single[39] and multiple defects.[40,41] Defects in these rough surfaces can have an effect on the hysteresis of the contact line[42] and effect its prewetting transition.[43] Investigating flowing films of individual molecules allows for the study of various phenomena that cannot be directly examined. We can visualize molecules as they flow past one another and directly visualize the amount of slip they undergo. Also it is known that polymer brushes of a certain side chain length break when they are adsorbed onto a surface. Up until now, this process has not been documented *in situ.* The imaging individual molecules as they flow in real time yields movies of these brushes breaking. This gives some insight into the forces that tear them apart. Despite this thorough compilation of data, there are still important questions that are left unanswered.

- Can we perform *in situ* studies to observe molecular slip?
- Do the individual molecules undergo a conformational change as they flow?
- Is it possible for crossed molecules to dissociate during flow?
- Can we monitor the scission process?

1.3.3 Controlled spreading. *Channels.* The understanding of spontaneous spreading on the molecular level is only the first step in this research. In microfluidics, some of the main goals are mixing and reacting chemicals,[44] sorting particles,[45] and synthesizing particles.[46] To achieve and enhance these processes and make them more efficient, it becomes necessary to study the conformation, shape, and flow behavior of the molecules in those channels. Fabrication techniques allow for the creation of smaller and smaller channels. As the size of these channels approaches that of the molecular size the conformation of molecules is affected by the confinement of the channels.[47] It then becomes necessary to investigate individual molecules as they flow through such channels. We lay groundwork to answer the following questions:

- How does confinement to narrow channels affect the molecules conformations?
- Do these channels induce order?
- Is there molecular slip at the channel walls?
- Do individual molecules undergo a plug flow while in these channels?
- Is there diffusion amongst the individual molecules?

Electric fields. Many researchers have studied the effects of electric fields on particles and fluids. There are many studies done with regards to electrowetting of fluids and their manipulation via dielectrophoresis.[48,49] Even individual particles have been manipulated and aligned using these methods.[50] These studies are all conducted using bulk fluids and techniques aimed at studying the macroscopic behavior of these fluids. Again due to the inability to resolve individual molecules in polymer melts it is unknown how introducing an electric field or confining the molecules to channels can affect their conformation, alignment, and spreading properties. The next step to control these polymer films is to use these methods to study individual molecules and their conformations along with their orientations and order with regards to their flow in electric fields. This leads to the following questions:

- What role do electric fields play in the orientation of molecules?
- How do the fields effect molecular conformations in thin films?
- Can we manipulate the bulk film using electric fields?
- Can we use these fields to confine molecular flow?
- Can we use an electric field to orient the molecules?

1.4 Strategies. Our experimental approach is based on imaging of individual molecules as they spread on a solid substrate. Molecular imaging is a challenging task. Not every technique can visualize molecules, and not every molecule can be visualized. We proposed to use AFM in combination with

cylindrical molecular brushes as model polymer molecules. While AFM has the spatial resolution (~10 nm) to visualize the polymers, it is the decoration of the polymer chains with side chains that enhances the contrast and ultimately allows for visualization. To study the concepts of individual molecules under flow, we must first develop strategies to accomplish this goal. We approach this in two parts: molecular visualization and polymer spreading. For the visualization of molecules, we will explain how the special architecture of cylindrical polymer brush molecules allows us to 'see' them with an atomic force microscope when other polymers remain invisible.

1.4.1 Model Molecules. As we stated earlier, it is impossible to achieve molecular resolution to image all polymer molecules in a melt. For this reason we turn to using large macromolecules with similar behavior to linear polymers for our studies. Our molecule of choice is a cylindrical polymer brush or polymer bottle brush (shortened to just 'brush' for the duration of this text). A polymer brush (Figure 1.6) consists of a linear polymer chain with a degree of polymerization (DP) = N with individual polymer side chains grafted to it, each with an average DP =n. During synthesis one can control both of these parameters thus directly controlling the brush's length and width. By altering N we can directly control the brushes width (higher N's yield longer lengths), while when we vary n we can directly control the brushes width or radius.

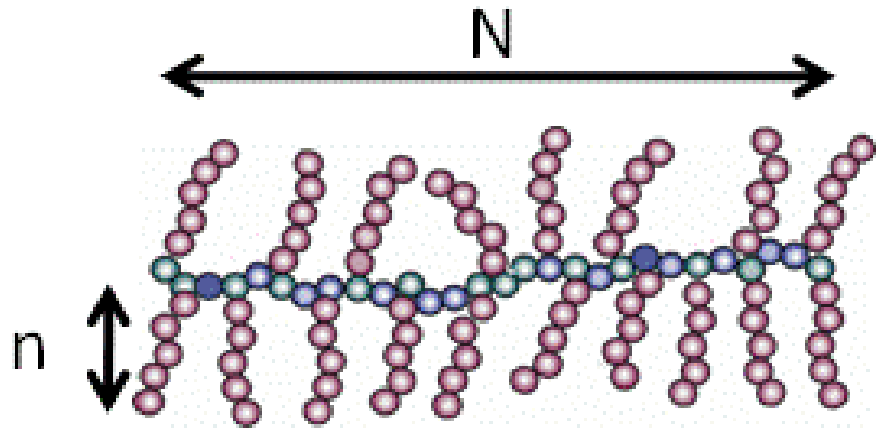

Figure 1.6 Architecture of a polymer brush. The architecture of a cylindrical polymer brush with a back bone degree of polymerization (N) and a side chain degree of polymerization (n).

We can use these parameters along with the grafting density (j) of the brush (the proportion of backbone monomers with a side chain grafted to them) to alter the shape of the brush. Parameters N, n, and j and their effects on the molecular properties are depicted in Table 1.2. The backbone degree of polymerization has a direct affect on the length of the molecule while the side chain degree of polymerization and grafting density are used to alter the chains width, stiffness, and backbone tension. For example, a brush with long side chains and a high grafting density will have many steric interactions between the side chains. These interactions will cause the side chains to repel, thus making the brush stiffer and more rod-like. (Figure 1.7) However, if we lower the grafting density by removing some side chains, or we shorten the side chains, the net repulsive force of the side chains will be weaker, thus allowing the brush to bend and flex. For the use of these brushes as model molecules we have universal

system that can be synthetically tuned to have a wide spectrum of structural properties.

Table 1.2 Brush parameters.

Synthetic parameter	Range	Changes:	Range
N	10-10000	Length (L)	50-10000 nm
n	10-200	Width(w)	10-300 nm
j	10-100%	Stiffness (l_p)	80-5000 nm
		tension	10-2000 pN

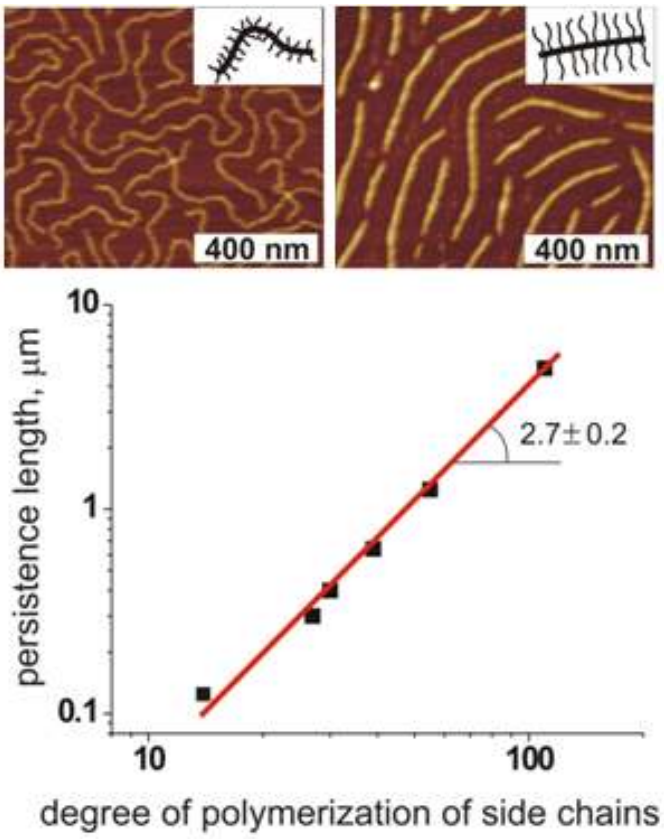

Figure 1.7 Various degrees of chain absorption onto surfaces. Coiled brushes with a low degree of chain adsorption and repulsion (top left) and extended chains with a high degree of adsorption and repulsion (top right). The graph on the bottom shows the relationship between n and the stiffness of the molecule.

When these brushes are in solution or in a melt phase, they take on a conformation that resembles a bottle brush: a back-bone at the core with side chains distributed around it. Although the fundamental architecture is different, the brush still maintains many of the physical properties of a polymer and it will still react to solvents in the same manner that the linear polymer will, swelling in good and athermal solvents and collapsing in poor and non solvents.

When these brushes come in contact with a surface, depending on its spreading coefficient, S (see Section 1.2.2), the side chains will either spread and adsorb onto the surface, or repel from the surface and form a globule (Figure 1.8). The spreading of the side chains is directed both parallel and perpendicular to the backbone and both are related to S. The parallel force becomes very important to the properties of the brush since it applies a tension on the backbone, thus causing it to extend. This tension is equal to $S \cdot d$, meaning it increases with the length of the side chains and thus their degree of polymerization. If this tension becomes sufficiently high the backbone can break as it spreads on the surface as in the case with some of our samples with the longest side chains.

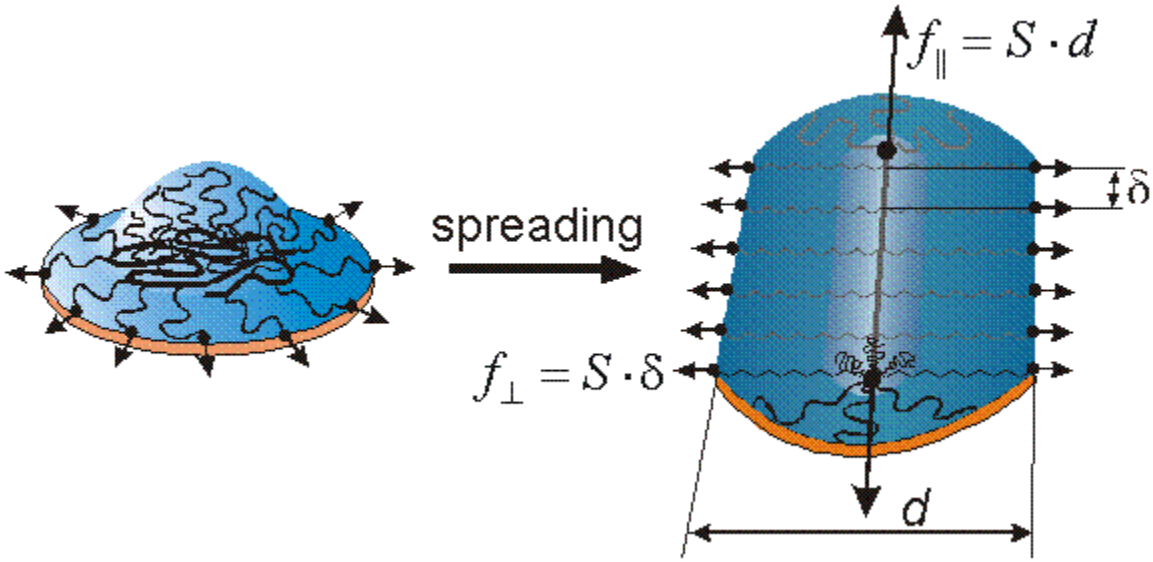

Figure 1.8 Single brush spreading. Schematic of a polymer brush spreading on a surface from when it is placed on the surface (left) to its equilibrium state (right). The spreading and tension forces on a brush are labeled.

When a brush is spread and fully absorbed onto a surface it takes on a unique conformation where approximately half the side chains spread and absorb onto the surface, while the other half form a ridge over the backbone (Figure 1.9 top). This ridge has a height of 2-4 nm and because of this gives contrast to the adsorbed side chains with a height of 0.8 nm. This height contrast is exploited using AFM. While on the surface, these side chains can take on a variety of conformations (Figure 1.9 bottom). With long side chains, the brush will stretch and become rod-like. When the side chains are uneven on each side of the backbone, the brush will begin to bend. Under high pressures the brush will compress by compacting, contracting, or coiling, depending on factors such as the grafting density of the brush, the surface energy, chain length, or back bone length.

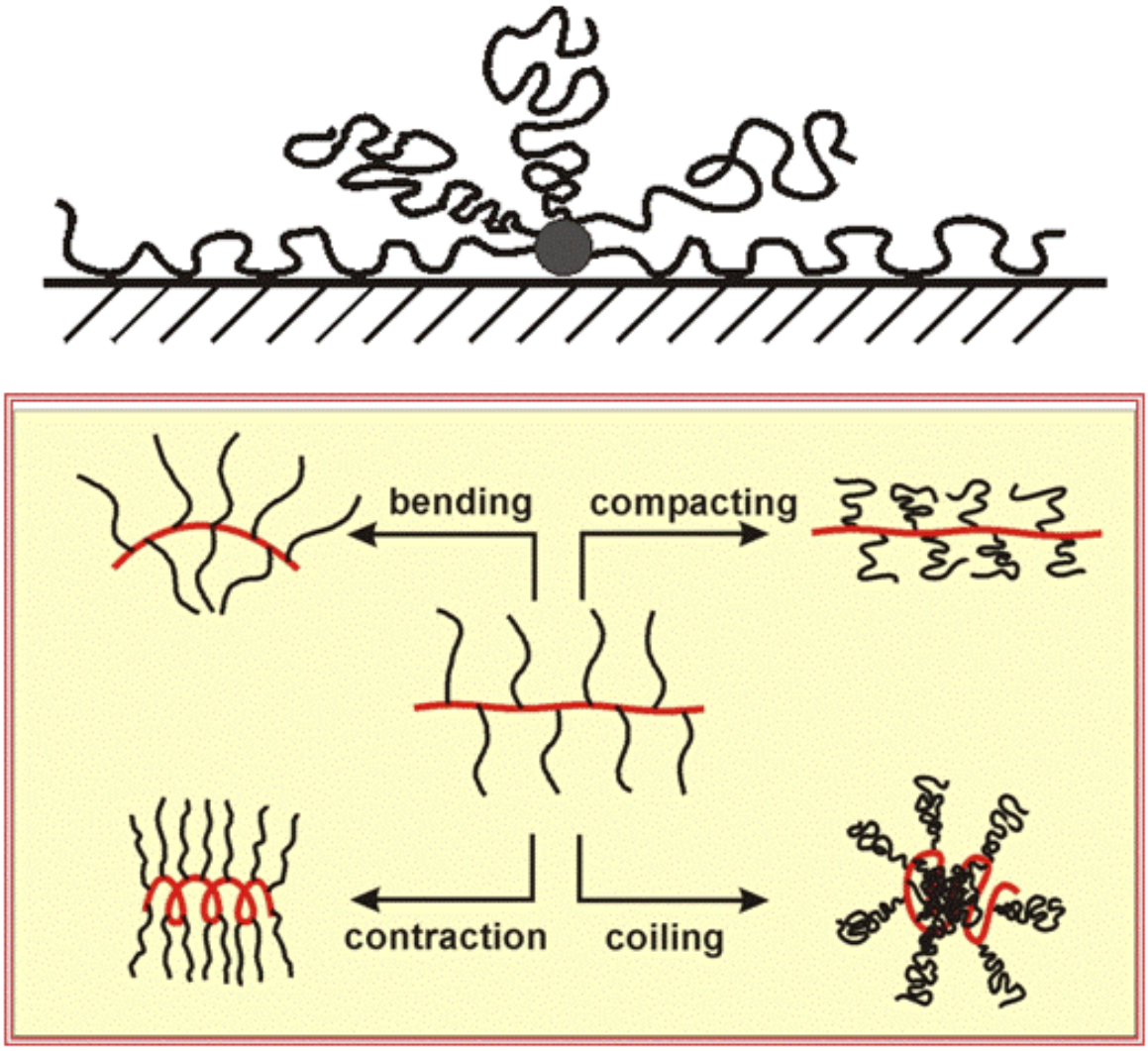

Figure 1.9 Various curvatures and conformations of polymer brushes. Top. Diagram of a polymer brush absorbed onto a substrate. Bottom. Various conformations a polymer brush can undergo.

The adsorbed nature of the side chains yields a switchable conformation from cylinder-like to a ribbon-like (Figure 1.10) that is easily visualizable.[51] This transition may occur during spreading as a result of pressure changes that undergo in a film. High pressures cause the side chains to collapse and lift the brush backbone off the surface, while causing it to form the cylindrical

conformation in Figure 1.10 (left). Lower pressures allow the side chains to absorb onto the surface and form the characteristic ridge in on the back bone.

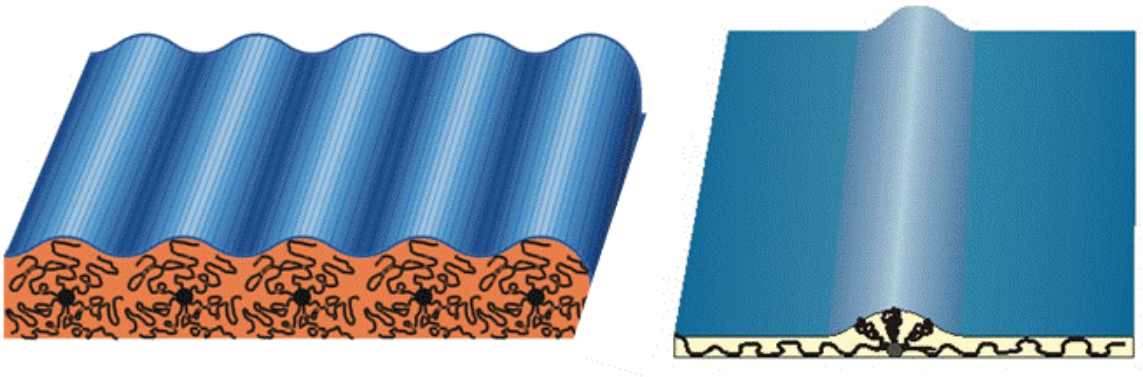

Figure 1.10 Conformations of a polymer brush on a surface. Left. Cylindrical conformation found in high pressure regions. Right. Absorbed conformation found in low pressure regions of a film.

The features of these polymer brushes that allow the molecular brushes to be imaged as single species can be exploited to do a variety of experiments as demonstrated in Figure 1.11. The top-left image consists of the polymer brushes in a matrix of linear polymer and their properties can be used to probe things such as film pressure and flow properties. The individual properties can be studied as well. Figure 1.11 (top center) shows an ultra high resolution image of a brush where its individual side chains can be seen. Fundamentals of crystallization can also be studied (Figure 1.11 top right). The images shown are of a brush with diblock side chains to with the center crystallizing. Most spectacular is the ability for these polymer brushes to model systems of polymer chains. Figure 1.11 (bottom) shows these polymer brushes on a dense monolayer. It is their architecture which allows each individual molecule to be visualized. It should be noted that although it is possible to image single

molecule chains (similar to the side chains in Figure 1.11 top center) it is impossible for the direct imaging and separation of linear polymer chains in dense films. To study the interactions and conformations of individual chains on each other it becomes necessary to use a model system, which these polymer brushes are able to mimic so well.

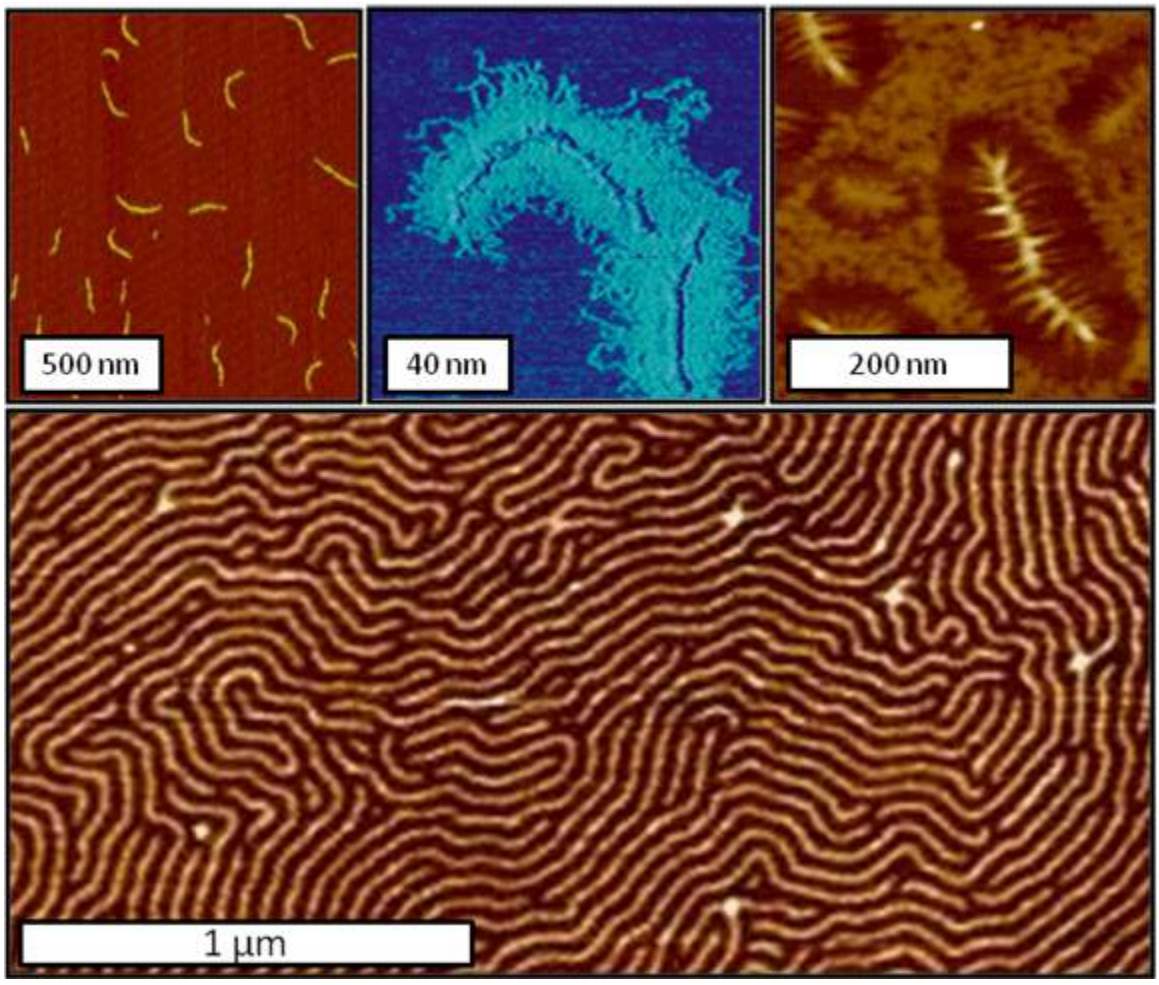

Figure 1.11 Images of polymer brushes as model systems. Top Right. Polymer brushes embedded in a linear matrix for use as probes. Top Center. High resolution AFM image of a polymer brush to study its structure. Top Right. Images of crystallized diblock polymer brushes. Bottom. Polymer brushes used as model polymer systems to study conformation, topology and structure.

1.4.2 Molecular Imaging. The study of individual molecules typically takes the form of one of two approaches. Investigate molecules you can see or label molecules with something you can 'see' (such as fluorescent microscopy). The latter approach usually requires only labeling a few probe molecules within the sample being studied. This approach works well for studying the kinetics and dynamics of single molecules, however it does not allow for the visualization of every molecule in a sample, which makes it difficult to study the interactions between molecules that are side by side and it is hard to properly study all anomalies within a sample. Studies on this topic have been conducted for decades, but each deals with the flow of the entire film[52-54] or molecular dynamic simulations.[55,56] Currently there is no technique with the ability to image each individual molecule in a polymer film, since linear polymer molecules are no more than 1 nm wide and have lengths from 5-10000 nm. Techniques such as ellipsometry[57] lack the spatial resolution (the best have resolutions of 100 μm) to study individual molecules, while more precise techniques, such as AFM (with resolutions of up to 1 nm), are unable to visualize and isolate individual polymers in films due to their interactions. To overcome these issues we utilize the high spatial resolution of the AFM, and couple it with a novel model polymer system which has the ability to be visualized (with 50 – 100 nm widths). This system allows us to individually image and monitor every molecule as they flow on a surface allowing for unique insight to how these molecules conform, mix, interact, and react with one another. This thesis uses this special system to study the five separate aspects of thin films and flows:

1.) How the preparation method affects the molecules conformation, topology, and packing in thin films (Chapter 3),

2.) How the flow of the thin films affects these properties (Chapter 4),

3.) The study of a friction induced fractionation of molecules as they flow in a chemically 'identical' matrix (Chapter 5),

4.) The study of the flow of molecules in real-time and the anomalies therein (Chapter 4),

5.) How molecules flow under the presence of external stimuli, such as an electric field (Chapter 7).

1.4.3 Substrates. When conducting spreading experiments it is important to select an appropriate substrate for the experiment. To measure molecularly thin layers of polymers the substrate must be atomically flat which is why we routinely use highly ordered pyrolytic graphite (HOPG), mica, or silicon as substrates. When choosing one of these substrates we need to consider the friction coefficients that the molecules have with the substrate. The friction coefficient is a very sensitive parameter and if it becomes too high ($\xi > \frac{D}{B}t^{4/5}$, where D is the spreading rate, B is a droplet spreading constant, and t is time) the film will spread much slower than the macroscopic drop. In the case of HOPG, the friction coefficient is in the range where spreading is possible ($\xi=2\text{x}10^{12}$ Ns/m^3). This makes it ideal for real time AFM studies of the flow process since the since the molecules spread at a rate of 1-10 nm/min. The AFM has the ability to capture images at 4 min intervals meaning that the distance the molecules move

in that time is on the order of their molecular size (4- 40 nm) so the conformational changes and individual molecules can be tracked in real time. However, the surface itself has many terraces and defects which make conducting long distance spreading experiments more difficult.

Earlier we mentioned that bare mica and silicon substrates have friction coefficients with the polymers we study that are too high to allow spreading. Friction can be reduced through lubrication. Given that water is one of best lubricants, we run spreading experiments under high relative humidity to deposit a water layer on the substrate. We do this by placing the substrate with a drop of the polymer in question into a chamber above a saturated salt solution to control relative humidity.[58] Silicon having a hydrophobic oxide layer does not allow for the water vapor to deposit on the surface so the humidity has no effect. The mica however, is hydrophilic and attracts the water. This water forms a thin layer on the surface (Figure 1.12) that allows it to be lubricated, thus drastically lowering the friction coefficient (to $\xi=2.1\text{x}10^{8}$ Ns/m^3) of the surface-polymer system orders of magnitude below that of the HOPG.[59] This allows for a controllable system that spreads when we expose it to a high RH and stops when we remove it.

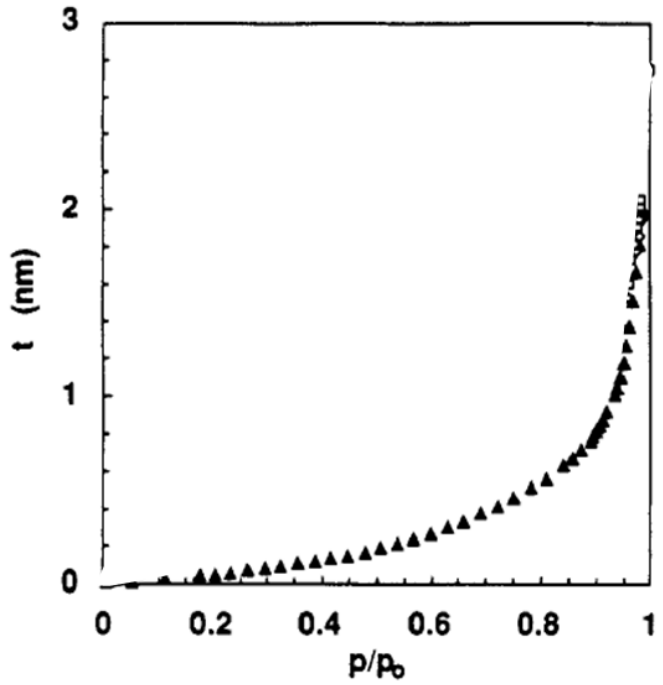

Figure 1.12 Thickness of water vapor on mica.[60] The thickness of water vapor layers determined from ellipsometry as a function of relative vapor pressure (p/p_0) at 18 C.

1.5 Conclusions. It is understood that while we can learn much about the spreading behavior of polymeric films using traditional methods, we cannot use those methods to extract information about the behavior of individual molecules in those films. Because of this, we turn to AFM and a model polymer system to study the physical properties of individual polymers both in static films and as they flow. Using these techniques we can answer the following questions:

- How does preparation method affect the conformation of molecules in a polymer film? What are the equilibrium and metastable conformational states in thin films?

- What effects does flow have on the conformations and topologies of individual molecules?

- Do these model molecules mix and fractionate under flow?

- How do the conformations and structures of molecules in flows change in real time?

- Can we control the flow of molecules?

Studying the molecular properties of films will hopefully lead to the ability to tune properties simply by engineering intelligent preparation methods.

This dissertation will delve into the area of thin spreading films and investigate these questions. I use AFM to visualize single polymer molecules under flow and characterize their motion. The questions mentioned above are carefully investigated and answered in the following text. Finally, I explore methods to manipulate the flow and conformation of the individual polymers using electric fields.

References

[1] Ginger, D. S.; Zhang, H.; Mirkin, C. A. *Angewandte Chemie International Edition* **2004***, 43*, 30-45.

[2] Hawker, C. J.; Russell, T. P. *MRS Bull* **2005***, 30*, 952-966.

[3] Bietsch, A.; Michel, B. *J. Appl. Phys.* **2000***, 88*, 4310-4318.

[4] McLellan, J. M.; Geissler, M.; Xia, Y. *J. Am. Chem. Soc.* **2004***, 126*, 10830-10831.

[5] Kleinbach, E.; Riede, T. *Chem. Eng. Process* **1995***, 34*, 329-337.

[6] Khan, H.; Fell, J. T.; Macleod, G. S. *Int. J. Pharm.* **2001***, 227*, 113-119.

[7] Pfohl, T.; Mugele, F.; Seemann, R.; Herminghaus, S. *ChemPhysChem* **2003***, 4*, 1291-1298.

[8] Zhang, H.; Mitsuya, Y.; Yamada, M. *J. Tribol.* **2002***, 124*, 575-583.

[9] Gans, B. -. d.; Duineveld, P. C.; Schubert, U. S. *Adv Mater* **2004***, 16*, 203-213.

[10] Sun, F.; Sheiko, S. S.; Moeller, M.; Beers, K.; Matyjaszewski, K. *Journal of Physical Chemistry A* **2004***, 108*, 9682-9686.

[11] Sheiko, S. S.; Prokhorova, S. A.; Beers, K. L.; Matyjaszewski, K.; Potemkin, I. I.; Khokhlov, A. R.; Moeller, M. *Macromolecules* **2001***, 34*, 8354-8360.

[12] Xu, H.; Sheiko, S. S.; Shirvanyants, D.; Rubinstein, M.; Beers, K. L.; Matyjaszewski, K. *Langmuir* **2006***, 22*, 1254-1259.

[13] Sheiko, S.S.; Sun, F.; Randal, A.; Shirvaniants, D.; Matyjaszewski, K.; Rubinstein, M. *Nature*, **2006,** 440, 191-194.

[14] Forrest, J.A.; Dalnoki-Veress, K.; Dutcher, J.R. *Phys. Rev. E.* **1997**, 56, 5705.

[15] Kawana, S.; Jones, R.A.L. *Phys. Rev. E.* **2001**, 63, 021501.

[16] de Gennes, P.E. Eur. Phys. J. **2000,** 2, 201.

[17] Forrest, J.A.; Dalnoki-Veress, K. Advances in Colloid and Interface Sci. **2001,** 94, 167.

[18] Vroege, G.J.; Lekkerkerker, H.N.W. *Rep. Prog. Phys.* **1992,** 55 1241-1309.

[19] Matsudomi, M.; Kato, A.; Kobayashi, K. *Agric. Biol. Chem*, **1982,** 46 (6), 1583-1586.

[20] O. Kahle, O.; Wielsch, U.; Metzner, H.; Bauer, J.; Uhlig, C.; Zawatzki, C. *Thin Solid Films.* **1998**, 314, 803.

[21] Kim, J.H.; Jang, J.; Zin W.-C. *Langmuir* **2001,** *17,* 2703-2710

[22] Frank B.; Gast, A.P.; Russell, T.P.; Brown, H.R.; Hawker, C. *Macromolecules.* **1996,** *29,* 6531-6534

[23] Bertrand, E., Bonn, D.; Broseta, D.; Dobbs H.; Indekeu, J.O.; Meunier, J.; K. Ragil, and Shahidzadeh, N. **2002,** *J. Pet. Sci. Eng.* 33, 217.

[24] Bergeron, V.; Bonn, D.; Martin, J.-Y.; Vovelle, L. *Nature.* **2000,** 405, 772.

[25] T.M., S.; S.R., Q. *Reviews of Modern Physics* **2005***, 77*, 977-1026.

[26] Xu, H.; Shirvaniants, D.; Beers, K.; Matyjaszewski, K.; Rubinstein, M.; Sheiko, S.S. *Phys. Rev. Lett*. **2004,** 93, 206103/1-4.

[27] Zhu, S.; Liu, Y.; Rafailovich, M.H.; Sokolov, J.; Gersappe, D.; Winesett, D.A. Ade, H. *Nature.* **1999**, 400, 49.

[28] Aoyagi, T.; Takimoto, J.-I.; Doi, M. *J. Chem. Phys*. **2001,** 115.

[29] Mugele, F.; Baret, J.-C. *J. Phys: Condens. Matter.* **2005,** 17, R705.

[30] Hughes, M.P. *Electrophoresis*. **2002,** 23, 2569-2582.

[31] Yang, M.; Chew Lim, C.; Liao, R.; Zhang, X. *J. Microelectromech. Syst.* **2006**, *15*, 1483–1491.

[32] Bonn, D.; Eggers, J.; Indekeu, J.; Menunier, J.; Rolley, E. *Rev. of Mod. Phys.* **2009,** 81, 739.

[33] Cazabat, A.-M. *Contemp. Phys*. **1987**, 28, 347-364.

[34] Leger, L.; Erman, M.; Guinet-Picard, A.; Ausserre, D.; Strazielle, C. *Phys. Rev. Lett.* **1988***, 60*, 2390.

[35] Heslot, F.; Cazabat, A. M.; Levinson, P. *Phys. Rev. Lett.* **1989***, 62*, 1286.

[36] Xu, H.; Sun, F. C.; Shirvanyants, D. G.; Rubinstein, M.; Shabratov, D.; Beers, K. L.; Matyjaszewski, K.; Sheiko, S. S. *Adv. Mater.* **2007***, 19*, 2930-2934.

[37] Xu, H.; Sheiko, S. S.; Shirvanyants, D.; Rubinstein, M.; Beers, K. L.; Matyjaszewski, K. *Langmuir* **2006***, 22*, 1254-1259.

[38] Valignat, M. P.; Oshanin, G.; Villette, S.; Cazabat, A. M.; Moreau, M. *Phys. Rev. Lett.* **1998***, 80*, 5377.

[39] Joanny, J.-F.; de Gennes, P.-G. *J. Chem. Phys.* **1984**, 81, 552.

[40] Ramos, S. M.M.; Charlaix, E.; Benyagoub, A.; Toulemonde, M. *Phys. Rev. E.* **2003,** 67, 031604.

[41] Prevost, A.; Rolley, E.; Guthmann, C. *Phys. Rev. B.* **2002,** 65, 064517.

[42] Decker, E. L.; Garoff, S. *Langmuir* **1997,** 13, 6321.

[43] Müller, X.; Dupont-Roc, J. *Europhys. Lett.* **2001,** 54, 533.

[44] Iida K.; Chastek T.Q.; Beers K.L.; Cavicchi K.A.; Jaehun Chun, J.; Fasolka, M.J**.** *Lab Chip.* **2009,** advanced article.

[45] Wang, M.M.; Tu, E.; Raymond, D.E.; Yang, J.M.; Zhang, H.; Hagen, N.; Dees, B.; Mercer, E.M.; Forster, A.H.; Kariv, I.; Marchand, P.J.; Butler, W.F. *Nature Biotechnology* **2004**, 23, 83.

[46] Song, Y.; Hormes, J.; Kumar, C.S.S.R. *Small.* **2008,** 4, 698.

[47] Aoyagi, T.; Takimoto, J.-I.; Doi, M. *J. Chem. Phys*. **2001,** 115.

[48] Zeng, J.; Korsmeyer, T. *Lab Chip.* **2004,** 4, 265.

[49] Cristini, V.; Tan, Y.-C. *Lab Chip.* **2004,** 4, 257.

[50] Herlihy, K.P.; Nunes, J.; DeSimone, J.M. *Langmuir* **2008,** *24,* 8421-8426.

[51] Xu, H.; Shirvaniants, D.; Beers, K.L.; Matyjaszewski, K.; Dobrynin, A.V.; Rubinstein, M.; Sheiko, S.S. *Phys.Rev. Lett*. **2005,** 94, 237801/1-4.

[52] Cazabat, A.-M.; Gerdes, S. ; Valignat, M. P.; Villette, S. *Interface Sci.* **1997,** 5, 129.

[53] Beaglehole, D., *J. Phys. Chem*. **1989,** 93, 893.

[54] Leger, L.; Erman, M.; Guinet-Picard, A.; Ausserre, D.; Strazielle, C. *Phys. Rev. Lett.* **1988***, 60*, 2390.

[55] Qian, T.; Wang, X.-P.; Sheng, P. *Phys. Rev. E* **2003,** 68, 016306.

[56] Ren, W., W. E. Phys. Fluids **2007,** 19, 022101.

[57] Valignat, M.P.; Oshanin, G.; Villette, S.; Cazabat, A.M.; Moreau, M. *Phys. Rev. Lett.* **1998,** 80, 5377 – 5380

[58] Rockland, L.B. *Anal. Chem.* **1960,** 32, 1375.

[59] Hu, J.; Xiao, X.-d., Ogletree, D.F.; Salmeron, M. *Surface Science.* **1995,** 344, 221.

[60] Beaglehole, D.; Christenson, H.K. *J. Phys. Chem.* **1992**, 96, 3395.

Chapter 2

Experimental Methods

As in any body of scientific work, in order to study thin polymer films under flow, we employed a variety of experimental techniques. For instance, (complex/complicated/intricate) polymer synthetic techniques were used to construct well-defined macromolecules that can be used to model linear polymers in films. These macromolecules allow for the tuning of their conformations and properties and, most importantly for this project, the imaging of the molecules as individual species. Various preparation techniques have been used to prepare films of single molecules and of dense monolayers that allow in-situ monitoring of single chains as they flow over a substrate. Analyses of digital images have been applied to monitor conformation and dynamics of the flowing macromolecules. Each of these steps utilizes unique techniques and instrumentation that will be described below.

2.1 Synthesis of polymer materials. The molecules studied throughout this work were synthesized in Professor Matyjaszewski's group at Carnegie Mellon University using a polymerization method known as atom transfer radical polymerization (ATRP). ATRP is a controlled radical polymerization technique, which results in molecules with a narrow distribution of molecular weights, i.e. a

low polydispersity index (PDI). Other types of polymerization, such as free radical polymerization yield little control over the size and the molecular weight distribution and topology of the polymer. Since a polymer's properties, such as viscosity, solubility, diffusion coefficient, and its conformation in the melt state, are all affected by its molecular size and PDI, it becomes important to keep this property as uniform as possible.

The synthesis of a linear polymer via ATRP involves the use of an initiator molecule, commonly alkyl halides, to initiate the polymerization. The halide atom in the initiator will reversibly bind to a catalyst forming a radical the polymer chain end. This radical facilitates the addition of a monomer to the chain end, causing the polymer to grow. At this point the halide atom is able to rebind to chain end, thus temporarily deactivating the reaction site and starting the process over again. The synthesis of the polymer brushes consists of a two step process[1] as illustrated in Figure 2.1. First, a macroinitiator, which becomes the backbone of the polymer, is synthesized. This macroinitiator is a polymer chain where the monomeric units consist of ATRP initiator molecules. In this specific case the macroinitiator synthesized was poly (2-(2-bromopropionyloxy) ethyl methacrylate) (PBPEM). Second, n-butyl acrylate monomers were grafted from this backbone using ATRP which allowed for the controlled growth of poly(n-butyl acrylate) (PBA) side chains.[2-4]

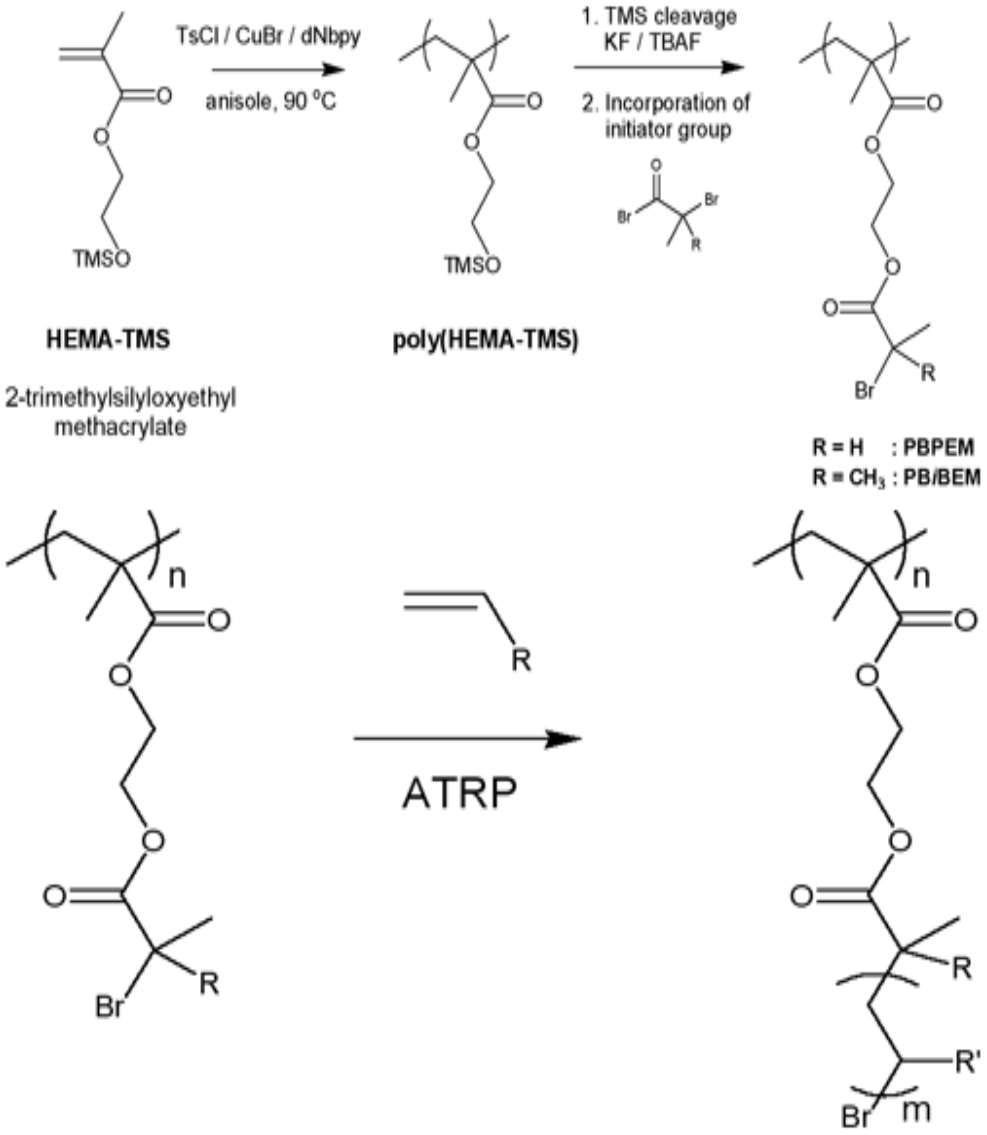

Figure 2.1 Synthesis of polymer brushes. Schematic detailing the synthesis of polymer bottle brushes using ATRP. The backbone synthesis is depicted on the top while the side chain synthesis is depicted on the bottom half of the figure.

The size control of the polymer brushes that this synthetic method supplies is crucial to analysis of these polymer films. This synthetic method allows for the control of many of the molecules parameters. We are able to vary the following parameters systematically:

- degree of polymerization of the backbone (N=100-5000)
- degree of polymerization of the side chains (n=10-150)
- the size distribution of both these parameters
- grafting density
- persistence length

2.2 Preparation of polymer films and flows. Three types of samples have been studied throughout the project: (i) single molecules, (ii) brush-like macromolecules imbedded into a dense layer of linear chains, and (iii) dense monolayers of molecular brushes (Figure 2.2). Single molecules were prepared by either adsorption from a dilute polymer solution by spin casting. Dense polymer films in this work were prepared using two methods: the Langmuir-Blodgett (LB) technique or spreading of a polymer film (Figure 2.2 bottom row). The latter preparation is solely used when studying the flow of polymers. What distinguishes one dense film preparation method from the other is the difference in the individual polymer configurations manifested for the two films (to be discussed in Chapter 3). The main difference between the two preparation methods is the original state of the individual molecules before they are forced into a film. With the LB method, the individual brushes are deposited on a surface as single species that are forced into a dense film upon lateral compression. Unlike the LB films, spreading deals with condensed polymer melts composed of overlapped and entangled macromolecules. One can also view LB and spreading techniques as two opposite (inverted) techniques: LB

yields films upon compression, while spreading yields films upon expansion. As such, one can prepare films at the same surface coverage (area per molecule).

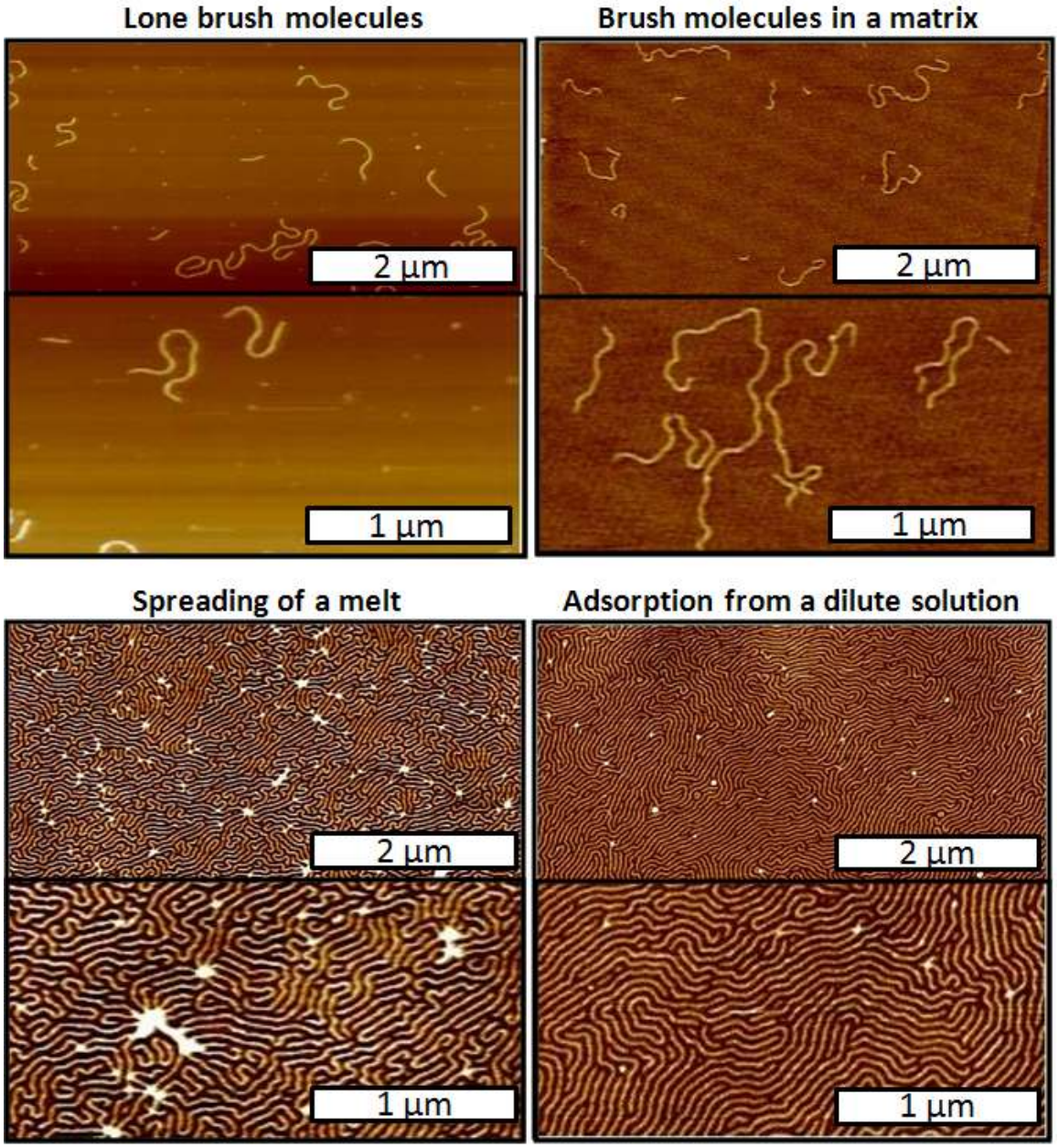

Figure 2.2 Polymer brush molecules in various configurations. Lone brush molecules on a substrate (top left). Brush molecules in a matrix of linear polymer (top right). Dense layer of brushes prepared from a spreading melt (bottom left). Dense layer of brushes prepared from a Langmuir-Blodgett trough (bottom right).

Both film preparation methods yield the ability to study the films at varying pressures. The LB method allows the user to tune the pressure, hence the conformation of the polymer in the film, by controlling the degree of film compression. It is this quantitative control of the surface pressure and molecular area that makes the LB method so attractive to study thin films. A major drawback of the method, however, is that it lacks the ability to study the flow of these polymer films. Moreover, it does not provide direct insight into the spreading behavior of polymers. For these reasons the LB method is used only as a characterization technique, for imaging and analysis of the conformation of molecular brushes at different states of equilibrium (Chapter 3) or to obtain properties of the bulk polymer itself when the spreading method is not adequate in doing so (Chapter 5). On the other hand, the preparation of films by spreading naturally has a gradient of pressures: ranging from a maximum where the film and drop intersect to zero at the edge of the film. To study the different pressures, one must image or observe at specific locations on the film with the pressure of interest.

2.2.1 Preparation of Langmuir-Blodgett films. LB films are an important method to prepare thin films since it can yield both molecularly thin films, as well as multilayered films. The LB trough works by compressing a known quantity of molecules on a surface with physical barriers, thus thereby controlling their surface pressure.[5] No other techniques (sputter coating, thermal evaporation, self assembly, or molecular beam epitaxy)[6] can yield such uniform control over

the thickness of the film, the number of layers it contains, or its surface pressure.[7,8]

In order to create a LB film from a particular molecule, we must first select a subphase that will not dissolve the molecule in question. This subphase typically has a relatively high surface tension (commonly water or mercury) and is physically contained by the trough itself (Figure 2.3). A solution of the molecule in a volatile liquid is placed drop wise onto the surface of this subphase. This both confines and disperses the molecules on the surface in a state that can best be described as a 2D gas. The barriers on the edge of the trough are then brought together in a controlled manner, thereby compressing the molecules into a uniform film. The surface pressure of this film is monitored by a Wilhelmy plate, which is a vertical plate hanging from a balance that measures buoyancy force supplied by the surface and film.

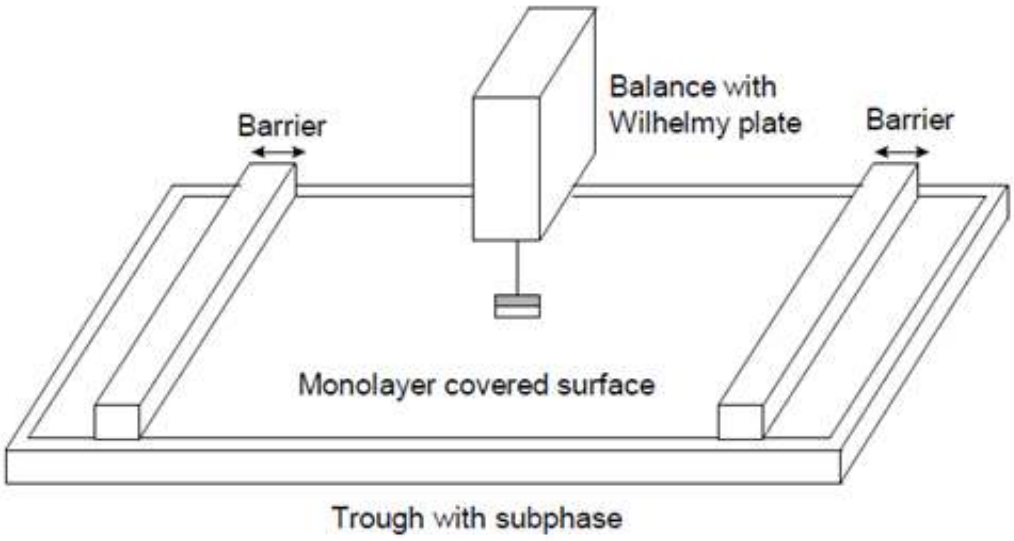

Figure 2.3 Langmuir Blodgett trough. A diagram of the Langmuir-Blodgett trough.

As the molecules are compressed and the surface pressure increases the film can proceed through various states and conformational changes. As stated earlier, at the lowest pressures the molecules are dispersed on the surface, similar to a 2D gas. Bringing the barriers together compresses the molecules into a state that is similar to a 2D liquid, thus forming a uniform monolayer. Increasing the pressure further can change the conformation of the molecules and eventually cause the molecules to form bi-layers, tri-layers, or possibly thicker films.

One of the most important features of the LB method is the ability to construct film pressure versus molecular area isotherms. As such, one can study molecular conformation at different degrees of surface coverage. Figure 2.4 shows molecular structure of thin films at different degrees of compression. One clearly sees that molecules change their conformation in response to compression. Furthermore, one can measure molecular weight from the known area per molecule and mass per unit area.[9] This allows accurate analysis of the molecular weight distribution of the studied molecules.

Figure 2.4 Images of brush molecules at various film pressures. The molecules all have the same dimensions, N = 500 and n = 35. The highest surface pressure ~18 mN/m is on the left side while the lowest ~1 mN/m is on the right side.

It is then possible to transfer the newly created film to a solid substrate such as mica, silicon, or glass.[10] This is another big advantage for LB films because you can use visualization techniques such as AFM to study the film you prepared. Theoretically, the conformation of the polymer on the LB substrate is preserved during transfer. Before the molecule is deposited on the subphase, the substrate in question is submerged into the subphase. When the desired pressure is obtained by the compression of the barriers, an elevator slowly pulls the substrate out of the subphase, thus transferring thin film from the surface of the liquid subphase to the surface of the desired solid substrate.

2.2.2 Creating molecular flows and films by spreading. The bulk of this thesis focuses on the flow of molecules in thin films. The theory and principles that govern these flows have been described in detail in Chapter 1, therefore only the experimental details will be given here.

The first step in creating these films is the deposition of a polymer liquid reservoir. This reservoir consists of the polymer melt being studied. A needle with a radius of approximately 100 μm is dipped into a surplus of the polymer melt. At this time, a drop of that melt is transferred to the needle, which is then placed onto the surface of the substrate being studied. Following this, a precursor layer will spread from the drop (Figure 2.5). In the case of a mica substrate, it will be necessary to place the drop into a humid environment (relative humidity about 85 %) to induce spreading. The humidity of this environment is controlled by a saturated salt solution that provides the necessary

relative humidity (RH) needed to experiment.[11,12] The removal of the drop from this humid environment will cause the spreading of the drop to cease, leaving a monolayer film for analysis. However, if the film spreads spontaneously without humidity, as in the case of a graphite substrate it becomes possible to monitor its progress *in situ* using an atomic force microscope.

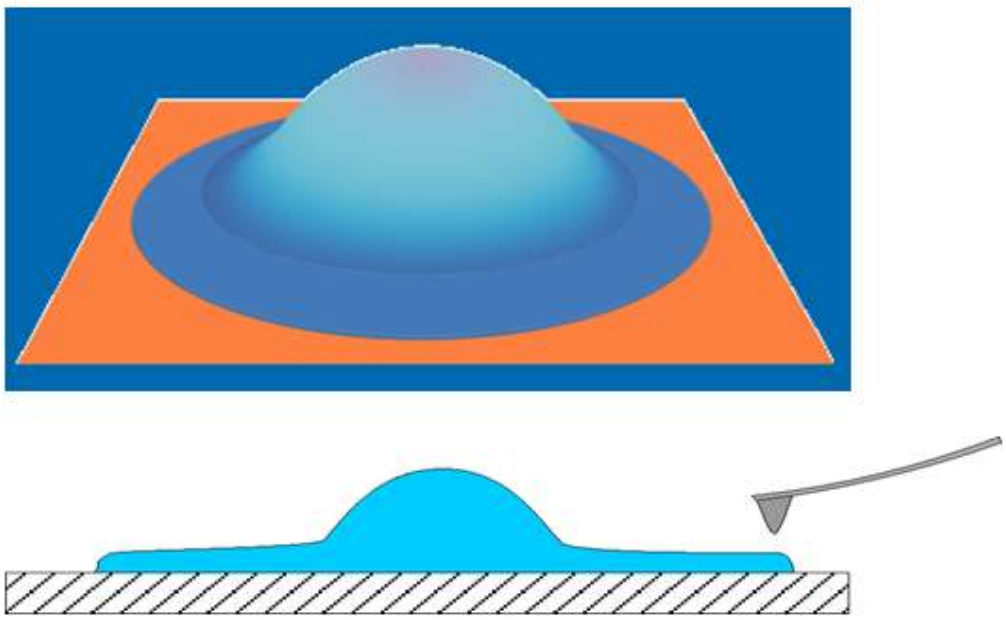

Figure 2.5 Diagrams of a spreading drop with its precursor layer. A 3D rendering of a spreading drop (top). The precursor layer forms a thin skirt around the drop. A cross section of a spreading drop (bottom).

Both methods of creating films (the LB and the spreading methods) are key to the study of the effects equilibrium has on these spreading films, while the LB method is of utmost importance to gain a base knowledge about the polymers in question when conducting spreading experiments. Spreading and the LB method are the main tools used throughout this dissertation to create molecularly thin polymer films.

2.3 Molecular Imaging. Imaging methods exploit a particular property of the object of interest to obtain contrast with its surroundings. For example, fluorescence microscopy contrasts molecules that fluoresce under a specific wavelength of light with those that do not. However, most optical microscopy techniques are limited in resolution by the Abbe diffraction limit where the best theoretical resolution of the image is half the wavelength of light. To image individual molecules, we must turn to techniques that can provide resolution on the nanometer scale, such as scanning tunneling microscopy (STM), scanning electron microscopy (SEM), or force microscopy. STM can resolve molecules with different electronic structures and is of not much use to uniform monolayers, while SEM requires a conductive surface to be imaged under vacuum; both are not conducive to our spreading experiments. Force microscopy[13] has the ability to use the scanning probe-sample interactions as the contrasting feature and has the ability to spatially resolve images to under 10 nm,[14-18], characteristics ideal for imaging our model polymer systems.

Force microscopy can operate in a variety of different contrast regimes: magnetic force microscopy measures differences in the magnetic force of a material, electric force microscopy measures the electric field of samples, while atomic force microscopy (AFM) resolves the interactions between the sample and the imaging probe. The latter is the best option to study our model polymer systems since it resolves the height contrast of the polymer brushes yielding the height images of an AFM.

The AFM consists of 3 major components: the probe tip, the detection system, and the scanning peizo (Figure 2.6). The probe tip is the sensor that collects the force information by interacting with the local force fields of the sample under study. It consists of a very sharp tip on the edge of a cantilever which deflects upon attraction or repulsion from the surface. This tip can be constructed of a variety of materials such as silicon, silicon nitride, tungsten, and carbon nanotubes. A laser is focused onto the back side of the cantilever and is directed towards a quad photo detector which can measure the deflection of the laser as the cantilever moves. The sample is controlled by a sensitive peizo system that scans the sample underneath the tip with nanometer precision.

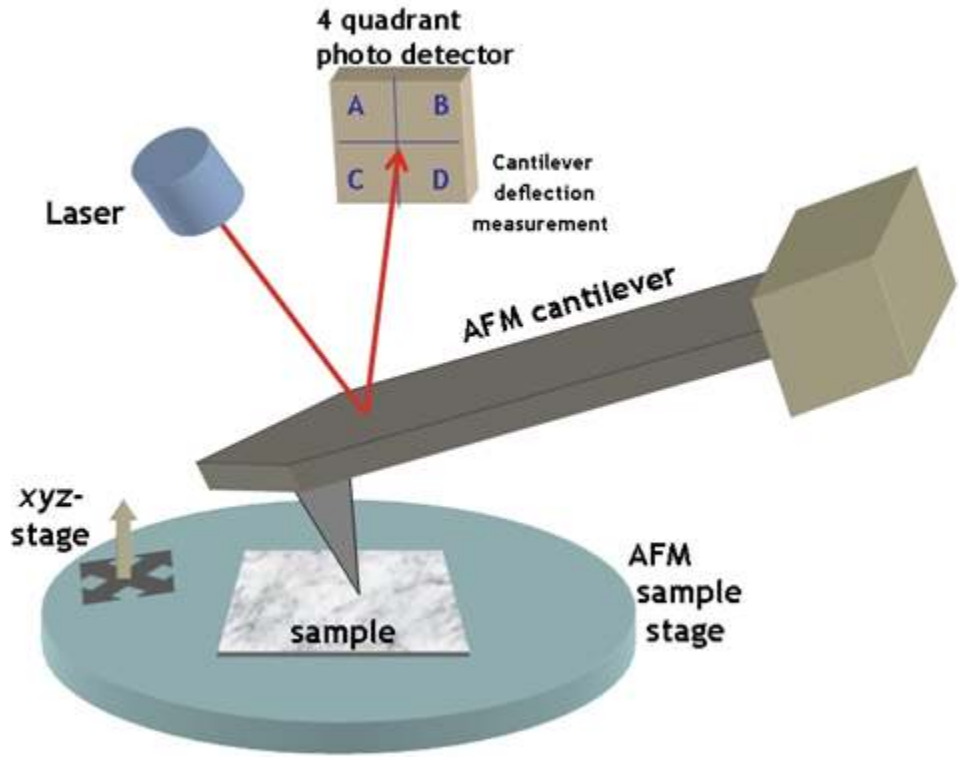

Figure 2.6 Atomic force microscope. Schematic of the workings of an atomic force microscope. The laser reflects off an oscillating tip which deflects as it moves over the surface. A four quadrant detector measures deflections in the cantilever as it scans over the surface.

In our experiments we operated the AFM in ‘tapping mode’ which operates by using a current to oscillate the cantilever and measures differences in its deflection as it passes over objects of different height. This method is preferred over contact AFM which slides the probe tip over the surface because it is less destructive when measuring soft or fragile samples. Since the backbone on our brush molecules have excellent height contrast, this method is ideal to image films of these polymers.

In addition to measuring a sample’s height, tapping mode can produce an image based on contrasting adhesion and viscoelastic properties. This imaging method is known as phase imaging (Figure 2.7). The distinction of phase imaging, compared to the height imaging, is instead of measuring the deflection of the cantilever, the AFM detects changes in the phase of the oscillation of the AFM tip as it comes in contact with the surface. A soft sample will shift the tips phase to a different degree than a hard sample and likewise attractive, adhesive, and repulsive samples will all have different effects on the phase of the oscillations. This method comes in handy when distinguishing different types of polymers with similar height contrasts.

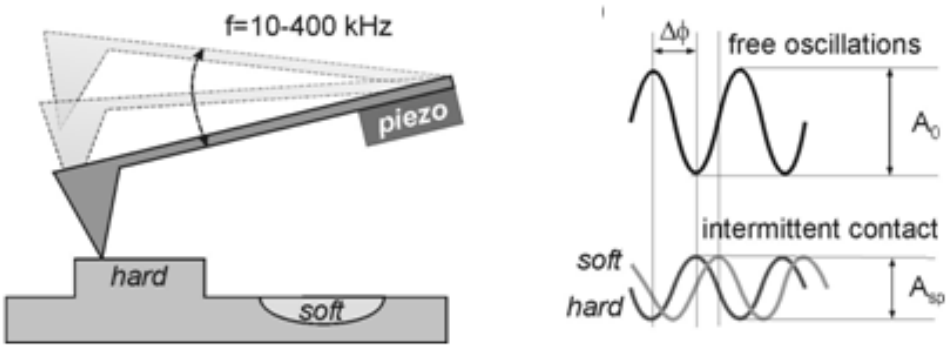

Figure 2.7 Imaging modes with atomic force microscope. Illustration of an AFM cantilever moving over a multi-component surface. The right side of the figure depicts the phase shift as the tip comes in contact with both hard and soft surfaces.

The capability of the AFM to image individual molecules with molecular resolution makes it the logical choice as the technique to image single molecules during and after their flow.

2.4 Image analysis. When images are obtained of our molecules we turn to a home built program known as 'Pen.' This software has the ability to identify individual molecules in an image and trace their contours (Figure 2.8). Once the contours are traced the program can extract a large wealth of quantitative data, such as molecular sizes, contour lengths, bond angles, histograms, order parameters, molecular distances and more, all automatically. The end result is a simple extraction of a vast amount of molecular properties.

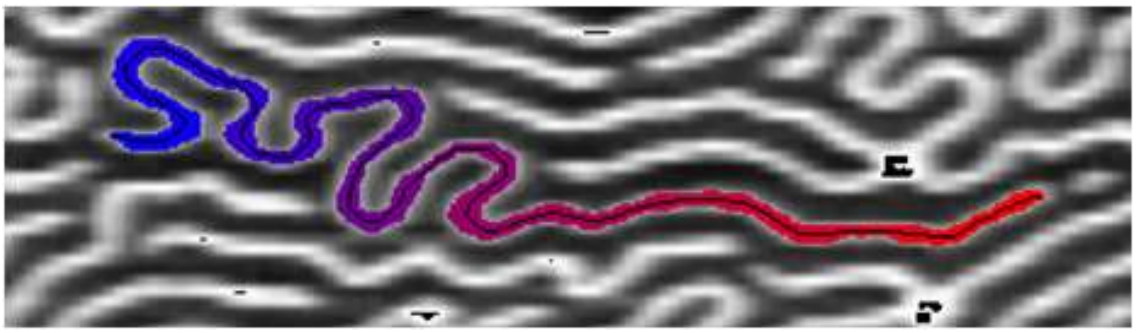

Figure 2.8 Diagram of molecular analysis. A polymer brush molecule isolated by the Pen program. The contour is traced.

To calculate the molecular properties described above, this program breaks up the molecules into individual vectors of a set length and coordinate. These vectors can then be measured to obtain the properties listed earlier. For example, to calculate the contour length of the molecule, it simply adds the absolute value of the lengths of all the segments while to calculate the end to end distance, it will sum the individual vectors to obtain a distance. Since the trace is broken up into vectors, the angles that each segment makes with one another can be measured. Using these measurements, we can calculate the correlation length that these molecules have with one another and obtain the molecules persistence length (Describe in more detail in Chapter 3).

2.5 Conclusion. Pioneers in the field have made important observations regarding the spreading of films. However, no previous studies were able to capture the effects and arrangements of individual molecules inside these films. With this combination of techniques and tools ranging from the areas of polymer

synthesis, to applied physics, to computer science, we can finally begin to understand the behavior of individual molecules in thin films both under static conditions and during flow.

References

[1] Borner, H.G.; Matyjaszewski, K. *Macromolecular Symposia,* **2002,** 177 1”15.

[2] Matyjaszewski, K.; Xia, J. *Chem. Rev.* **2001**, *101*, 2921-2990.

[3] Matyjaszewski, K.; Tsarevsky, N.V. *Nature Chem*. **2009**, 1, 276-288

[4] Sheiko, S.S.; Sumerlin, B.S.; Matyjaszewski, K. *Progress in Polymer Science* **2008,** 33, 759-785.

[5] Langmuir, I. *J. Am. Chem. Soc.*, **1917,** 39, 1848.

[6] Petty, M.C. *Thin Solid Films*, **1992,** 210/211, 417.

[7] Roberts, G., Ed. *Langmuir-Blodgett Films*, Plenum Press, New York **1990**.

[8] KSV – Application Notes #107

[9] Sheiko, S.S.; da Silva, M.; Shirvaniants, D.; LaRue, I.; Prokhorova, S.; Moeller, M.; Beers, K.; Matyjaszewski, K. *J. Am. Chem. Soc.* **2003,** 125, 6725.

[10] Blodgett, K.B. *J. Am. Chem. Soc.*, **1935**, 57, 1007.

[11] Young, J. F. *J. of Appl. Chem.* **1967**, 17, 241-5.

[12] Rockland, L. B. *Anal. Chem*. **1960**, 32 1375-6.

[13] Binnig, G.; Quate, C.F.; Gerber, Ch. *Phys. Rev. Lett*. **1986**, *56*, 930.

[14] Scheuring, S.; Fotiadis, D.; Moller, C.; Muller, S.A.; Engel, A.; Muller, D.J. *Single Molecules* **2001** 2, 59-67.

[15] Rivetti, C.; Guthold, M.; Bustamante, C. *J. Mol. Biol.* **1996** 264, 919-932.

[16] Kumaki, J.; Hashimoto, T. *J. Am. Chem. Soc*. **2003** 125, 4907-4917.

[17] *Minko, S.; Roiter, Y. Current Opinion in Colloid & Interface Science* ***2005*** 10(1,2), 9-15.

[18] Sheiko S.S.; Möller M. *Chem. Rev*. **2001** 101, 4099-4123.

Chapter 3

Molecular Conformation of Polymers Confined to Monolayers.

3.1 Introduction. Thin polymer films are at the heart of many technologies such as thin film transistors,[1] membranes,[2] Surfactants,[3] and light emitting diodes.[4] The development of such applications is built upon the theoretical and practical knowledge gained from previous studies. Early on, these studies centered on the dewetting of thin films consisting of fluids on surfaces[5-8] and later on thin films consisting of polymers.[9-14] Since this dewetting behavior can negatively impact these high performance applications, a need arises to develop films which have more durable properties on the molecular level.

The conformation and packing (based upon conformation, orientation, and density) of polymer chains has been proposed as a mechanism to explain various thin film phenomena. For instance, in poly(styrene) films, the glass transition temperatures (T_g) are reported to be both depressed,[15,16] when the film is confined to a thin film, and elevated,[17] when that thin film is grafted to a surface. The explanation of these phenomena revolves around the confinement structure of these polymer chains.[18,19] The proposed surface-induced changes of polymer structure at the surface of the substrate have lead to the study of the dynamics of these chains[20-22] with the goal of obtaining a better understanding of these bulk processes.

The experimental techniques used to study these properties are focused on the bulk films, such as optical microscopy, ellipsometry, and fluorescence spectroscopy. These techniques provide information about the film thickness, macroscopic morphology, and average molecular orientation; however, they fail when addressing the microscopic structure on the scale of the individual molecules. This leaves open many questions about the molecular conformation, chain entanglements and overlaps, as well as the packing arrangements in thin films. Furthermore, due to the large size of polymer molecules, the slow equilibration process yields metastable conformations with a life-time longer than typical industrial processes (days-years). Fundamental understanding of the real (off-equilibrium) structure of polymer films on a molecular scale can provide a great deal of insight that will allow accurate tuning of the film properties such as surface tension. This is evidenced by the importance of macromolecular packing and order of thin films in the optical and electrical properties of liquid crystals[23] and unimolecular wires.[24] At the same time, molecular entanglements in thin films can approach a woven conformation thereby changing a films surface tension[25] and robustness to make coatings more durable.

The study of individual molecules in thin films requires a technique that has the ability to image the individual macromolecules. The goal is to resolve the complete contour, including chain ends and microscopic curvatures on a scale below 10 nm (typical persistence length of polymer chains). This would be a significant advancement compared to optical microscopy, which is currently used as a main molecular imaging tool. As shown in Figure 3.1, a fluorescence optical

microscope is able to image long (~10 μm) DNA molecules;[26] however, the technique fails to resolve the curvature on the scale of the DNA persistence length of 50 nm. Our approach is to use Atomic Force Microscopy (AFM) to image individual polymer molecules and capture their various conformations and structures in thin films. Typically, AFM resolution of soft systems, such as polymer films, is on the order of 5 nm, which does not allow resolution of conventional polymer chains like poly(ethylene), poly(styrene), and poly(methyl methacrylate). Therefore, a strategy proposed to overcome this shortcoming is to employ model macromolecules: polymer chains decorated with short side chains. The combination of AFM and model molecules enable us to image individual polymer chains and measure their surface features such as topology, conformations and packing arrangements.

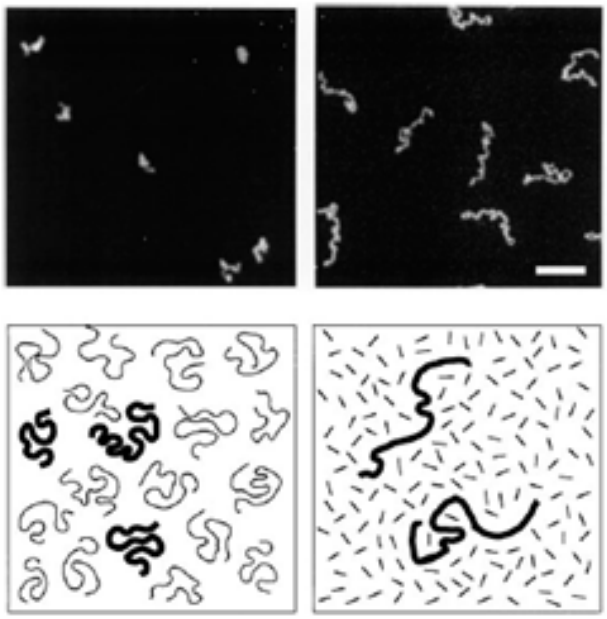

Figure 3.1 Fluorescent images of DNA.[27] Fluorescent images of single DNA molecules (top) with their cartoon depictions (bottom). The left side is an image of a DNA film with 1 % of the molecules fluorescently labeled, while the right side consists of labeled DNA in a matrix of unlabeled oligonucleotides. In both cases it would be impossible to image every individual molecule to characterize properties such as crossing and in the left image, it is difficult to make out the contours of the individual strands.

3.2 Molecular system. To conduct these experiments, we first select our molecular brush dimensions to appropriately model a polymer system. We have chosen a series of poly(butyl acrylate) brushes with a back bone degree of polymerization (DP) N = 7280 with a polydispersity index of about 1.9. This backbone is sufficiently long to properly emulate the entanglements and overlaps present in a single molecule system. However, as the side chain DP (n) becomes larger the brush becomes stiffer making it necessary to conduct these experiments with the shortest brush possible. These dimensions in the number of monomers express themselves as molecules of a particular size each with different properties i.e. the longer side chain molecules are the stiffest and more

rod-like while the molecules with the shorter side chains are more flexible and more closely resemble linear polymers. Since we are using these molecules as models for polymer systems the most suitable molecule for these experiments are the series with n = 40. Due to the polydispersity index of N, we see a large range in molecular lengths ranging from 100 nm to over 5000 nm. The side chains have a polydispersity also; however, this does not affect the overall width of the brush since each brush has many side chains and the width is a function of the average lengths. For chains with n = 40 the width of the brushes are consistent at 45 nm.

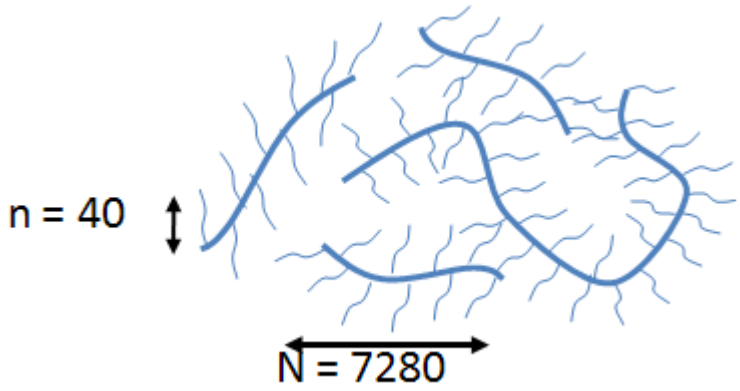

Figure 3.2 Schematic of molecular brush. The dimension of the molecules used in this chapter is as labeled.

3.3 Samples. In this study, we compare two types of samples: dense monolayers of the polymer brush molecules (Figure 3.3 left) and solutions of the brush molecules imbedded in a matrix of a linear polymer (Figure 3.3 right). The two different samples are used to make 3 separate films: (1) spreading preparation of the dense melt, (2) a Langmuir-Blodgett (LB) preparation of the dense melt, and (3) an LB preparation of the brush embedded in the matrix. The

brushes used in these films are the PBA brushes described in the previous section (N = 7280, n = 40) and the polymer matrix consists of linear PBA with a degree of polymerization m = 214 and a PDI of 1.2.

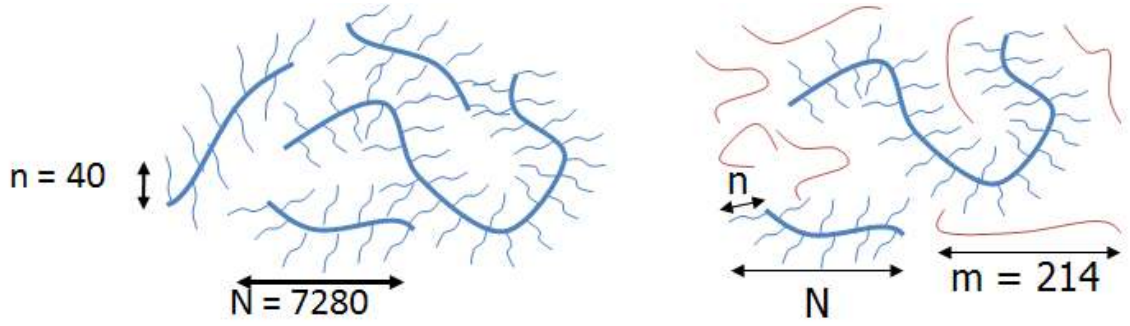

Figure 3.3 Schematic of the sample systems used. Left. A dense film of polymer brushes with n = 40 and N=7280. Right. A system of brushes in a matrix of linear polymers with n = 40, N = 7280, and the linear degree of polymerization, m = 214.

3.4 Film preparation. We have used two methods that created monolayers of these polymer brushes: adsorbing the model polymer molecules from a solution and spreading from a drop. The adsorption from solution involves depositing a dilute solution of the probe molecules on the subphase of an LB trough and compressing the polymers using the trough barriers (Figure 3.4). This preparation method allows the molecules to take an extended conformation on a surface before being physically forced into a dense monolayer. The molecular interactions, conformations and topologies are a direct result of the compression. For comparison we also prepared a film by spreading a drop of a polymer melt, where the molecules are first in their native melt state before they are forced into a film. In practice, the contrast between the two methods entails films formed

from individual molecules compressed into a film (LB method) versus films formed by molecules leaving a bulk melt state (spreading drop method).

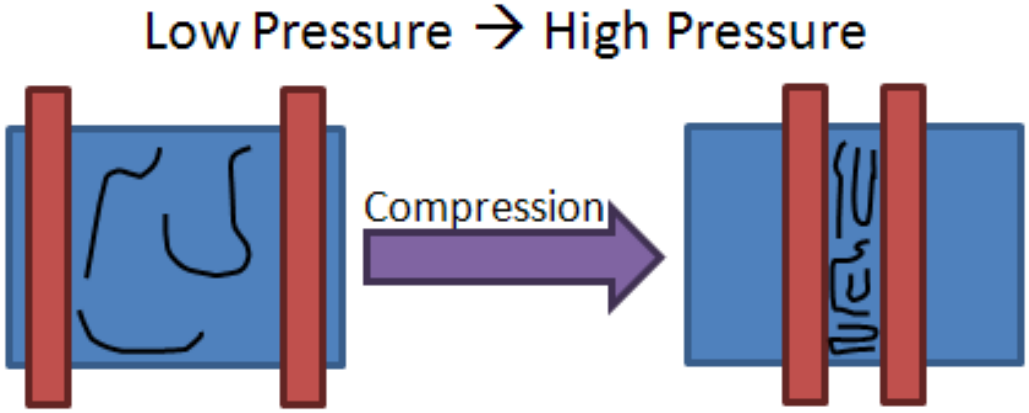

Figure 3.4 Diagram of LB. Diagram of the polymer molecules before and after compression on the LB trough.

Figure 3.5 shows a typical molecular organization of the prepared films at a surface pressure of 18 mN/m. Using the LB method, this pressure was achieved by laterally compressing the film on a water subphase to the desired film pressure and the same pressure was achieved in the spreading films simply by imaging the region of the film with the desired pressure.[28] Upon first observation, there are many obvious differences between the 3 films. The most notable feature in each film are that the dense adsorbed LB film appears to have extended macromolecules, while the spreading film demonstrates chain folding and crosses, while the adsorbed film with the linear matrix have random coils with no order. As stated above, these observations are ascribed to slow equilibration of the polymer films composed of large macromolecules. We grouped the molecular features into the following categories: (i) conformation of

individual molecule (length, Rg, and l_p), (ii) molecular topology (loops, folds, crosses), (iii) molecular assemblies (overlap, networks, ordering). Detailed analysis of these molecular structures will be presented in the following sections.

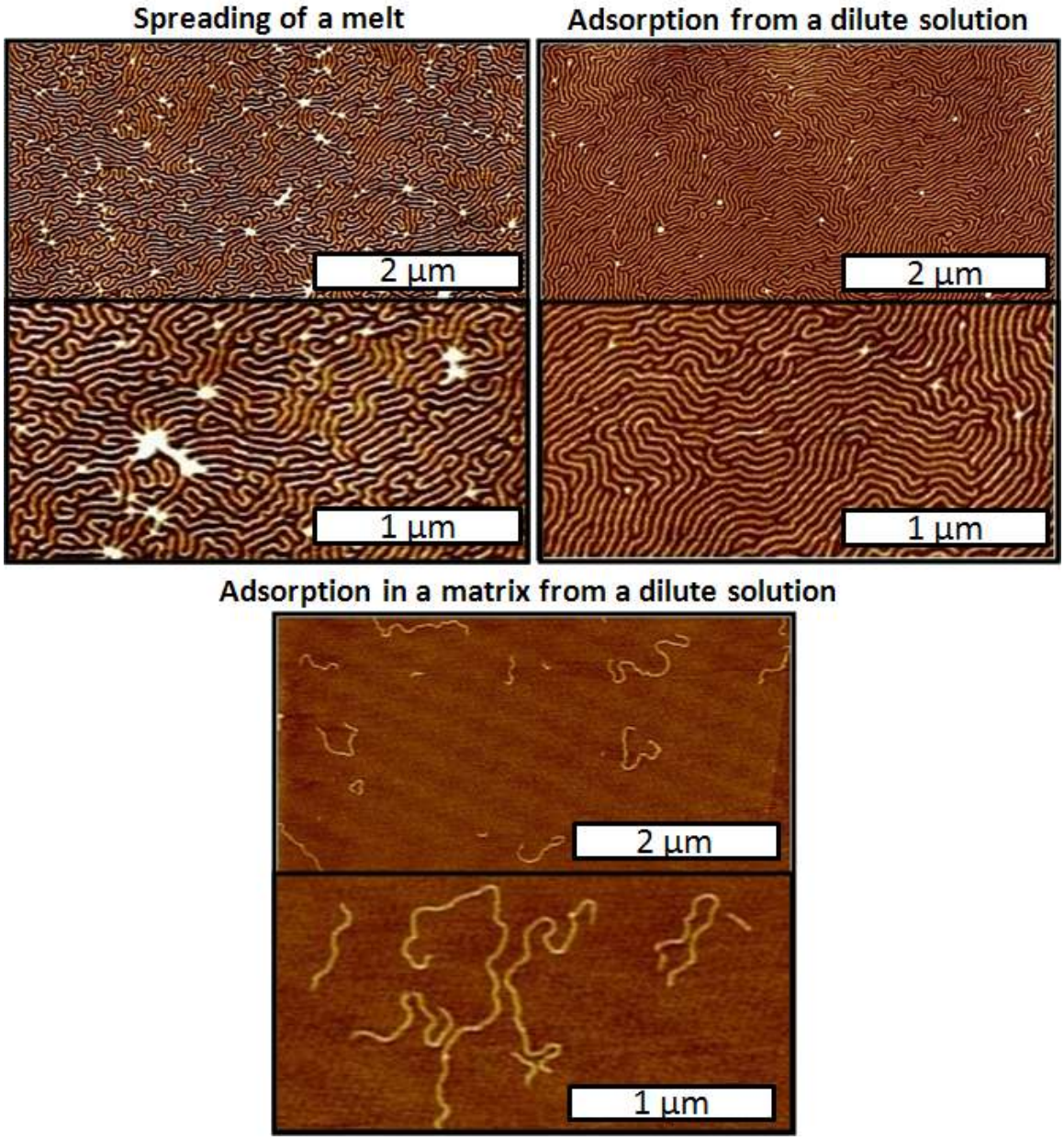

Figure 3.5 Images of prepared monolayers. AFM images of monolayer films of polymer brush molecules prepared from spreading (top left), adsorption (top right), and adsorption of brushes in a linear matrix onto a surface from a dilute solution (bottom). Two separate scales are shown for each film.

3.5 Conformations of individual molecules. The conformations taken by the model polymers vary with the preparation method. We have isolated 4 distinct conformations of the molecules in our film: extended, folded, collapsed and coiled (Figure 3.6). Each molecular conformation has its own unique characteristics, such as molecular length (L) , fractal dimensionality (D), persistence length (l_p), and molecular size (R_g). Using these properties and how they relate to conformation, we can determine the conformational make up of these films and how they are affected by the preparation method.

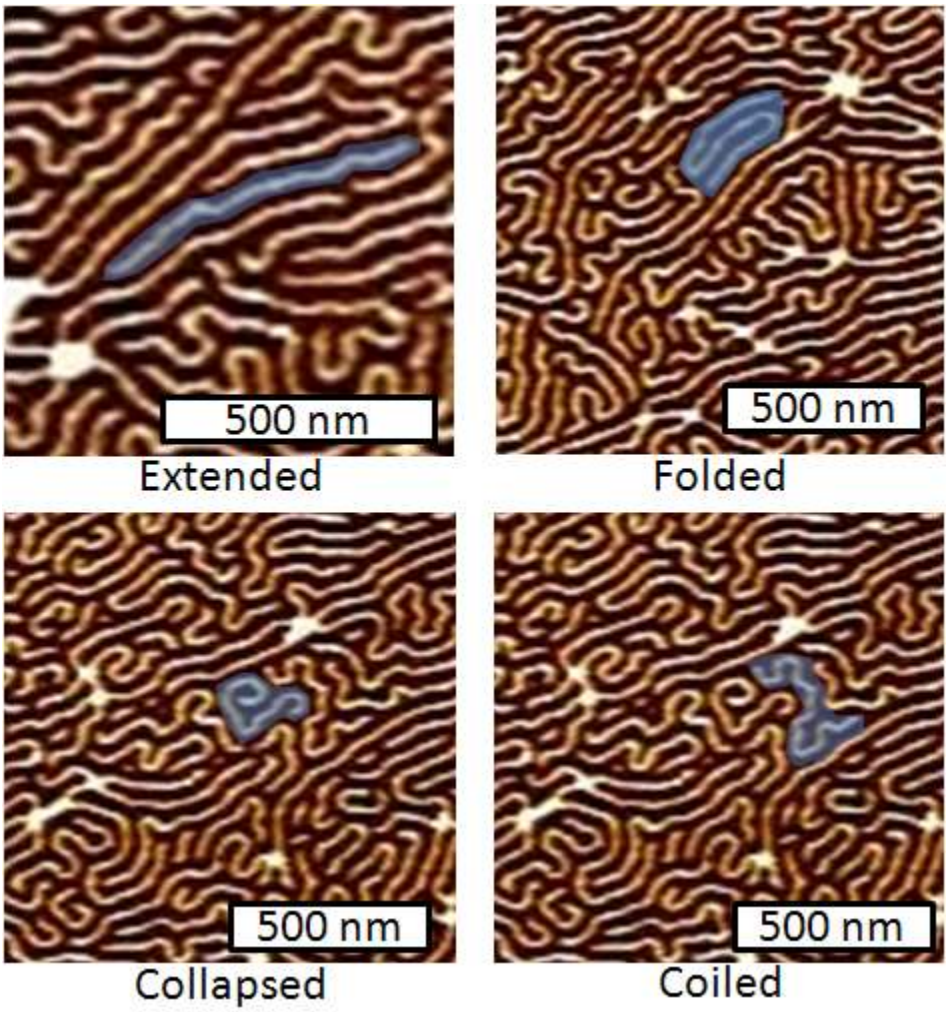

Figure 3.6 Images of molecular conformations. AFM images highlighting the various conformations of the polymer molecules that are seen in the film: extended (top left), folded (top right), collapsed (bottom left), and coiled (bottom right).

3.5.1 Radius of gyration. The radius of gyration (R_g) describes the distribution of masses with respect to the center of mass of the polymer. For a 3D chain, the scaling analysis predicts $R_g \sim N^{3/5}$ for a polymer chain in a good solvent (where there is a net repulsion between monomers) and $R_g \sim N^{1/2}$ in an ideal solvent (where there is no net repulsion or attraction between individual monomers). On

the other hand, in a 2D system, $R_g \sim N^{3/4}$ for a polymer in a good solvent. When the polymer is in a collapsed state, i.e. poor solvent, $R_g \sim N^{1/3}$, thereby forming a globule in 3D, while $R_g \sim N^{1/2}$ which forms a disk in the 2D case. The conformation of a molecule confined to a melt of polymers of differing sizes depends on the relative sizes of the probe molecule (N_A) with respect to the size of the surrounding melt molecules (N_B). For 3D, if $N_A < N_B^2$, the probe molecule collapses and is in the ideal state if the sizes are identical ($N_A = N_B$). In a 2D system, the collapse of the probe molecule occurs when $N_A < N_B$. Experimentally, the R_g is either measured by scattering techniques (e.g. light scattering in solution) or molecular imaging techniques of the molecules on a 2D surface.

To analyze the conformations of polymer brushes on a surface, we first obtain a base line average for the contour lengths of the brushes in both dense films prepared. These lengths of the brushes from both preparation methods are similar, 524 nm, 590 nm, and 610 nm for the spreading, the absorption, and the molecules embedded in the linear matrix respectively. We then use this average as a base line to compare the radius of gyration and end to end distances of the molecules in both films. As it turns out, both parameters approximately double their values when the film is prepared from solution, as opposed to spreading from a drop. The end to end distance jumps from 199 nm to 409 nm to 284 nm and the R_g increases from 73 nm, 134 nm, and 106 nm for the spreading film, the film adsorbed from solution, and the molecules embedded in the linear matrix respectively. If the molecules in the films had similar conformations, we would expect the end to end distances of the molecules and their radius of gyration (R_g)

to remain unchanged with the preparation method. This indicates that the individual molecules are more extended when they are adsorbed to the LB subphase where they become more rod-like, while when the molecules are in the linear poly(butyl acrylate) matrix, they are in their ideal state.

3.5.2 Persistence length. The persistence length (l_p) can be understood by breaking up a chain into many segments represented by the vector **r**. These segments are considered to be freely jointed and can rotate about an angle θ (in 2D a chain, it would consist of one of two angles +θ or -θ). This leaves the correlation between two segments, i and j, to be $\left\langle \vec{r}_i \cdot \vec{r}_j \right\rangle = l^2 \left(cos\,\theta\right)^{|j-i|}$, where l is the length of the segments. The value $\left(cos\,\theta\right)^{|j-i|}$ decays in value rapidly at increasing separation between i and j. Using the relationship $\left(cos\,\theta\right)^{|j-i|} = exp\left[\left|j-i\right| ln\left(cos\,\theta\right)\right] = exp\left[\frac{-\left|j-i\right|}{s_p}\right]$, we can define the term $s_p = -\frac{1}{ln\left(cos\,\theta\right)}$, where s_p is the number of bonds needed for this correlation to decay. Given that s_p is the number of bonds for the function to decay and l is the length of those bonds we can define the persistence length to be $l_p = l * s_p$ and obtain the relationship $ln < cos(\theta) >= -\frac{l}{l_p}$. It is an equilibrium property, that is, it assumes that chains freely fluctuate. In our case, we analyze the frozen (quenched) conformation which is presumably formed by equilibrated systems (like snapshots). By averaging the orientations of these snap shots we can

determine the typical orientation of any molecules as it fluctuates in a film. In addition to the R_g and end to end values, the extension of the molecules can be quantified by calculating the persistence length (l_p) of the molecules and comparing it from technique to technique. The persistence length is a measure of flexibility and is defined as the correlation length of the bond angles between discrete segments on an individual chain. It is calculated by plotting the angle of the two segments versus their separation along the chain in the equation $ln < cos(\theta) >= -\frac{l}{l_p}$, where l is the distance between the segments and θ is the angle between segments.

The plots of the persistence lengths of the various preparations are shown in Figure 3.7. The slopes of the curves were found to be -0.012, -0.0015, and -.0115 for the spreading, adsorption, and adsorption in a matrix preparation methods respectively, which corresponds to l_p's of 84 nm, 650 nm, and 87 nm. This means that the molecules adsorbed from solution are about 8 times stiffer then the molecules within the film spread from the drop or the film in the matrix. This is an unusual result considering the nature of the preparation methods. Of the two events that make up these films (preparation method and dense film versus molecules in a matrix) the two with the most similar persistence lengths (spreading from a film and the molecules in a linear matrix) do not have either of these in common. This is most likely caused by the forced folding during the compression of the LB film. In a dense film the molecules must arrange as tiles with no gaps in between while in the matrix empty space is filled with linear polymers thus preventing the pressure from forcing these molecules into

unnatural conformations. The extension in these molecules also gives the adsorbed film a great deal of order.

The order parameter of the spreading film was found to be roughly equivalent to the persistence length, while the domain size in the film prepared by adsorption from solution is about 1.5 μm. From the persistence length plot for the film prepared from spreading, we see an increase in the correlation function at long distances. This can be attributed to the combination of two events. The first is simply statistics of the chains. There are a greater number of short measurable chains, thereby resulting in very good statistical data for the shorter lengths. In contrast, there are relatively few very long chains, thus giving poor statistical data. This means that a few random orientations of molecules can greatly influence the outcome of such a plot at large distances from the drop. The second factor is the longest chains are more likely to be folded than shorter chains due to the probability of them folding. This gives order to areas of the chain separated by a large distance, since the folds create parallel regions of the chain. If this is true in the case of only a small number of chains, giving the amount of influence they have on these graphs at long distances, it is easy to comprehend how the chains can appear to increase their correlation over large distances. However, if we record enough data these trends should disappear.

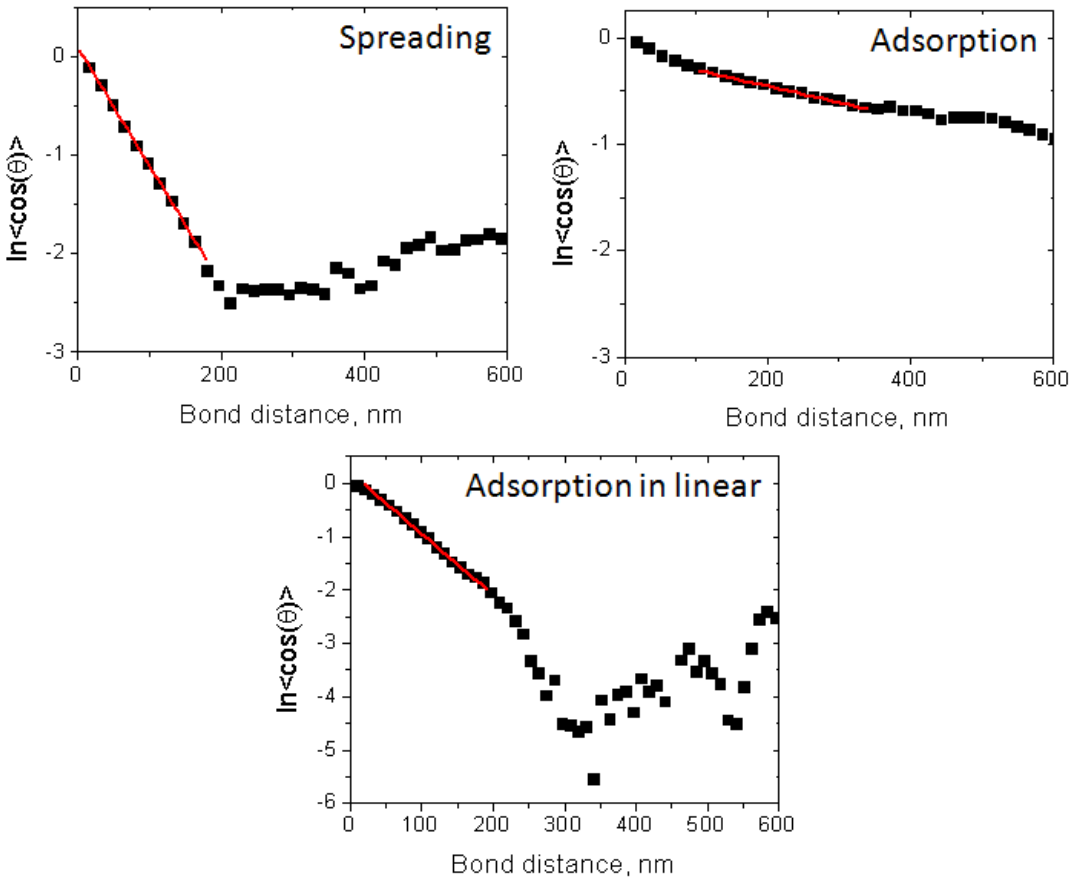

Figure 3.7 Persistence lengths of brushes. Plots of the average cosine of the bond angles versus the distance between the bonds for molecules in a monolayer film prepared by adsorption from a dilute solution (top left) and spreading from a melt (top right) and for a film prepared from the adsorption from a solution of the brush in a matrix of linear (bottom). The negative inverse slopes of these plots are equal to the molecules persistence length.

The origin of this extension can be understood using the mechanism with which the molecules adsorb onto the surface from their original state. When the brushes are deposited on the water subphase in the LB trough, the side chains spread away from the drop and it is energetically favorable for as many of these side chains to be on the surface as possible.[29] The preferred conformation of

these brushes will then be rod-like due to the stiffening caused by the spreading interactions of the side chains. The packing and rearranging of the film and the lack of space in between molecules prevent them from taking on a more natural state, as seen in the film prepared from the matrix. To the contrary, the high pressure inside of the melt drop and in the film as the brushes first leave the drop prevents the side chains from fully extend when the brushes are spread from the drop. This keeps the brushes from forming rod like structures, thus giving them more bends and folds.

3.5.3 Fractal dimensionality. Polymer chains are considered fractal objects that are (i) self-similar and (ii) have a define dimensionality: $R \sim M^D$, where R is the molecular size, M is the mass of the molecule, and D is the fractal dimensionality of the polymer. A peculiar property of polymer fractals is that they are statistical objects that change their conformation in time. Therefore, one typically uses an average dimensions (e.g. mean square Rg). On scales greater than the persistence length of the molecule, the fractal dimensionality, or the rate at which the molecular area increases with respect to its molecular length, can relate information about the conformation of the molecules.. Extended molecules form rods and have a characteristic dimensionality of 1, while collapsed molecules form disks and have a dimensionality of 2. The ideal coiled molecules however follow a random self-avoiding walk which yields a dimensionality of 1.33 on the surface. This is the expected conformation of a 2D melt of these brushes. However the folded molecules exhibit a certain degree of order and therefore

their specific dimensionality cannot be defined on all length scales since it is not self similar on all length scales.

To find the average conformations the molecules are comprised of, we measure (using the methods described earlier) and then plot the molecular lengths or mass versus the radius gyration of each individual molecule (Figure 3.8). The slopes of averages of these points (when plotted on a log-log scale) are equal to 1/D. As expected, the shortest brushes from both preparation methods have a dimensionality of 1. This occurs below the l_p of the molecule since there is no curvature on that scale and the molecule is rod-like. At lengths greater than the persistence length, the molecules in the film prepared by the adsorption from solution technique (Figure 3.8 left-green points) have a dimensionality of 1.19. Although these molecules are rod-like in nature they have a considerable deviation from 1. We attribute this deviation to the folded molecules within the film. The longer the molecules are, the more folds they are likely to have and the occurrence of the folds varies with preparation method. However when we look at the molecules in the matrix they have a dimensionality of 1.35. This is the precise value expected for the random self-avoiding 2D walk. This demonstrates that the preferred conformation of a molecule outside of the dense film is its ideal 2D state. The folds in the molecules play a role in their extensions in the dense films. In the film prepared from the adsorption of the molecules from solution, there is on average 1 fold every 5163 nm as opposed to 1 fold every 478 nm for the film prepared from spreading, an order of magnitude difference. Although a folded molecule is still extended, its R_g is considerably

shortened, thus accounting for the majority of the stray points below the majority of the points on the plot.

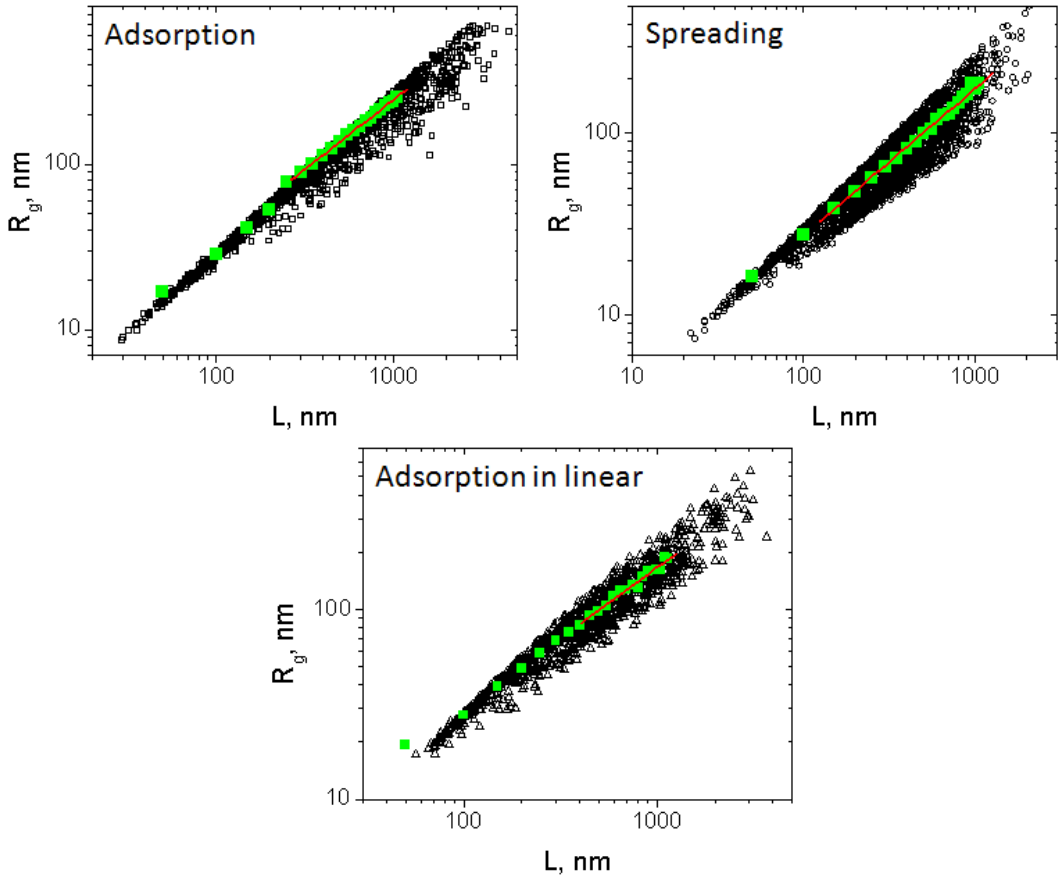

Figure 3.8 Radius of gyration versus molecular length. Plots of the molecular lengths of the individual molecules versus their radius of gyration for both the preparation of films by adsorption from a dilute solution (top left) and spreading from a melt (top right) and for a film prepared from the adsorption from a solution of the brush in a matrix of linear (bottom). The green points are the root mean squared average of the R_g for a particular range of lengths and the red slope of those averages is the inverse of the dimensionality.

The L versus R_g prepared from spreading plot in Figure 3.8 (top right) shows a much denser continuum of points. If one would find the range of the

molecules in the continuum, we find a minimum dimensionality of 1.05, or very rode-like molecules, at one extreme and 1.59, or semi-collapsed coils at the other. When the average values of these molecules are determined, we find an average dimensionality of 1.23. This number is considerably close to the self-avoiding random walk described earlier (D~1.33). However, because of this large variation of values for the R_g versus L plot we proceeded to investigate the averages further by plotting a density plot of the values in question (Figure 3.9). This density plot immediately revealed two dominant populations with dimensionalities of 1.05 and 1.41. This indicates that majority of the molecules prefer two specific conformations; the extended and self-avoiding random walk configurations. In other words, polymer molecules are quenched into two metastable states: extended and coiled, both with characteristic fractal dimensionalities. We will show later that spreading causes a transition from the coiled to extended state.

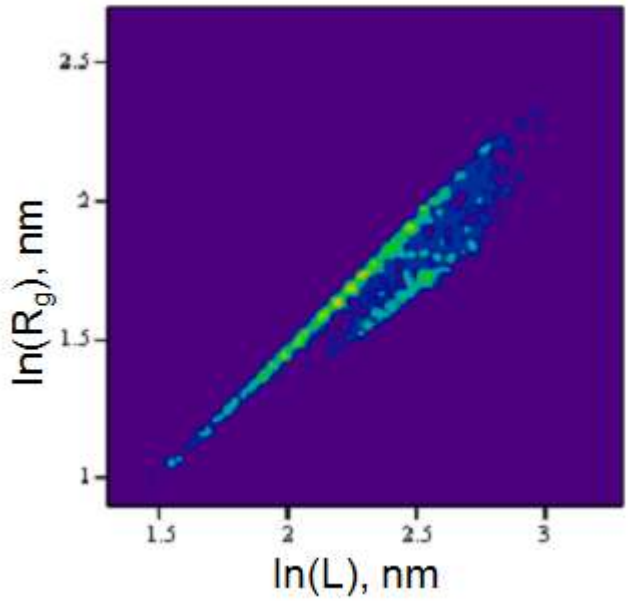

Figure 3.9 Radius of gyration versus molecular length density plot. Density plot of the molecular lengths of the individual molecules versus their radius of gyration polymers in films prepared by spreading molecules from a melt. The higher densities are the warmer colors and two distinct populations emerge. From the slops of the two high density populations we can extract the fractal dimensionality of the two types of polymers.

3.6 Molecular topology. For the purposes of this text we define the topology of a film as the features of the individual molecules in relation to one another. The various topologies can be seen in Figure 3.10. The molecules can be either be crossed or uncrossed with the uncrossed molecules forming one of many conformations (discussed in section 3.4). Crossed molecules form when the back bones of the individual polymer chains overlap at one or more point and they undergo one of 3 forms: loops, crosses, or networks. We define molecular loops to be single molecules that cross over themselves one or more times. Similar to loops, crosses are two molecules that overlap at one or more places

while networks include many molecules overlapping at many different points, creating a weave-like structure inside the monolayer.

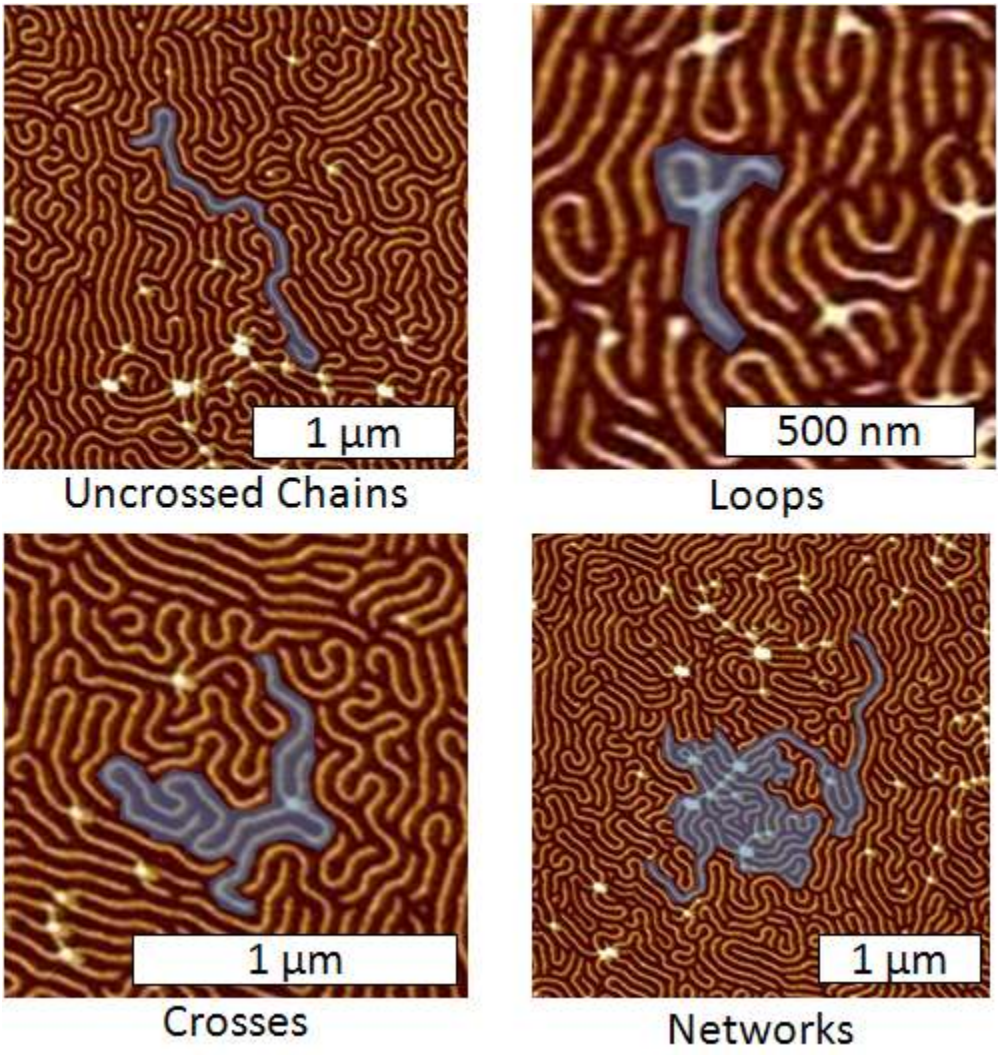

Figure 3.10 Molecular topologies. Various topologies that the polymer chains are observed in uncrossed chains (top left), loops, (top right), crosses (bottom left), and networks (bottom right). The molecules in question are highlighted in blue.

The structures created from the various topologies can have effects on the dynamics of molecules, their molecular packing, optical and physical properties, as well as the flow of the molecules. When these molecules form crosses or

networks and the crossing points are sufficiently strong, the movement of the molecules can be affected. For example, if two identical chains (with B Kuhn mononers with length b) are crossed at the center we get one structure with a mean squared radius of gyration $\left\langle R_g^2 \right\rangle = \frac{5}{48} Bb^2$ as opposed to two individual molecules with $\left\langle R_g^2 \right\rangle = \frac{Bb^2}{6}$. During the creation of these films, the crossed structures move as one piece (in Chapter 4 we show that they do not dissociate during flow). This movement can restrict the thermal diffusion of the brushes since the friction of the brush on brush is higher than the brush on surface friction (see Chapters 5 and 6). Through this dampening, these structures can slow down an already slow equilibrium process. Their shapes and crosses can affect their packing arrangements also. The arms of the crosses are for the most part 90 degrees. If the natural equilibrium conformation is an extended packing this perpendicular nature can obstruct these structures making it hard for them pack in a favorable manner. The ability of these molecules to stick together also can affect the flow of these molecules. It has been documented that these molecules exhibit a flow induced diffusion.[30] The ability of these molecules to diffuse through the melt as they flow depends on the size of the molecules and these very large networks will diffuse slower than the individual molecules.

The major effects of the preparation method has on the molecular topology can be seen in 2 major areas: when the film is prepared by adsorption from solution, more single molecules and loops present themselves, while when the film is prepared from the spreading of a melt there is a much higher

proportion of crossed molecules and networks. Table 3.1 shows the precise values of each.

Table 3.1. Proportions of crosses, loops, and networks for the two preparation methods

Property	**Spread**	**Absorption**
Crosses, cross/mol.	.315	.050
Loops, loop/mol.	.0038	.011
Network, %	55.3	9.4

The qualitative differences of the two methods can be predicted. When spreading a polymer film the molecules move in a plug flow, meaning all the molecules move as one, and the rear end of the film is replenished from the drop reservoir as the front of the film progresses. The molecules that replenish the surface film as it flows away from the meltcome from the drop, where they are entangled, and they move onto the surface as one unit projecting those entanglements onto the surface. However, when the brushes are deposited onto the surface from a very dilute solution they are few and far between, leaving little opportunity for overlap. When these molecules land onto the surface, their 3D conformations are projected onto the surface, in contrast to sliding out of the drop, creating more loops one the surface.

3.7 Molecular assemblies. Of the features we see in these thin films their assemblies and arrangements seem to be the most consequential. It is not just the conformations of the individual molecules that provide the physical properties of the films; it is how the molecules interact with each other. Encompassed in these interactions are structures formed by the molecules in their films such as

networks, along with the order and packing arrangements they undertake. By preparing identical films using two different techniques we can control how these molecules pack along with the extent that they form networks. Learning how to control these molecular properties can eventually lead to thin films with tunable physical and optical properties.

The packing arrangements in molecules confined to films can undergo one of three basic formations: collapsed molecules, coiled molecules, and extended molecules (Figure 3.11), each with distinct features and dimensionalities. Collapsed molecules behave as if they are attracted solely to themselves (or repulsed by their neighbors). This causes the individual sections of the molecules to seek out themselves on the surface and form a tight coil with a fractal dimensionality of 2. This formation is only observed in a handful of molecules not considered to be statistically significant in either film so we can rule out this being an important feature. The coiled molecules are what would be observed if the 2D melt was ideal: a random self-avoiding walk with a fractal dimensionality of 5/3. Finally, the extended molecules create rod-like structures on the surface that have a fractal dimensionality of 1. As presented earlier both these structures are present in the films prepared by both methods.

Figure 3.11 Packing arrangements. The various packing arrangement that are possible in the monolayer systems: a collapsed disk-like packing (left), an ideal packing in a self-avoiding 2D walk (center), and an extended packing (right).

The conformations of the molecules calculated earlier can give us partial evidence as to the packing arrangements of the molecules in the films. For the films prepared by the LB method, we see strong evidence that the molecular conformation is mostly that of extended molecules. This can be further tested by measuring the domain size that the molecules undertake (Figure 3.12). The domain size is the correlation length of the order parameter of any two segments from any molecule in the film. The LB film yielded a correlation length of approximately 1.5 μm. These large domain sizes comprised of molecules, largely oriented in the same direction, emphasize the rod-like extended packing of the LB film. It is our belief that harnessing this rod-like packing of these LB films can eventually lead to enhanced optical properties of these films.

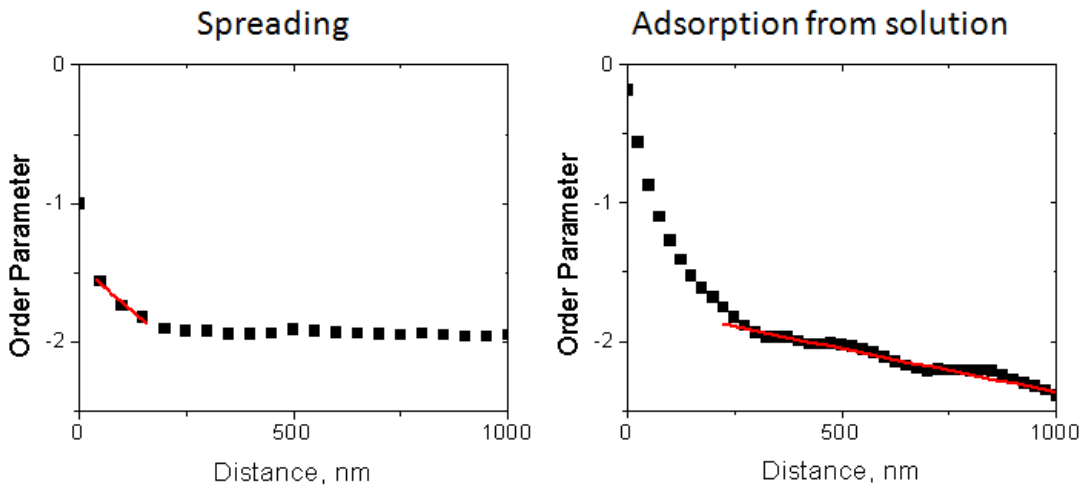

Figure 3.12 Orientational order parameter plotted against distance. Both films are present and the plots were used to calculate the domain size. The steep slope at small distances is attributed to the persistence length.

The packing arrangements of the films prepared from spreading are a harder to interpret. We have shown that there are two dominant conformations in the film and because of their molecular curvature their domain sizes are impossible to calculate using their order parameters. Figure 3.12 shows how the domain size calculated by this method is below that of the persistence length of the individual molecules (l_p=84 nm). This can be explained by the fact that as each individual molecule has no short range order, no order between adjoining molecules will ever be achieved. These seemingly random orientations of two molecular conformations with no real long range packing arrangement can be attributed to the presence of molecular networks in the film. The amount of these molecular networks varies greatly between the LB and spreading preparation methods, 9.4 and 55.3% of brushes are confined to the networks for the respective film preparation method.

Since over half the molecules belong to such networks during spreading, they can occupy enormous size thus obstructing the packing arrangements of the individual molecules. Figure 3.13 demonstrates just how massive these networks can grow. It shows the location and sizes of various networks inside a polymer film. As one can see their sizes can grow to well over 25 μm^2 and cover a large percentage of the surface. The presence of these networks could be a positive phenomenon. These networks can behave as woven networks in the films, thus increasing their robustness and surface tension. These two different preparation methods each yield a separate packing and orientations that when exploited correctly could give different sets of physical properties. This emphasizes the importance of preparation method when preparing films for specific applications.

Figure 3.13 Images of networks. AFM images of a large span of surface. The networks are lined with red and blacked out to make them easy to see. The sizes of the individual networks can grow greater than 25 μm^2.

3.8 Conclusions. The comparison of the preparation of these films yielded some unigue observations.

1) The compacting of these brush molecules into a tile configuration by the LB trough causes an extension of these molecules. This extension is not seen in the sample prepared by spreading, nor the sample prepared in the matrix.

2) The fractal dimensionality of the 3 samples prepared was calculated. The molecules prepared in a dense film from solution had a dimension of 1 (a rod-like dimensionality), while the sample of brushes embedded in the matrix has a dimensionality of 1.35 (a self-avoiding random walk). However the dense film prepared from the spreading of the melt yields both the ideal coiled and the extended conformations.

3) The preparation methods affect the packing of the individual molecules in the film. We observe 2 separate packing arrangements (extended and coiled) in the film prepared from spreading and a primarily extended packing arrangement in the molecules prepared from LB. We explained this by considering the mechanisms in which the molecules are adsorbed onto the surface. The brushes in the sample adsorbed from solution spread out and then are forced together, where as the molecules in the sample prepared from spreading are adsorbed onto the surface from their entangled melts.

4) We have observed networks or overlapping molecules present in the monolayers. These networks dominate the topology in the sample prepared from spreading but they are rarely observed in films prepared by the LB method. They affect the molecular properties and behaviors in the films from the extension of the molecules to their packing and fractal dimensionalities. They can also

influence some of the physical (surface tension) and optical properties of these films.

These results show that the molecular arrangement of films is strongly dependent on their preparation method. Asignificant consequence of this arises when we consider the equilibrium states of these films. The energy required to rearrange the films is much greater than their thermal energy alone, thus making equilibrium a very slow (if not an infinite) process. Comparing the properties of the films prepared from a flow to that of films prepared from the adsorption from a solution show drastically different results. The spreading films shows many more crosses and a greater percentage of molecules are confined to networks, suggesting a possible enhancement of surface tension. On the other hand, the film prepared from the solution contains mostly extended brushes and a great deal of order. This can possibly enhance the optical properties of the film. In addition to these phenomena, it has been observed that when the film is prepared from a spreading drop there is two populations of brushes that include both the extended and coiled molecules. In the future we hope to learn how we can begin to manipulate these conformations and topologies to affect the film properties.

References

[1] Klauk, H.; Halik, M.; Zschieschang, U.; Schmid, G.; Radlik, W.; Weber, W. *J. Appl. Phys.* **2002,** 92, 5259.

[2] Kreuer K.D. *Journal of Membrane Science* **2001,** 185, 1, 29-39.

[3] Torchilin, V.P. *Journal of Controlled Release* **2001,** 73, 2-3, 137-172.

[4] Sirringhaus, H.; Tessler, N.; Friend, R.H. *Science* **1998,** 280, 5370, 1741.

[5] Taylor, G.I. *Proc. R. Soc. London*, Ser. A **1959,** 253, 313.

[6] McEntee, W.R.; Mysels, K.J., *J. Phys. Chem*. **1969,** 73, 3018.

[7] Culick, F.E.C. *J. Appl. Phys*. **1960**, 31, 1128.

[8] Debregeas, G.; Martin, P.; Brochard-Wyart, F. *Phys. Rev. Lett.* **1995,** 75, 3886.

[9] Reiter, G. *Phys. Rev. Lett.* **2001**, 87, 186101.

[10] Saulnier, F.; Raphael, E.; de Gennes, P.G. Phys. Rev. Lett. **2002,** 88, 196101.

[11] S. Herminghaus, R. Seemann, and K. Jacobs, Phys. Rev. Lett. 89, 056101.

[12] Shenoy, V.; Sharma, A. *Phys. Rev. Lett.* **2002,** 88, 236101.

[13] Dalnoki-Veress,K. *et al.*, Ph*ys. Rev. E.* **1999,** 59, 2153.

[14] Saulnier, F.; Raphael, F.; de Gennes, P.E. *Phys. Rev. E.* **2002,** 66, 61607.

[15] Forrest, J.A.; Dalnoki-Veress, K.; Dutcher, J.R. *Phys. Rev. E.* **1997**, 56, 5705.

[16] Kawana, S.; Jones, R.A.L. *Phys. Rev. E.* **2001**, 63, 021501.

[17] Tate, R.S.; Fryer, D.S.; Pasqualini, S.; Montague, M.F.; de Pablo, J.J.; Nealey, P.F. *J. Chem. Phys.* **2001**, 115, 9982.

[18] de Gennes, P.E. Eur. Phys. J. **2000,** 2, 201.

[19] Forrest, J.A.; Dalnoki-Veress, K. Advances in Colloid and Interface Sci. **2001,** 94, 167.

[20] Forrest, J.A.; Fakhraai, Z. Phys. Rev. Lett. **2005,** 95, 025701.

[21] Ayalur-Karunakaran, S.; Blumich, B.; Stapf, S. *Langmuir* **2009**, 25(20)

[22] Plum, M.A.; Steffen, W.; Fytas, G.; Knoll, W.; Menges, B. *Optics Express,* **2009,** 17, 10364-10371.

[23] Vroege, G.J.; Lekkerkerker, H.N.W. *Rep. Prog. Phys.* **1992,** 55 1241-1309.

[24] Choi, S.J.; Park, S.M. *Adv. Mater.* **2000**, 12, 20,1547.

[25] Matsudomi, M.; Kato, A.; Kobayashi, K. *Agric. Biol. Chem*, **1982,** 46 (6), 1583-1586.

[26] Gurrieri, S.; Rizzarelli, E.; Beach, D.; Bustamante, C. *Biochemistry.* **1990**, 29,

3396-3401.

[27] Maier, B; Rädler, J.O. *Phys. Rev. Lett.* **1999,** 82, 1911.

[28] Xu, H.; Sun, F. C.; Shirvanyants, D. G.; Rubinstein, M.; Shabratov, D.; Beers, K. L.; Matyjaszewski, K.; Sheiko, S. S. *Adv. Mater.* **2007***, 19*, 2930-2934.

[29] Sheiko, S.S.; Sun, F.; Randal, A.; Shirvaniants, D.; Matyjaszewski, K.; Rubinstein, M. *Nature*, **2006,** 440, 191-194.

[30] Xu, H.; Shirvaniants, D.; Beers, K.; Matyjaszewski, K.; Rubinstein, M.; Sheiko, S.S. *Phys. Rev. Lett*. **2004,** 93, 206103/1-4.

Chapter 4

Flowing Polymer Films

4.1 Introduction. Spreading and wetting properties are of fundamental importance to a vast amount of applications on every length scale. Macroscopic wetting and spreading enhances our ability to recover petroleum from shale,[1] safely coat our crops with pesticides,[2] and even drain our highways.[3] It is essential in microscopic applications such as nano lithography[4,5] and inkjet printing.[6] Perhaps the field most influenced by spreading interactions is that of open channel microfluidics.[7,8] This branch of microfluidics uses channels open to air and relies heavily on the spreading interactions between the molecular fluid and the surface. The molecular behavior of these fluids play important roles in the spreading rates of the polymer in the channels, molecular mixing, conformations, topology, and fractionation of molecules. All of these details will give us insight to a very important goal of microfluidics: controlling chemical reactions.

The physics of macroscopic flows are well understood.[9] When placed on a surface, a bulk drop spreads until it reaches its equilibrium state, which can be measured by its contact angle.[10-13] It has been found that both the radius of the drop[14] (R_0) and the contact angle (θ_c) both obey power laws, $R_0 \sim t^{1/10}$ and $\theta_c \sim t^{-3/10}$. However, a precise understanding of the microscopic behavior of the contact

angle requires an inclusion of the precursor film into the studies[15,16] (Figure 4.1). The precursor film follows a completely different power law, $R \sim t^{1/2}$ (which resembles a diffusion law) than the spreading of a bulk drop itself, as it more resembles a diffusion law. There have been numerous studies done to characterize the profile,[17] spreading rates,[18] and spreading conditions[19] of the precursor film using macroscopic techniques (usually optical microscopy and ellipsometry). Yet, to this day, very little information (if at all) is available about the molecular mechanism of spreading. Several fundamental questions remain. For instance, how does the flow rate depend on MW? And how does the flow rate depend on conformation? Finally, how does flow affect conformation and orientation of the flowing macromolecules? It is our goal to study these flowing precursor films in the context of the individual molecules to resolve these questions.

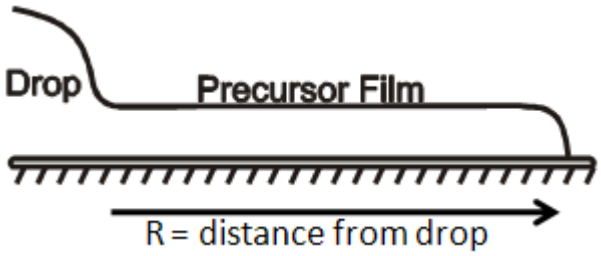

Figure 4.1 Sketch of the polymer drop and precursor film. The polymer drop is the reservoir melt of the polymer blend while the precursor film flows to the right.

In chapter 3, we learned that molecular properties, such as molecular conformations, topologies, orientation, and packing, of thin films vary with their preparation methods. In this chapter, we explore how these film properties are

affected as a film progresses under flow. To do so, we spread polymer films on a surface and observed their molecular properties, such as length, conformation, and topology along the film. We also investigated these properties as the individual properties, such as width, stiffness, and length, of the brushes are tuned.

4.2 Experimental. To conduct these experiments, we place a drop of polymer melt onto a mica surface. This is then placed into a humidity chamber at with a relative humidity (RH) of 97%. Since the friction between the mica and the polymer is too high for spreading to spontaneously occur, the humidity plays the role of a lubricant as it reduces the friction coefficient between the two. The sample is then taken out of the humidity chamber after a measured time and the spreading subsequently halts due to the desorption of the water layer. This static film is then imaged and analyzed at various points across the film. The individual molecules in the polymer films were then measured using atomic force microscopy (AFM).

A polymer brush system was chosen that would best emulate a linear polymer. This requires the brush to be as long as possible (L_n=800 nm) with side chains as short as possible (w=40 nm) to allow for maximum flexibility, but still long enough to allow for a suitable height contrast for imaging. The system selected had the parameters N = 7280 and n = 40 (Figure 4.2). As we show below, the persistence length of this polymer is on the order of 100 nm which is larger than the tip radius allowing for full resolution of the chain curvature.

Studies were then conducted to compare the effects of spreading on the topological and conformational features of different brushes with varying degrees of flexibility. To do this, n was varied from 40, to 50, 80, 110, and 140. These dimensions provide a backbone with lengths that range from 100-5000 nm, with brush widths that vary from 45 – 170 nm depending on the pressure of the film and the side chain degree of polymerization.

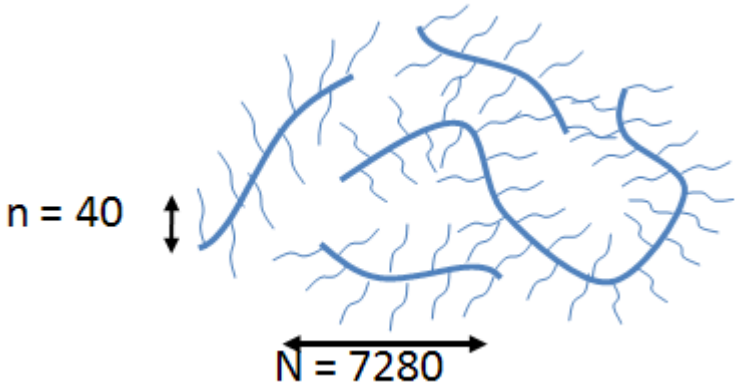

Figure 4.2 Schematic of the polymer brush. This experiment uses brushes with a long back bone. Comparison studies were also done by varying n to 40, 50, 80, 110, and 140.

4.3 Spreading of polymer films. When the polymer melt is deposited on the surface under humidity, the thin film precursor layer spreads. This occurs because the spreading coefficient, S (the change of the surface energies of all the interfaces between the spread and unspread states of the film), is positive. To describe the spreading of the film, we first must describe the forces that act on the film. The driving force of the spreading is a pressure gradient in the direction of the spreading and this is balanced by a sliding friction of the film yielding the relation $\frac{d\Pi}{dr} = -\xi \vec{V} A$, where $\frac{d\Pi}{dr}$ is the pressure gradient along the

film, ξ is the friction the film has with the surface, V is the film velocity, and A is the area of the film. To balance the energy gained by spreading with the energy loss from friction, both sides can be integrated resulting in $S = -\xi \vec{V} R$, where R is the length of the film.

We first spread a polymer brush molecule with dimensions N=7280 and n=40. After 45 minutes, the spreading of the polymer drop was ceased and images of individual molecules were taken at various locations along the film (Figure 4.3). The total length of the polymer film was 230 μm. As clearly seen, the flowing macromolecules change their conformation and topology at various locations along the film. Some of the molecular dimensions and structural features are visible (folding, extension, brush width), while the other ones are not immediately apparent (contour lengths, radius of gyration). In order to quantify the flow-induced variations of molecular conformation, we have used software allowing accurate analysis of the contour lengths, radius of gyration, order parameters, and persistence lengths of the individual molecules. The flowing film provides energy and additional diffusion for the individual molecules in the film to rearrange[20] as well as a changing pressure as the film flows.[21] Both scenarios play significant roles in the molecular dynamics of these flowing films.

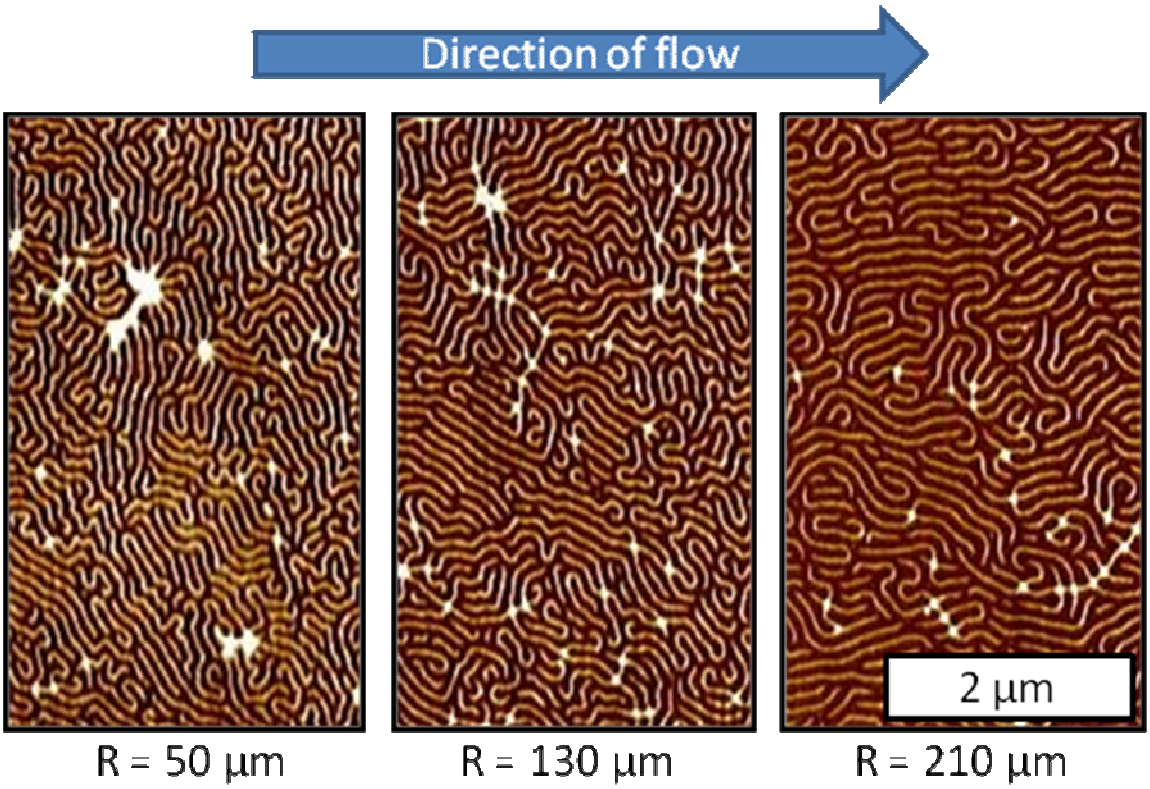

Figure 4.3 Images of a polymer film after flow. Images of a film of molecules (N = 7280, n = 40) at various distances from their reservoir drop (spreading coordinate).

4.4 Molecular Topology. As seen in Figure 4.3, spreading films are composed of crossed and lone molecules. The crossed molecules may have multiple crosses and can form large networks. Upon investigation, we find that there are glaring differences between the brushes that make up the lone molecules and the crossed molecules. These differences are illustrated in Figure 4.4 (left) which shows distributions of the lone brushes in the film, the brushes confined to the networks, and all the brushes in the film. We can see that the distribution of the brushes in the networks is skewed towards the longer brushes then the length distribution of lone brushes, i.e. the lengths of the brushes that belong to

the networks are longer than the lengths of the brushes outside the networks. The average lengths of the brushes in both topological structures are plotted as a function of film length (Figure 4.4 right). In all cases, the average lengths of the molecules in the bulk melt is far greater than the average lengths of the lone molecules while the network molecules were typically longer than the average molecular length in the bulk melt. This indicates that there is a preference for the longer brushes to form networks. This is what we would expect considering longer brushes are more likely to become wrapped up and entangled deeper into the melt. The network formation reflects the entangled structure of polymer melts and depends on the method in which the brushes leave the drop.

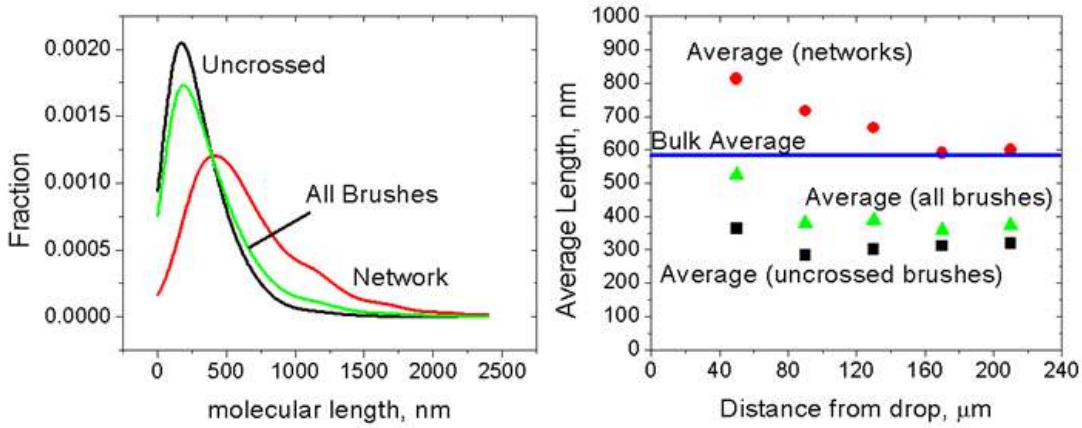

Figure 4.4 Lengths of polymer brushes in a film. Length distribution of brushes (N=7280) confined to different topologies (Uncrossed brushes (─), Brushes in networks (─), and all brushes combined (─)) at a distance of 50 μm from the drop (left) and the average lengths of those brushes (uncrossed brushes (■), brushes in networks (●), all the brushes in the film (▲), and the bulk average(─)) at various spreading coordinate (right).

In polymer melts, there is an entanglement threshold or a size where chains in a melt become entangled. We estimate the entanglement threshold (M_e

- average molecular weight between entanglements) for linear poly(butylacrylate) to be about 10000 g/mol. We use this entanglement threshold to find the scaling relation between the length of the side chains, n, and the entanglement length of the brush, ($L_e=N_eb$, where b is the Kuhn length and N_e is the number of Kuhn monomers per entanglement). We start with the relation that defines the number of strands inside an entanglement, $P_e = \frac{b^3}{v_0}\sqrt{N_e}$, where v_0 is the volume of the Kuhn monomer. If we make the assumptions that P_e is constant, the width of the brush, $w \sim n^2$, and $b/d \sim n^{9/8}$ then we obtain the relation $L_e \sim n^{-11/8}$. In other words, the amount of entanglements in the melt increases with the length of the side chains. We can use the relationship between side chain length and the amount of entanglements to test whether the increase of entanglements in the melt translates into entanglements, networks, and crosses on the surface. Figure 4.5 shows the images of the precursor film at various locations along the film. At first glance the number of crosses and length of the brushes in those films appears to stay similar, and a detailed analysis below confirms this.

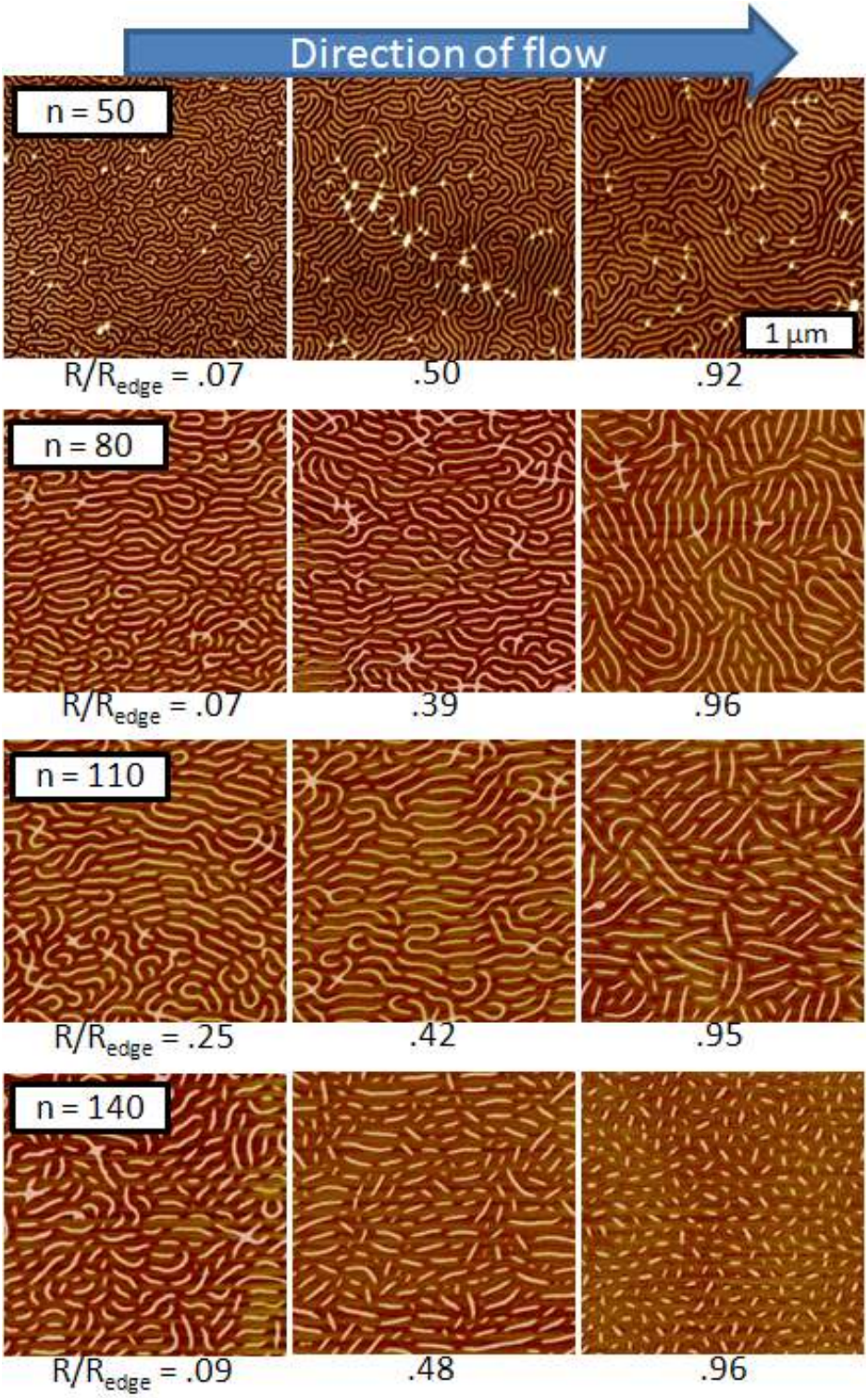

Figure 4.5 Flow of brushes with various side chain degrees of polymerization. Images of films prepared by spreading of molecules with the same backbone degree of polymerization (N = 7280) and varying side chain degree of polymerization (n).

When we analyze the average brush length during the flow for different n values (n=40 and 80) for the uncrossed brushes, we observe no change in the average length of the brushes as we vary n and the normalized spreading coordinate (R/R_{edge}) (Figure 4.6). According to our analysis, we should expect to see much shorter brushes for the longer side chains (n=80) considering the entanglement length is 1/3 then that of the short side chains (n=40). The reasoning is the shorter entanglement length would trap shorter molecules within the melt and confine them to more networks. However, both samples have similar average lengths which are consistently below the average length of the sample inside them melt (~600 nm) (obtained using the Langmuir-Blodgett method). It is a curious observation that the lengths of the brushes would be below this value and yet not change with the degree of entanglements. Possible explanations for this are discussed below.

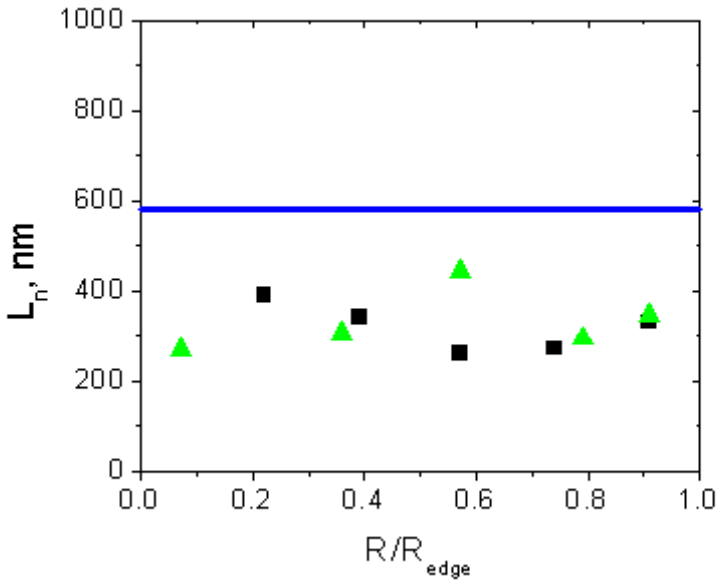

Figure 4.6 Average brush lengths for different side chains during flow. Average lengths of brushes with different side chain lengths, n = 40 (■) and n = 80 (▲), as they spread away from the drop. The average value of the sample in its bulk melt state is represented by the blue line (—).

To examine the role the side chain degree of polymerization has on these networks of crossed molecules, we count the number of crosses per length in the film for various side chain lengths (Figure 4.7 left). Between the samples with n=40 and n=80, there is no measurable difference in the amount of crosses per length of brush. One would reasonably deduce that if the entanglements in the drop projected themselves onto the surface at the drop film interface, then the more entangled brushes with the long side chains would have more crosses and networks. This is not the case. This suggests that the crosses and networks are simply a 2D projection of the chains physically overlapping in space and not due to their becoming entangled.

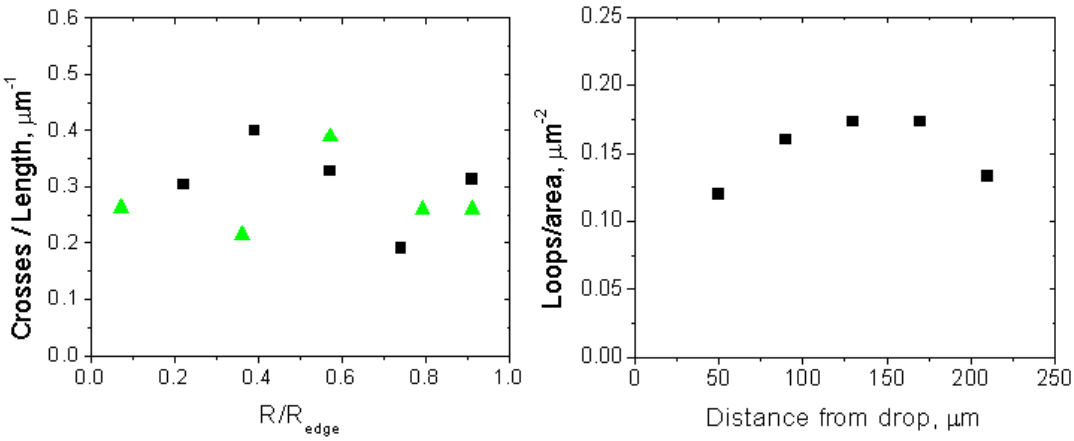

Figure 4.7 Polymer brush crosses during flow. The number of crosses per brush length in the film as it spreads for two separate samples of brushes (left) and the number of loops per area in the film as it spreads (right). For all the samples N = 7280 while the side chains of different lengths are indicated by n = 40 (■) and n = 80 (▲).

We now turn our attention to the stability of these networks. To do so we monitor the amount of crosses and loops against their spreading coordinate (Figure 4.7). Loops do not vary within error for this sample (N=7280, n=40). To remain thorough, we examine crosses during flow for two separate samples (N=7280, n=40 and N=7280, n=80). Both samples remain constant over flow. This indicates little or no dissociation of the crosses as the film spreads. Although we have seen evidence of almost no dissociation of these crosses, in chapter 6, we will present direct evidence of this dissociation phenomenon.

4.5 Molecular conformations. In addition to topological changes, flow also causes conformational changes in the film. The most important is the stiffening and extension of the individual molecules. The stiffness is characterized by the

molecule's persistence length (l_p). The persistence length can be obtained from the end-to-end distance and from the curvature distribution (Figure 4.8). Upon examination of the film, we see constant end to end distances of the molecules with the exception of the region of the film furthest from the drop. Here, we see an increase in the end to end distance which suggests that only near the very edge of the film do we see the chains become completely unfolded, which is confirmed by the persistence lengths of these molecules. This increase in stiffness is due to adsorption of side chains as the pressure decreases along the flowing film. The increasing amount of adsorbed side chains also leads to the increase of the brush width. The latter can be tracked by monitoring the brush widths of the individual molecules (Figure 4.8 right). Since the polymer chains take up physical space when they are adsorbed to the surface, increasing their numbers also increases the area that the brushes occupy, thus increasing their width.

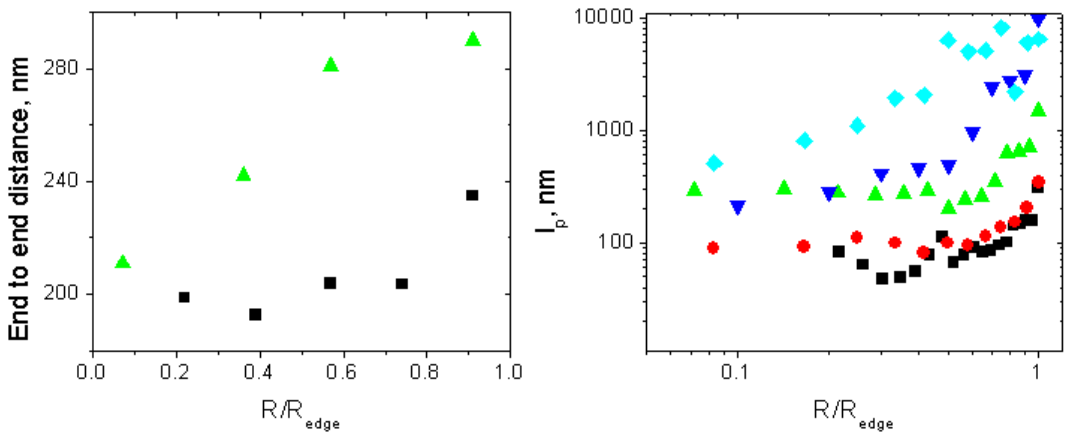

Figure 4.8 Persistence length and end to end distances of brushes during flow. Plots characterizing the extension of the brushes with varying n: End to end distance (left) and persistence length (right). n = 40 (■), n = 50 (●), n = 80 (▲), n = 110 (▼), and n = 140 (♦).

The plots in Figure 4.8 all follow the same basic trend: their persistence length and end to end distances stay relatively constant close to the drop and extend rapidly at the edge of the film. These two regimes seem to be following two separate processes: 1) as pressure decreases from its highest point to lowest, there is little or no effect on the extension of the brushes and 2) when a low enough pressure is reached, the brushes drastically extend. One possible explanation for the presence of these two regimes during flow is the fact that the brush itself has two separate conformations: coiled and extended. When the persistence length does not change with spreading coordinate, the brush is altering its conformation. At a certain point, the backbone begins to become extended thus rapidly increasing the persistence length. To account for this conformational change, we turn to chapter 3, where it was discussed that the different conformations of molecules express themselves by different scaling of

their radius of gyration to the contour length. Density plots of these variables revealed that there is indeed two dominate conformations: an extended conformation with dimensionality D=1 (the upper branch) and a coiled conformation with D=1.33 (lower branch). If we view these density plots at different spreading coordinates, it becomes clear that the coiled conformation gives way to the extended conformation since the lower branch gradually fades as the spreading progresses. This is direct evidence of a flow induced conformational change. The origin of this change revolves around the pressure decrease along the spreading coordinate. As the pressure decreases, the individual molecules are able to spread more and this unimolecular spreading induces a tension on the backbone. This tension causes the brushes to extend and uncoil, thus a conformational change during flow.

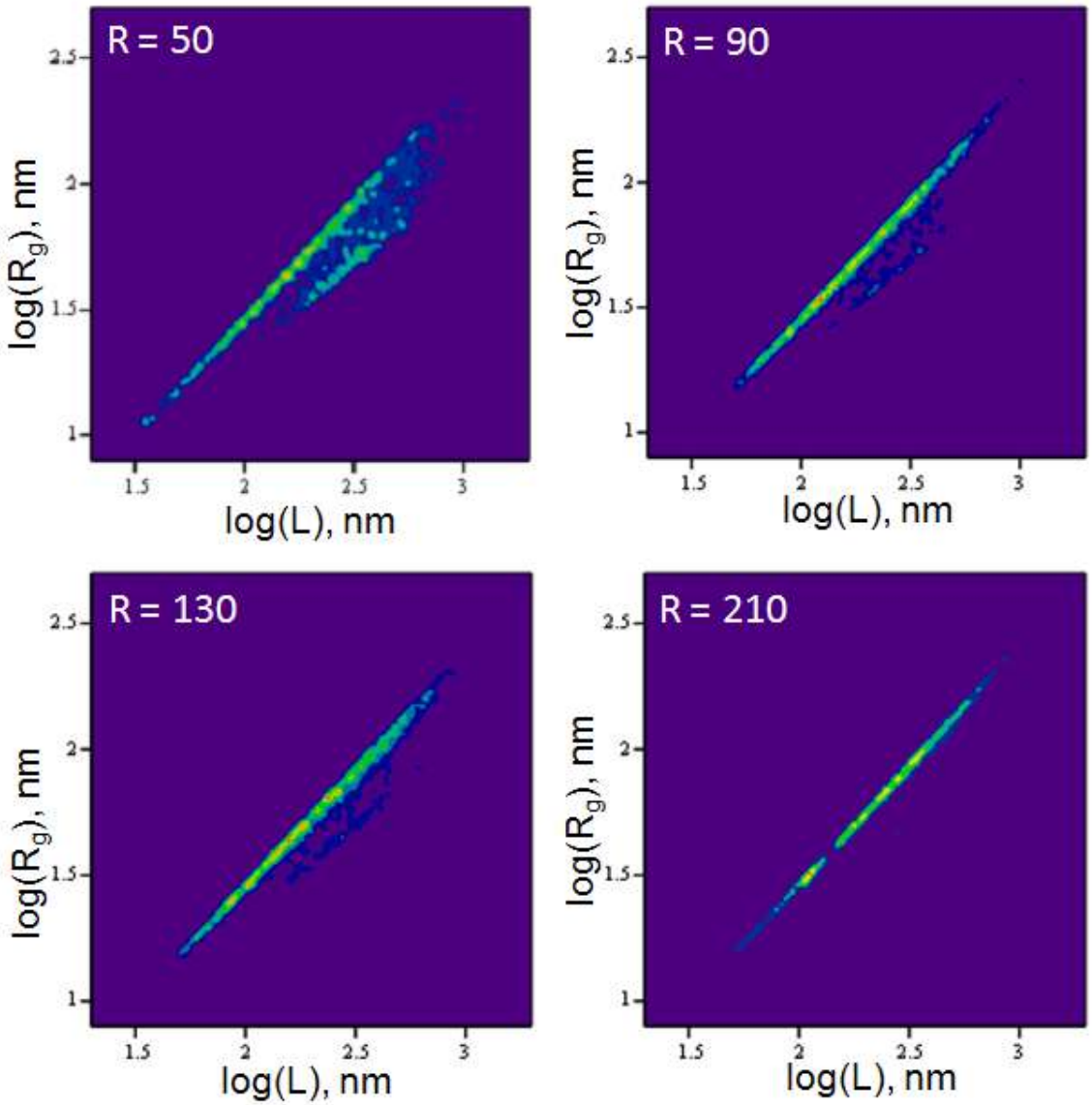

Figure 4.9 Contour lengths versus radius of gyration for individual molecular at various spreading coordinates. The closest to the drop (top left) shows two distinct conformations: the coiled and folded conformation. The coiled conformations disappear as the spreading coordinate increase.

It is also known that the stiffness of molecular brushes increases with the width. Figure 4.10 is a plot of the brush widths as a function of the spreading distance and n. As expected, the brush width has a positive correlation to both n and distance along the film. The longer side chains occupy more space on the

surface thus creating more space between them. Also as they spread along the film, the pressure of the film becomes smaller, thus allowing more of the side chains to adsorb to the surface and occupy a greater area and spreading the brushes out.

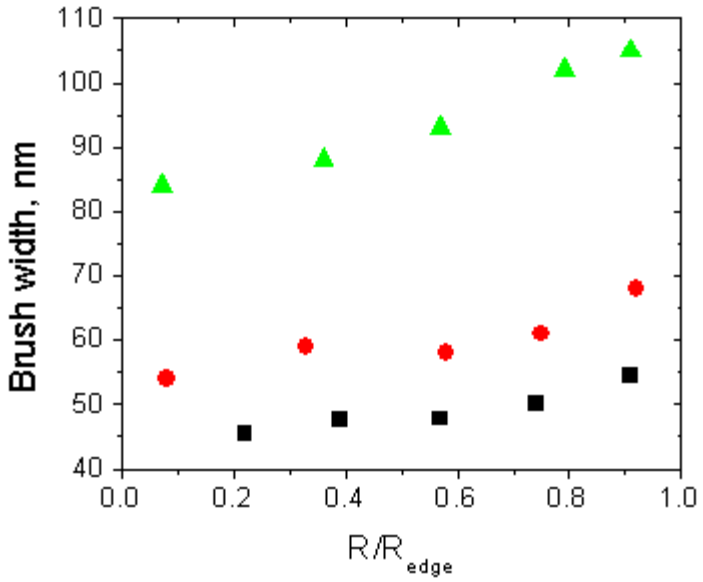

Figure 4.10 Brush widths for different side chains during flow. Molecular width as a function of the spreading coordinate for brushes with side chain DP of n = 40 (■), n = 50 (●), and n = 80 (▲).

It has previously been reported that the persistence length of the brush molecules scales with the degree of polymerization of the side chains,[22] $l_p \sim n^{2.7}$. However, by comparing the brush widths and the corresponding persistence lengths, we obtain the plot in Figure 4.11. This log-log plot of the persistence length versus the brush length at different locations of the film for different brush lengths gives an interesting result. As it turns out, the persistence length of the

molecules is not related to n but they are instead related to the brush width, w. We verify this by finding the scaling relation of $l_p \sim w^{2.4}$ which is within error of the previous scaling relation involving n. In other words as the physical width (not n) of the brush increases, the persistence length increases. This conclusion can be verified with two pieces of information. The first is portrayed by Figure 4.8 where the persistence length increases along the film even though n does not change. This result should suggest that another factor is responsible for the stiffening of the molecules. The second verifying fact can be found in the description of a breaking brush.[23] The tensile force responsible for elongating and ultimately stiffening the brushes is $f_t = S \cdot w$, where S is the spreading parameter. This means that the width is directly responsible for the tension on the backbone that extends and stiffens the molecules.

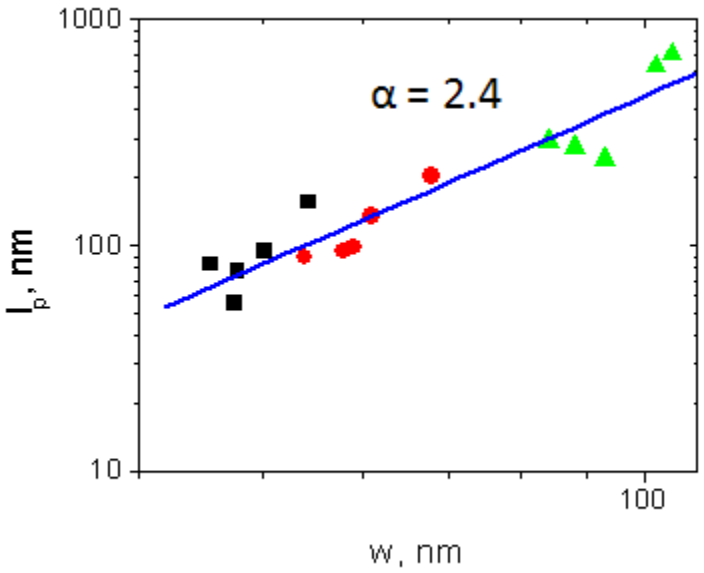

Figure 4.11 Brush widths versus persistence length. The straightening of brushes of different side chain lengths (n = 40 (■), n = 50 (●), n = 80 (▲)) as there width changes with the pressure of the film.

Another major indicator of the conformational changes is the amount of folds, molecules that bend 180 degrees, in the film as it progresses (Figure 4.12). As the film flows the amount of folds decreases with the progression of the flow. This unfolding is caused by stiffening of molecular brushes. In addition, there is a drop off in the number of folds as the side chains become longer, the brushes are harder to fold. This is evident in the number of folds per lengths at the points closest to the drop, where the molecules do not have the opportunity to rearrange and unfold.

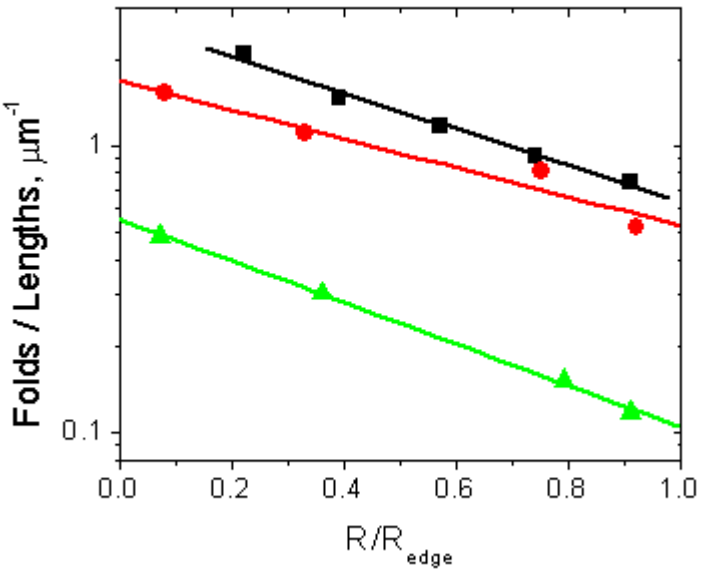

Figure 4.12 Folds per length during flow for different side chain lengths. Number of folds in 1 μm total length of polymer brush molecules for various side chain lengths at various spreading coordinates as they spread: n = 40 (■), n = 50 (●), and n = 80 (▲).

As the pressure drops along the film, more of the brushes' side chains become adsorbed to the surface, which increases the persistence length, straightens the chains, and thus ultimately unfolds them. This increase is best illustrated by plotting the persistence length against the number of folds per unit length (Figure 4.13). The plot shows an inverse relationship between the amount of folds per unit length and the persistence length of the molecule. This suggests that the same mechanism that causes the stiffening of the brushes facilitates their unfolding. As the side chains spread out on the surface they increase the area of the molecules forcing the molecules to unfold and assume extended conformations in order to maximize their area.

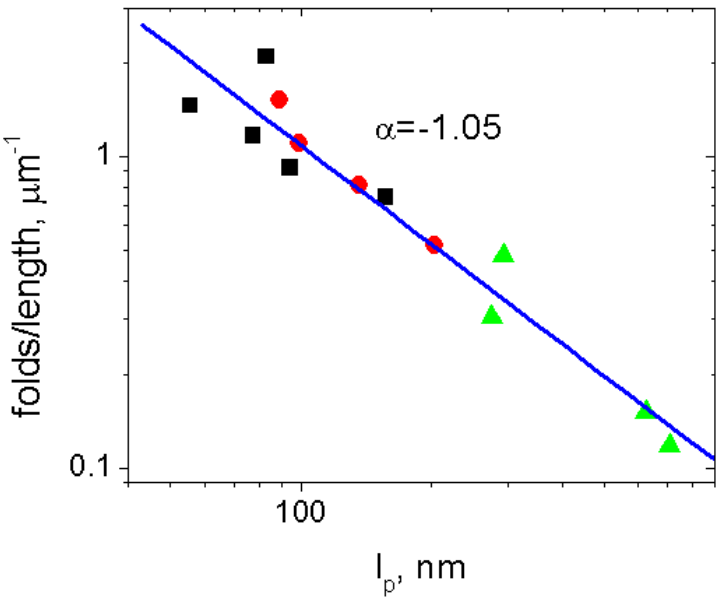

Figure 4.13 Chain folding as a function of persistence length. The folds per length is plotted against the persistence length of individual molecules for the same length (N=7280) and various side chain lengths (n = 40 (■), n = 50 (●), and n = 80 (▲)). The slope of the plot is -1.05.

4.6 Flow induced scission. The effects of brush stiffness are measured by spreading films of the brushes with different side chain lengths described in the experimental section. We tune the stiffness of the brushes by tuning the degree of polymerization or number of monomeric units present in the side chains of the molecules. However, this process leads to a few side effects, including the increase of the brush width, an increase of the height contrast, as well as changes in the melt properties such as viscosity. The results of this spreading are shown in Figure 4.5. In the samples with the longest side chains (n=110 and n=140) it can be observed that there is significant shortening of the brushes as

the spreading coordinate progresses. This can be attributed to a flow induced scission. Scission occurs when the side chains of an individual brush spread away from the back bone and induce tension. The tension force on the backbone is proportional to the width of the brushes; therefore brushes with longer side chains have greater backbone tensions. As the spreading coordinate moves away from the drop, the surface pressure decreases causing the tension on the backbone of the brush to increase.[24]

4.7 Ordering. An interesting aspect of flow that we were able to uncover is as the brushes become stiffer, we begin to see an order during their flow. To measure the order parameter our home built program breaks the individual molecules into small units of a controllable length. In this case the length selected was 20 nm (a length roughly 3 times the resolution of the AFM images obtained), well below the persistence length of the brushes. These small units are considered vectors by the analysis software and their angles (with respect to the direction of flow) are calculated. The square of the cosine of the angles are then found and an order parameter is calculated, $O.P.=2\langle\cos^2\theta\rangle-1$, where θ is the angle the molecules make with the direction of flow. This order parameter results in a value between -1 and 1. A -1 order parameter would mean the molecule is oriented perpendicular to the direction of flow, while a parameter of 1 would mean the molecule is oriented parallel to the direction of flow. An order parameter of 0 would indicate either randomly ordered molecules or molecules oriented 45 degrees to the direction of flow. For the purposes of this document,

we consider an order parameter between -0.2 and 0.2 for the molecule to be randomly oriented.

We can see this ordering visually in the films with n = 80 and above (although for n =140 the scission occurs so rapidly the remaining brushes are approximately disks and hence cannot have any order). This order orients the molecule in the direction of the flow and dissipates near the edge of the film. Figure 4.14 shows the correlation functions for brushes of two separate side chain lengths (n = 40 and n = 80). There is strong correlation for the brush with n = 80 compared to n = 40 where the correlation is weak along the entire film. There are subtle variations of friction that are present along the backbone of the brush that help orient the brushes during flow. It is the rod-like nature of the brushes with the longer side chains that allows the entire brush to be oriented with the flow then rather small parts of the brush which will continually reorient themselves.

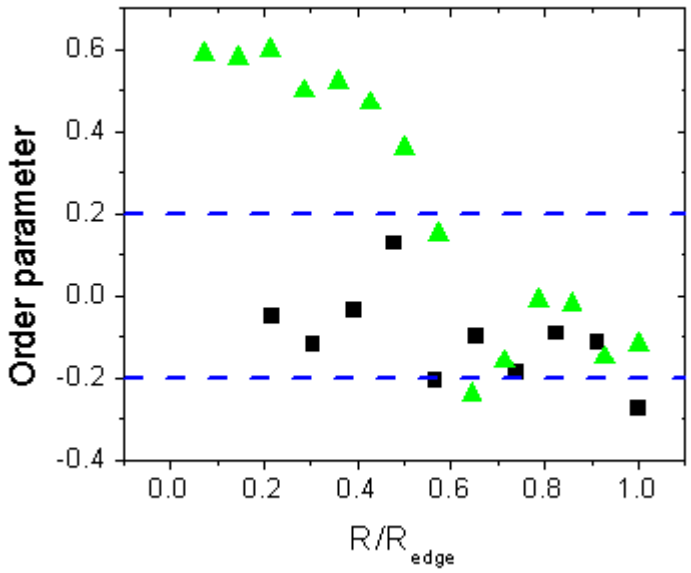

Figure 4.14 Order of molecules during flow. The order parameter of various size brushes, n = 40 (■) and n = 80 (▲), at various distances along a spreading film. The area between the dashed blue lines is considered to have no order.

4.8 Conclusion. We have learned a great deal about how the properties of films change as they spread along a surface as a part of a monolayer film. As a polymer spreads along a film, it undergoes a surface pressure change. This pressure change not only serves as a driving force for the flow of the molecules, it serves as a force that can change molecular conformations.

1) During the process of spreading we observe the molecules extending due to the decrease in the film pressure. As the pressure decreases, more side chains adsorb onto the surface, thus stiffening the brushes and extending them.

2) Chains unfold as they flow. The amount of folds in the systems decays exponentially as they move away from the drop. This behavior is true for the

brushes of all lengths however there are less overall folds in the brushes with the longest side chains. There is an energy loss due to the unfolding process, however this loss is negligible compared to the energy gained from the flowing film.

3) The persistence length of each of the sets of molecules increases during the flow. This is attributed to the extra side chains adsorbing to the surface at the lower pressures, which creates tension on the backbone. This causes an increase in the width of the brushes. We have also shown that the persistence lengths do not scale to n, but the width of the brushes.

4) The amount of crosses in the flowing films does not seem to be affected by the flow or the length of the side chains. In other words, they do not dissociate during flow. This is evidence that these networks can be quite strong considering the additional energy supplied to the film through flow induced diffusion is not enough to break them apart.

5) We have determined that these brushes have a flow induced order that is related to the degree of polymerization of the side chains. The longest side chains align with the direction of flow while the shorter side chains have a disordered arrangement. This difference is at least partially due to the larger entanglements that the shorter brushes exhibit, which, with the tight packing of the molecules, prevents them from organizing with the flow.

This chapter focused on the changes in the film properties as they flow. These flows allow the films to change in multiple ways: the film pressure is reduced during flow, flow induced diffusion allows additional energy for the films

to rearrange, and helps the film progress towards its equilibrium conformation. The understanding of these polymer flows is a first step in developing tunable film properties. By controlling aspects of the flows of these polymers such as film velocity, spreading time, and film pressures, we can begin to control how these films progress towards their equilibrium and how far they proceed. As shown in this chapter the films in different stages of their progression have molecules with different conformations, topologies, and orientation, thus having an effect on the physical properties of the films.

References

[1] Bertrand, E., Bonn, D.; Broseta, D.; Dobbs H.; Indekeu, J.O.; Meunier, J.; K. Ragil, and Shahidzadeh, N. **2002,** *J. Pet. Sci. Eng.* 33, 217.

[2] Bergeron, V.; Bonn, D.; Martin, J.-Y.; Vovelle, L. *Nature.* **2000,** 405, 772.

[3] Shahidzadeh, N.; Bertrand, E.; Dauplait, J.-P. ; Borgotti, J.-C.; Bonn, D. *Transp. Porous Media.* **2003**, 52, 213.

[4] McLellan, J.M.; Geissler, M.; Xia, Y.N. *J. Am. Chem. Soc.* **2004,** 126, 10830.

[5] Hawker, C. J.; Russell, T. P. *MRS Bull* **2005***, 30*, 952-966.

[6] Tabeling, P., *Microfluidics* **2004**, (EDP Sciences, Paris).

[7] Squires, T.M.; Quake, S.R. *Reviews of Modern Physics* **2005***, 77*, 977-1026.

[8] Pfohl, T.; Mugele, F.; Seemann, R.; Herminghaus, S. *ChemPhysChem* **2003***, 4*, 1291-1298.

[9] Bonn, D.; Eggers, J.; Indekeu, J.; Menunier, J.; Rolley, E. *Rev. of Mod. Phys.* **2009,** 81, 739.

[10] de Gennes, P.-G., *Rev. Mod. Phys*. **1985**, 57, 827.

[11] Brenner, M. P.; Bertozzi, A. L. *Phys. Rev. Lett.* **1993,** 71, 593.

[12] McHale, G.; Newton, M. I.; Rowan, S. M.; Banerjee, M. *J. Phys.D* **1995,** 28, 1925.

[13] Oron, A.; Davis, S. H.; Bankoff, S. G. *Rev. Mod. Phys.* **1997**, 69, 931.

[14] Tanner, L. H. *J. Phys. D* **1979,** 12, 1473.

[15] Cazabat, A.-M.; Gerdes, S. ; Valignat, M. P.; Villette, S. *Interface Sci.* **1997,** 5, 129.

[16] Beaglehole, D., *J. Phys. Chem*. **1989,** 93, 893.

[17] Leger, L.; Erman, M.; Guinet-Picard, A.; Ausserre, D.; Strazielle, C. *Phys. Rev. Lett.* **1988***, 60*, 2390.

[18] Heslot, F.; Cazabat, A. M.; Levinson, P. *Phys. Rev. Lett.* **1989***, 62*, 1286.

[19] Valignat, M. P.; Oshanin, G.; Villette, S.; Cazabat, A. M.; Moreau, M. *Phys. Rev. Lett.* **1998***, 80*, 5377.

[20] Xu, H.; Shirvaniants, D.; Beers, K.; Matyjaszewski, K.; Rubinstein, M.; Sheiko, S.S. *Phys. Rev. Lett*. **2004,** 93, 206103/1-4.

[21] Xu, H.; Shirvaniants, D.; Rubinstein, M.; Shabratov, D.; Beers, K.; Matyjaszewski, K.; Sheiko, S.S. *Advanced Materials* **2007,** 19, 2930-2934.

[22] Sun, F. C.; Dobrynin, A. V.; Shirvanyants, D.; Lee, H.; Matyjaszewski, K.; Rubinstein, G.; Rubinstein, M.; and Sheiko, S.S. *Phys. Rev. Lett.* **2007,** 99, 137801.

[23] Sheiko, S.S.; Sun, F.; Randal, A.; Shirvaniants, D.; Rubinstein, M.: Lee, H.I.; Matyjaszewski, K. *Nature*, **2006.** 440, 191-194.

[24] Park, I.; Nese, A.; Matyjaszewski, K.; Sheiko, S.S. *Macromolecules* **2009,** 42, 1805-1807.

Chapter 5

Fractionation of Brushes in a Matrix

5.1 Introduction. Understanding the spreading behavior of thin polymeric films is vital for the advancement of lithography,[1-4] coatings,[5,6] microfluidics,[7,8] lubrication,[9] and printing.[10] Thermodynamic and kinetic properties of a spreading process are largely controlled by the interaction between the flowing macromolecules and the substrate. It is possible for these interactions to change molecular conformations,[11-13] ordering,[14] and even chemical structure[15] of the adsorbed macromolecules. The short-range molecular interactions also have an effect on sliding friction and thus can control dynamics of individual molecules on a surface.[16,17] The friction coefficient between these macromolecules and the surface depends on the chemical structure, conformation, and orientation of the adsorbed macromolecules and may also exhibit minute variations due to the intrinsically heterogeneous structure of a substrate surface. Controlling interfacial interactions provides an opportunity to induce diffusion within a plug flow, enhance mixing of spreading macromolecules, facilitate their ordering, and perform molecular fractionation.

In a spreading experiment, a fluid drop is placed on a substrate and depending on the value of the spreading parameter (S), the fluid will either wet ($S>0$) or not wet ($S<0$) the substrate.[18] Under the favorable wetting conditions,

intermolecular van der Waals forces will drive a monolayer of liquid, called the precursor film, to spread ahead of the drop (Figure 5.1). The dynamics of the precursor film's spreading process is controlled by the pressure gradient driving the flow and by the sliding friction responsible for the film-substrate interactions as follows

$$-\frac{d\Pi}{dr} = \xi \cdot V(r) \tag{5.1}$$

where Π(r) is the local film pressure, ξ is the friction coefficient per unit area, and, in the case of radial spreading, $V(r)=V_{front}R/r$ is the local velocity of the film. Integration of Equation 5.1, first over distance r (Equation 5.2) and then over time t (Equation 5.3), provides a local flow velocity and the time dependence of the precursor film radius R(t) as a function of the film spreading rate D ≅ S / ξ and the drop radius R_0.

$$\dot{R} = \frac{D}{R(t)\ln\frac{R(t)}{R_0}} \tag{5.2}$$

$$\left(\ln\frac{R(t)}{R_0} - \frac{1}{2}\right) + \frac{R_0^2}{2} = Dt \tag{5.3}$$

Where $\dot{R} = V_{front}$. Both the spreading parameter, S, and the friction coefficient, ξ, are determined by the polymer-substrate interactions. The friction coefficient has been shown to exhibit a strong dependence on the substrate structure and

composition.[11,14] On heterogeneous substrates, the local variations in polymer-substrate friction may enhance local molecular diffusion in the frame of the flowing film.[16] On homogeneous substrates, a spreading process shows features of a plug flow, i.e. all species (e.g. molecules) move with the same velocity. It is especially true for large macromolecules that can be viewed as microscopic objects with linear dimensions 10-100 nm.[16] This coupling between molecular dimensions, interaction with the substrate, and flow properties could induce molecular separation during spreading of multi-component polymeric films (spreading-induced fractionation). To test this hypothesis and to establish how the fractionation is influenced by molecular parameters, we have studied spreading of a mixture of brush-like macromolecules and linear polymer chains of the same chemical structure. By considering mixtures of chemically similar species, we have suppressed the tendency for phase separation. Unlike the plug-flow behavior of single-component melts,[19] the mixtures revealed the difference in spreading velocity between brushes of different sizes resulting in spreading-induced molecular fractionation.

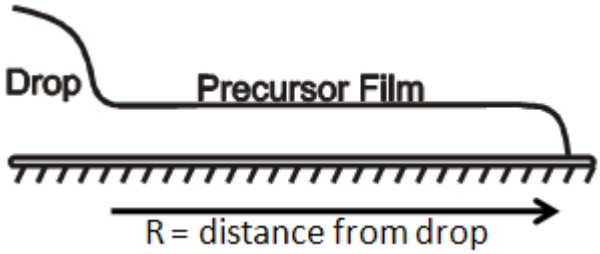

Figure 5.1 Sketch of the polymer drop and precursor film. The polymer drop is the reservoir melt of our polymer blend while the precursor film flows to the left.

The rest of the chapter is organized as follows: The molecular weight dependence of the spreading velocity was obtained using Atomic Force Microscopy (AFM). These results were used to develop a model which ascribes the origin of the fractionation to the difference in friction coefficient between the poly(*n*-butyl acrylate) (PBA) brushes and PBA linear chains. The assumptions of the model were tested in molecular dynamics simulations of the Poiseuille flow in brush-linear chain mixtures.

5.2 Experimental. Brush-like macromolecules with PBA side chains that are densely grafted to a poly(2-hydroxyethyl methacrylate) backbone have been synthesized by Atom Transfer Radical Polymerization.[20-22] Two different architectures of brushes have been prepared: (i) a backbone degree of polymerization, N = 500, and a side chain degree of polymerization, n = 35, with an average length of about 100 nm, called short brushes (for the short average length of their backbone), and (ii) N = 7280 and n = 50, with an average length of about 800 nm, dubbed long brushes. The polydispersity index (PDI) of the two brush polymers are 1.2 and 1.6 respectively. Our collaborators have also synthesized a series of linear PBA with various degrees of polymerization, where m = 174, 214, 235, 477, 563, all with PDI's between 1.1 and 1.2. Four homogeneous molecular systems have been prepared by mixing solutions of each type of polymer in the appropriate ratio and subsequently evaporating the solvent in a vacuum oven (Figure 5.2). The compositions of each of the mixtures are summarized in Table 5.1.

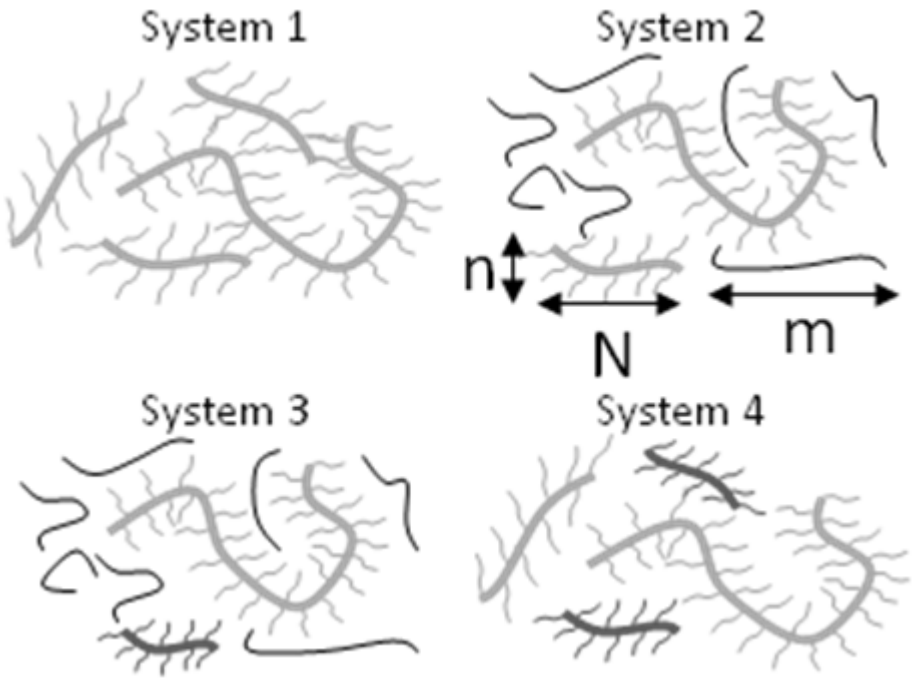

Figure 5.2 Polymer melts. Four molecular systems have been studied. System 1 consists of a melt of molecular brushes. System 2 is a melt of linear polymers and molecular brush. System 3 is two different types of polymer brushes mixed with a melt of linear chains. System 4 is a melt of two different molecular brushes. The architecture of a molecular brush and linear chain is seen (depicted) under System 2. N is the degree of polymerization of the brush's backbone, n is the degree of polymerization of the polymers side chain, and m is the degree of polymerization of the linear polymer.

Table 5.1 Polymer melt mixtures.

System	Brush 1[a)] Weight fraction	Brush 2[b)] Weight fraction	Linear PBA[c)] Weight fraction
1	1.00	-	-
2a	0.05	-	0.95
2b	-	0.05	0.95
3	0.05	0.05	0.90
4	0.95	0.05	-

[a)] Brush 1: N=500, n=35, PDI=1.2
[b)] Brush 2: N=7280, n=50, PDI=1.9
[c)] Linear PBA: N=214

Drops of the polymer melts with a radius of R≅100 μm were deposited onto a mica substrate using a needle with a diameter of 100 μm. The polymer melts were then allowed to spread at 25°C under a relative humidity of 97% on a time scale ranging from minutes to several hours.

Atomic force microscopy was used to image individual molecules within the precursor layer at different distances from the drop after a defined spreading time. The AFM measurements were conducted with a Nanoscope IIIa AFM (Veeco Metrology Group) using Si probes with a cantilever spring constant of 6 mN/m and a resonance frequency of 160 kHz. The imaged molecules were characterized for length distribution using home built software for analysis of the digital images.

5.3 Fractionation. We first carefully examine flow characteristics and spreading of the polymer brushes and linear chains alone. Respectively, two 100 μm drops of linear (m=214) and brush-like (N=500, n=35) poly(n-butylacrylate) were allowed to spread for 45 minutes under the identical environmental conditions (mica substrate, T=25°C, and relative humidity 97%). The precursor layers of both the brush-like and linear drops spread to radii of 235 and 1195 μm, respectively. Since the interfacial tension of both polymers is the same, the significant difference in the spreading rates is ascribed to the differences in the friction coefficients of the linear and brush-like PBA (Eq. 1). From Equations 5.2 and 5.3, one determines the corresponding friction coefficients between the polymers and the substrate to be $\xi=2.1\text{x}10^{8}$ $N\cdot s/m^{3}$ for the brush and

ξ=2.5x10^6 N·s/m^3 for the linear, i.e. the brush-like PBA has ca. two-orders of magnitude higher friction coefficient than its linear counterpart.

The studies of the individual (single-component) systems have been followed by experiments on their mixtures. A 96 μm drop of System 2b (see Table 5.1) was prepared and was spread for 45 minutes on a mica substrate. As shown in Figure 5.3, PBA brushes are finely dispersed with the matrix of linear PBA. The mixing is consistent with the prediction of the Flory theorem for structurally asymmetric mixtures, namely the mixture of the molecular brushes (N=7280, n=50) and linear chains (m=214).[23] After the 45 minutes spreading, the precursor film had a length of R=2800 μm. However, when the film was examined using AFM, the brushes were found to have propagated a smaller distance of 1195 μm from the drop, a significantly shorter distance then the matrix of linear chains. AFM images of flowing macromolecules were taken every 40 μm along the precursor film. Figure 5.3a shows a few selected AFM images at various distances from the drop. It is clear that the contour length of the molecular brushes decreases as one looks further away from the drop edge. The image analysis revealed that the average brush length remains constant close to the drop edge and begins to decrease at distance x=300 μm (Figure 5.3b). We have coined the region of the film where the average length decreases the 'fractionation region' of the film. The fractionation was confirmed by analyzing the length distributions at different distances from the drop edge (Figure 5.3c). The individual distributions in Figure 5.3c progressively shift towards shorter brushes, confirming their fractionation upon spreading. The

observed depletion of shorter brush macromolecules is consistent with their faster spreading velocity.

One may suggest that the difference in the bulk and film length distribution occurs due to fractionation upon the transition from the drop to the precursor film. In order to rule out this reason, we have summed up the length distributions at regular intervals along the spreading film (Figure 5.3c) to compile a cumulative distribution of the entire film. As shown in Figure 5.3d, the cumulative distribution fully matches the bulk distribution (measured by from a Langmuir-Blodgett film). The length distributions in the precursor film and bulk polymer had the same shape and size, and yielded the same PDI=L_w/L_n=1.18. This indicates that the exchange rate of brush molecules from the drop to precursor film does not depend on the size of molecular brushes.

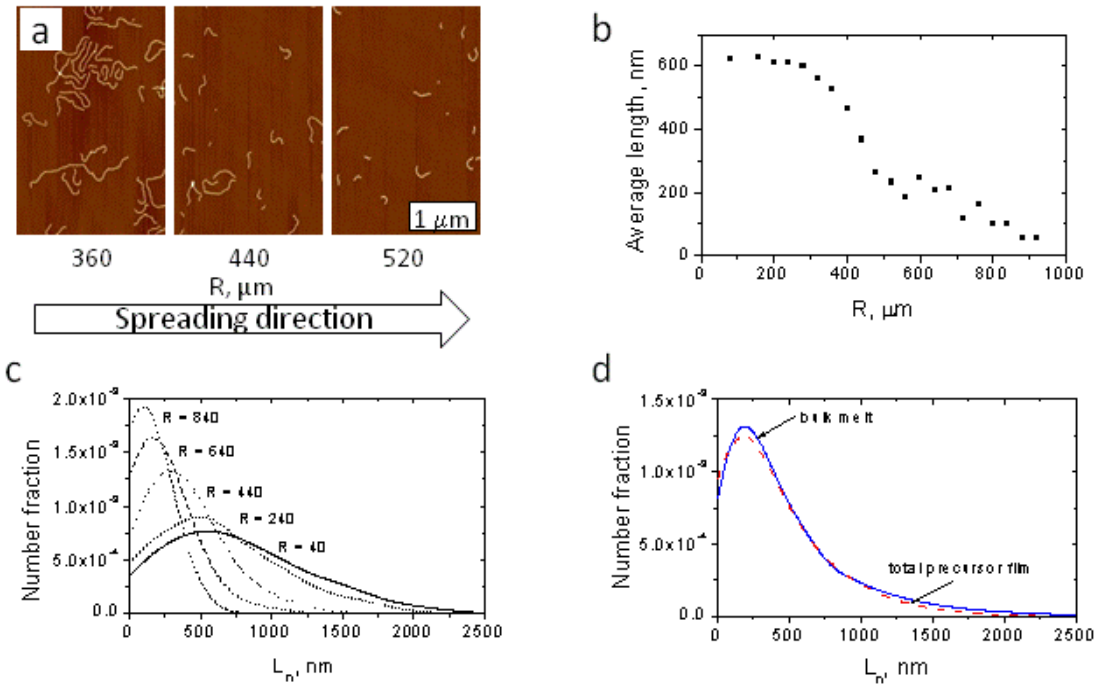

Figure 5.3 Fractionation of brushes in a linear matrix. (a) Images of the precursor film from a drop spread from System 2b. As one looks further away the brushes are generally shorter. (b) Number average length of the molecular brushes, from System 2a, in the precursor layer at various distances from the drop. (c) Length distributions of the bulk melt (solid line) compared to the distribution of the total film (dashed). (d) The length distribution of the polymer brushes, from System 2a, at various distances from the drop along the precursor film.

The total length distribution was used to calculate the instantaneous velocity of the brush molecules with different degrees of polymerization (DP) of the backbone. The calculation was based on the assertion that faster moving, short brush molecules have lower relative concentrations on the surface than in the bulk compared to slower moving longer brushes. This behavior can be rationalized by the following scaling argument: $V_N \sim R_N \sim 1/\phi_N$, i.e. instantaneous velocity of molecular brushes with DP=N is proportional to the maximum distance

$x=R_N$ which these molecules traveled during time t and inversely proportional to their local number fraction ϕ_N in the plateau region, i.e. at short distances from the drop edge. It is tempting to use this scaling relation to directly calculate the brush velocity relative to that of linear chains, V_0, as $V_N/V_0=\phi_0/\phi_N$, where ϕ_0 is the number fraction of linear PBA chains in the plateau region. However, this calculation will be inaccurate since AFM does not resolve the linear chains and thus forbids their counting for determination of ϕ_0. Therefore, we have calculated the relative velocity from the fraction of the shortest brushes by applying the scaling relation as

$$\frac{V_N}{V_0} = \frac{R_1}{R_0}\frac{\phi_1}{\phi_N} \tag{5.4}$$

where V_0 is the spreading velocity of the linear PBA, $x=R_0$ is the total length of the precursor film, (R_0=2800 μm after spreading during t=45 min), $x=R_1$ is the maximum distance traveled by the shortest (L=50 nm) brush molecules (R_1=1195 μm at t=45 min), and ϕ_1 is the fraction of the shortest brushes within the cumulative film. Figure 5.4 shows the dependence of the relative velocity of molecular brushes on their number average contour lengths. The graph corresponds to the results in Figures 5.3a, b and c and suggests a decrease of the brush velocity with increasing the brush contour length. The solid line is a fit of a physical model for the heterogeneous spreading process developed that will be discussed later in this chapter.

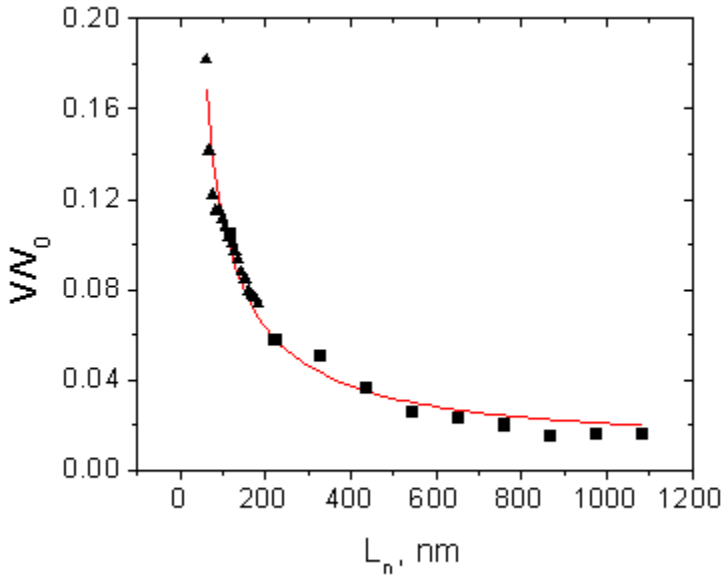

Figure 5.4 Velocities of polymer brushes in the spreading film. Velocity of the brushes relative to the spreading velocity of the matrix of linear chains is presented as a function of the number average contour length. The data points were obtained for two molecular systems: ▲System 2a (N=500, n=35) and ■ System 2b (N=7280, n=50). The solid line is representation of the fit from the model (Appendix A).

Harnessing the phenomena described above, we have conducted experiments to separate two types of brushes that differ in the degree of polymerization of the backbone. The melt described by System 3 contained a mixture of long brushes having a number average length of L_n=550 nm and short brushes having an average length of L_n=95 nm. The difference in the side chain lengths shows itself as a variation of heights on the backbones and therefore different contrasts in AFM images (see excerpt in Figure 5.5a). The difference in contrast allows us to easily monitor and separate the two kinds of brushes when analyzing their length distribution.

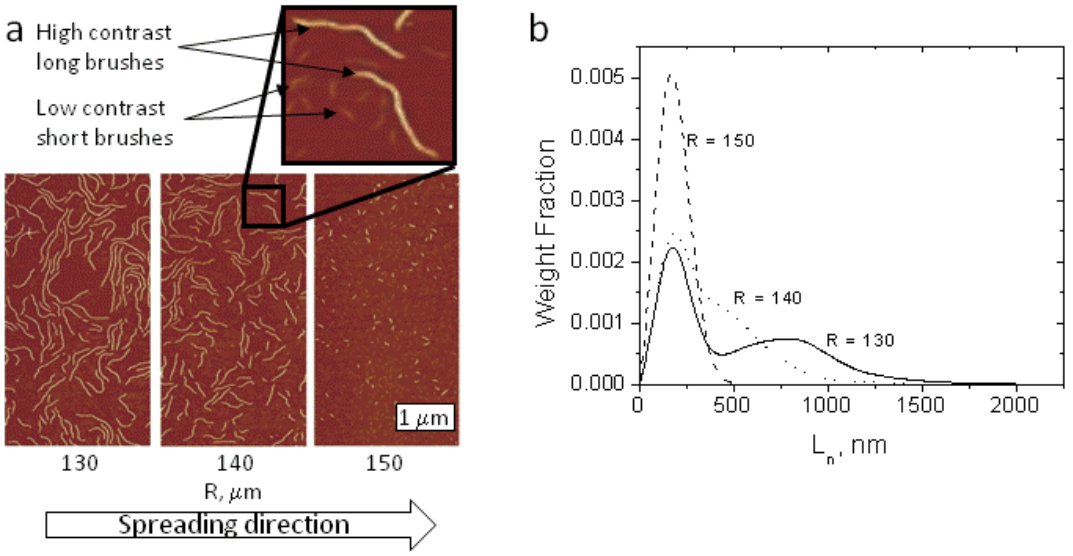

Figure 5.5 Separations of brushes. (a) Height images of a mixture of molecular brushes within a matrix of linear chains (System 3) have been captured along the precursor film. The long brushes disappear far from the drop. (b) Length distributions of the brushes from system 3 taken at various distances from the drop: R=150 μm (dashed line), R=140 μm (dotted line), and R=130 μm (solid line).

Figure 5.5a shows selected images captured within the fractionation region of the film. As before, the longer brushes of both types moved slower than the shorter molecules. At shorter distances (e.g. R=130 μm), one can clearly see the bimodal distribution of the mixture. At longer distances (e.g. R=150 μm) away from the drop edge, only the short brushes of both kinds are present in the image. This confirms successful separation of a bimodal distribution. It is important to note that short brushes of two different architectures (with short and long side chains) flow with a similar velocity. This indicates that that the fractionation of the brushes with large aspect ratios is dominated by the contour length of the spreading macromolecules, as opposed to their widths. To

independently verify this claim, we compared the ratio of the weight fractions of the short to long molecules with L_n<350 nm to that of the bulk mixture. In both cases, we have found a ratio of 9:1 w/w, i.e. the composition of the bulk mixture. The fact that the fractionation is determined by the contour length is consistent with the theoretical model discussed below.

5.4 Model. The observed fractionation is attributed to the difference in friction coefficient of the linear and brush-like PBA with the substrate during the spreading process. This difference in friction coefficients could be both chemical and physical in origin. For the former, the poly(methacrylate) (PMA) backbone has a slightly different chemical composition than the PBA side chains. However, the "chemical" contribution of the PMA is negligible, since its molar fraction is less than 2% and it is surrounded by the PBA side chains. A possible physical explanation for the difference in friction is attributed to the difference in packing density and orientation of the PBA monomeric units at the interface. The extremely high grafting density causes the butyl units in the extended side chains to align perpendicular to the substrate unlike the random orientation of conformationally relaxed linear chains. Due to the perpendicular orientation of the butyl units, the friction dissipation is dominated by the stronger interactions between the more hydrophilic acrylic groups and the hydrophilic substrate.[24]

The difference in friction causes a drag force between the faster moving matrix (linear PBA) and the slower moving PBA brushes. The drag force may have two mechanisms: (i) viscous drag at a nonslip boundary (Model 1) and (ii)

slip between a brush molecule and the linear matrix (Model 2). Both models are discussed in Section 5.4.1 and yield the relative velocity V/V_0 (the velocity of molecular brushes relative to the velocity of the matrix) as function of the molecular area and contour length respectively, and also predict the velocity dependence on the friction coefficients and matrix viscosity. Ironically, both models allow quantitative description of the experimental data with decent accuracy (Figure 5.A1). Therefore, additional experiments have been conducted to select the right model.

5.4.1 Derivation of models. We consider two models of the flow-induced fractionation. To simplify the results, each brush is approximated to take on the conformation of a disk flowing on the surface. Looking at Figure 5.3a one can see the brushes are generally coiled and when the extended side chains are considered, this becomes a reasonable approximation. Both models assume that the major cause of the fractionation is the difference in friction coefficient with the substrate between the matrix of linear PBA and the molecular brushes with PBA side chains. The difference between the two models is that Model 1 assumes no slip between the matrix and brush molecules, while Model 2 assumes complete slip at the brush-matrix interface (infinite slip length). In both models we assume that the brush has a rectangular shape with length L, width d and thickness h.

Model 1. Figure 5.6 depicts four major forces acting on a brush molecule: F_p - The force created by the changes in pressure along the film.

$$F_p = -\frac{\partial \Pi}{\partial x}\pi L^2 \tag{5.5}$$

where l is the length of the brush, d is the width of the brush, and $\frac{\partial \Pi}{\partial x}$ is the pressure gradient along the film. This force drives the flow of every component of the film. In a dilute 2D solution, the film can be approximated by the spreading of the matrix alone. Using Equations 5.2 and 5.5 we obtain:

$$F_p = V_0 \xi_0 \pi L^2 \tag{5.6}$$

where V_0 is the velocity of the linear matrix and ξ_0 is the friction coefficient between the linear matrix and the surface.

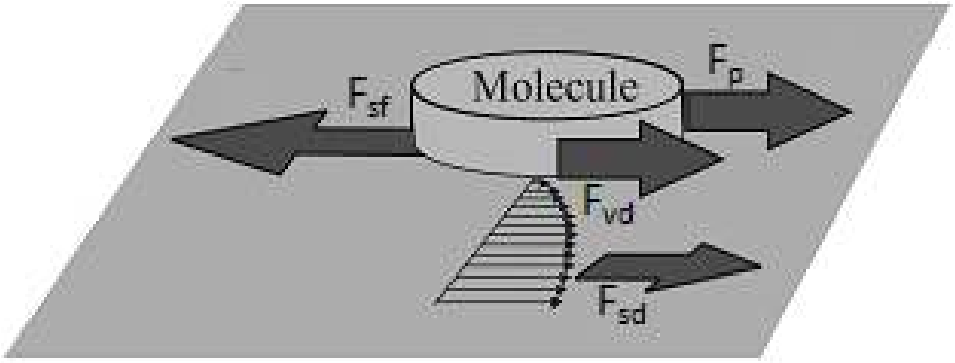

Figure 5.6 Diagram of molecule in non-slip film. Depiction of the various forces that act on a polymer brush spreading in a linear matrix using a no slip model.

F_{sf} - The friction force that arises from the interaction between the brush and the surface and is dependent on the velocity of the brush and its friction coefficient (surface friction).

$$F_{sf} = V\xi\pi L^2 \tag{5.7}$$

where V is the velocity of the brush and ξ is the friction coefficient between the brush and the surface This force is dependent on the velocity of the brush relative to the surface it travels on.

The Stokes equations for thin films such as these requires the consideration of two types of drag[2526], 1) a surface induced drag, F_{sd} (surface drag) and 2) a viscous drag F_{vd}.

$$F_{sd} = -\xi_0\pi L^2(V_0 - V) \tag{5.8}$$

and,

$$F_{vd} \cong \frac{-4\pi\eta(V_0 - V)h}{2 - lnRe} \cong \frac{-4\pi\eta(V_0 - V)h}{2 - ln\left[\frac{\rho(V_0 - V)}{\eta}\right] - lnL} \tag{5.9}$$

where η is the viscosity of the matrix, Re is the brushes Reynolds number in the fluid, h is the thickness of the film, and ρ is the density of the film. For the parameters for our experiment Equation 5.9 can accurately be approximated by

$$F_{vd} \cong -0.16\eta h(V_0 - V) \tag{5.10}$$

The viscous drag component is similar to the drag that occurs when a thick liquid flows around pipe. The surface induced drag is a more complicated phenomenon that arises from the decrease of friction force between the matrix

and the substrate, which is caused by the slowing of the matrix. These forces are then balanced to obtain the relationship

$$\frac{V}{V_0} = \frac{2\beta L^2 + \gamma_{slip}}{(1+\beta)L^2 + \gamma_{slip}} \quad (5.11)$$

Where $\gamma_{slip} = 0.16\eta h/\pi\xi$ and $\beta = \xi_0/\xi$ and are fitting parameters. Using the values for friction and bulk viscosity we can calculate approximate values for γ_{slip} and β (η_{bulk} = 290 Pa*s for linear PBA of m=214, ξ=2.1x10^8 $\frac{Ns}{m^3}$, ξ_0=2.5x10^6 $\frac{Ns}{m^3}$, and h=8 Å in spreading films). This yields measured values for γ_{slip} and β to be 0.00018 μm^2 and 0.012 respectively.

Figure 5.7 demonstrates the effects of altering the parameters β and γ on the relative velocity. As seen in Figure 5.3a, parameter β (the ratio of friction coefficients) controls the speeds of the longest brushes compared to that of the linear film. As β→1 the friction coefficients of the brushes with the surface and the linear matrix with the surface become equal resulting in a plug flow (Figure 5.7a). Parameter γ (proportional to the monolayer viscosity) determines the width of the fractionation region. As seen in Figure 5.3b, for low viscosities of the matrix (e.g. γ<10^{-4}) we should see no fractionation within the studied range of molecular sizes (0.1<L<1.5 μm). Since the viscous drug force is very low, all molecules regardless their size will move with a finite velocity determined solely by parameter β. However, when γ increases, then the difference in velocities (and hence the spreading distances) between brushes of different lengths within

the 0.1<L<1.5 μm range will become pronounced resulting in a sizable fractionation interval within the spreading film.

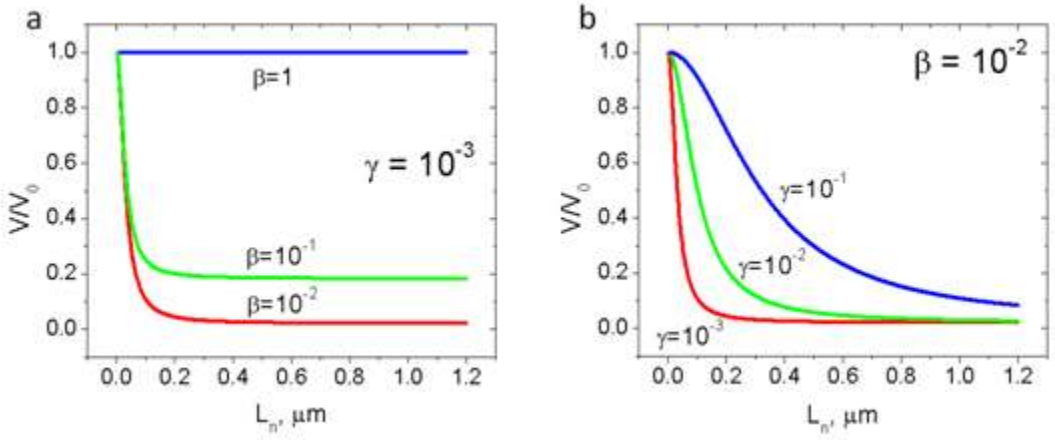

Figure 5.7 Plots of the fractionation from model 1. (a) The effects of altering the β parameter while holding γ constant. (b) The effects of altering the γ parameter while holding β constant.

In Model 2, we assume full slip and the forces considered in this model are depicted in Figure 5.8. The pressure gradient and the surface frictions remain the same as model 1 so the equations for F_p and F_{sf} are the same in both models. However, the origin of the F_{vd} force (drag force) is different as it is caused by the friction between the matrix and brush molecule (matrix-brush friction, mf). One can write the additional friction force as

$$F_{mf} = 4(V - V_0)\xi_{BM} hL \tag{5.11}$$

where ξ_{BM} is the friction between the brush and matrix. Similar to the no slip model we then balance these forces and get

$$\frac{V}{V_0} = \frac{\beta L + \frac{4\varphi h}{\pi}}{L + \frac{4\varphi h}{\pi}} \quad (5.12)$$

, where $\varphi = \frac{\xi_{BM}}{\xi}$ is a fitting parameter for the equation, i.e. (brush-matrix friction / brush-surface friction).

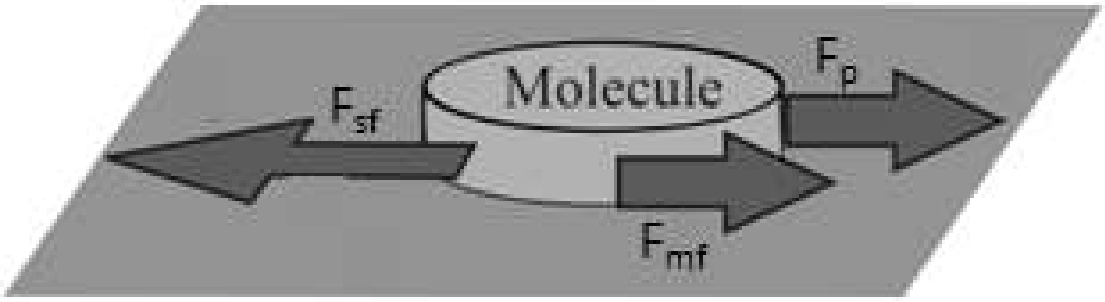

Figure 5.8 Diagram of a molecule in a slip film. Depiction of the various forces that act on a polymer brush spreading in a linear matrix using a slip model.

The effect of the model parameters is presented in Figure 5.9. Parameter β is identical to Model 1, i.e. it controls the velocity of the brush molecules compared to that of the linear film (Figure 5.9a). The effect of parameter ϕ (friction drag) is similar to that of parameter γ in Model 2. The increase in the friction drag results in expanding the fractionation region to match the size range of the studied molecules (0.1< R<1.5 μm). (Figure 5.9b).

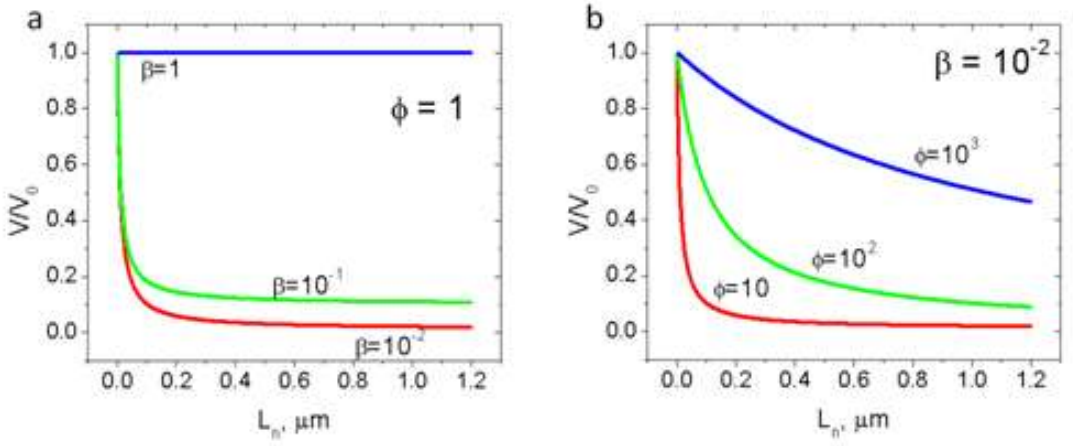

Figure 5.9 Plots of the expected fractionation from model 2. (a) The effects of altering the β parameter while holding φ constant. (b) The effects of altering the φ parameter while holding β constant.

5.4.2 Analysis of models. Model 1 (viscous drag, nonslip boundary) predicts that the velocity of the spreading brush macromolecules depends on the viscosity of the matrix (Section 5.4.1). In order to verify this prediction, we have measured the velocity in as a function of the molecular weight of linear PBA. In the studied range of molecular weights (22-73 kDa) the zero-shear bulk viscosity ranges from 250-3000 Pa·s. One would prefer using viscosity values for polymer monolayers; however, these data, to the best of our knowledge, are not available in the current literature. Figure 5.10 demonstrates that the velocity of all the molecular brushes decreases with the matrix molecular weight and thus matrix viscosity. This behavior contradicts Model 1, which predicts the increase of the drag force with matrix viscosity. In other words the model predicts that the velocity of the brushes should decrease as the molecular weight of the matrix increases, however we observe the opposite. As such, the drag force is believed to be at least partially caused by friction at the brush-matrix interface (Model 2),

which also implies a non-zero slip length between a brush molecule and the linear matrix. The decrease in brush velocity (Figure 5.10) is tentatively ascribed to the decreasing penetration of linear chains into the corona of side chains in molecular brushes, which in turn facilitates slip at the matrix-brush interface.

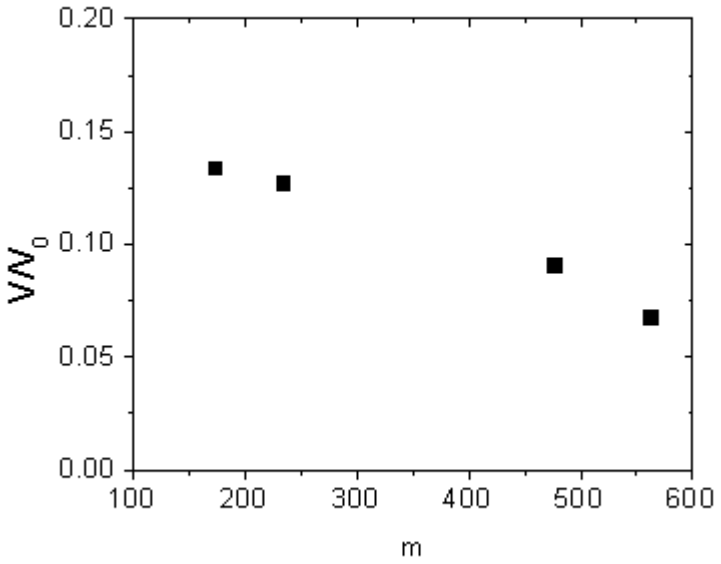

Figure 5.10 Fractionation at different matrix viscosities. V/V_0 of the shortest brushes for various molecular weights of the linear matrix.

To describe our data we have considered a second model, Model 2, which is based on a complete slip (the matrix flows at the same velocity at all points) between the polymer brush and the linear matrix (Appendix A). This model gives the following relation for the relative velocity shown in Equation 5.12, where $\varphi = \frac{\xi_{BM}}{\xi}$ is the ratio of the brush-matrix friction coefficient and brush-substrate friction coefficients, and $\beta = \xi_0/\xi$ is the ratio of the matrix-substrate friction

coefficient and brush-substrate friction coefficients considered to be a fitting parameters of the model, *L* is the brush length, d is the brush width, and *h* is the thickness of the side chains.

Equation 5.12 was used to fit the experimentally measured relative velocities as a function of the molecular size with two fitting parameters β and φ. As shown in Section 5.4.1, parameter β controls the position of the longest brushes compared to the front of the linear matrix, while parameter φ determines the width and magnitude of the fractionation interval. As shown in Figure 5.A2, the fractionation occurs only when the brushes and the matrix have different friction coefficients with the substrate (β<1). The fitting results yield β=0.009 and φ=11.3. In other words, the matrix has approximately 100 times less friction coefficient with the substrate compared to the brush molecules. This difference is in excellent agreement with the friction coefficients $\xi=2.1\times10^{8}$ N·s/m^3 and $\xi_0=2.5\times10^{6}$ N·s/m^3 that have been independently determined from the spreading rate at beginning of the Section 5.3. To estimate φ within an order of magnitude, we use the viscosity of linear PBA with a radius comparable to the thickness of the film (η ~ 1 Pa·s) and divide that by the radius of the polymer to give us a friction coefficient per area ($\xi_{BM}\sim 1\cdot10^{9}$ N·s/m^3). This gives us the approximate value φ = 10, which is in agreement with our model.

When both materials have the same friction with the substrate, one observes a plug flow, i.e. all species move with the same velocity. To test this prediction, we have studied a mixture of two different brush molecules (System 4). Figure 5.11a shows the images at various distances over the spreading

precursor film. As shown in Figure 5.11b, the average lengths of the brushes don't change throughout the precursor film, i.e. there is no fractionation present in System 4. This observation is consistent with the model since the frictions of both the short brush matrix and the longer brushes are equal meaning their velocities should be the same i.e. a plug flow.

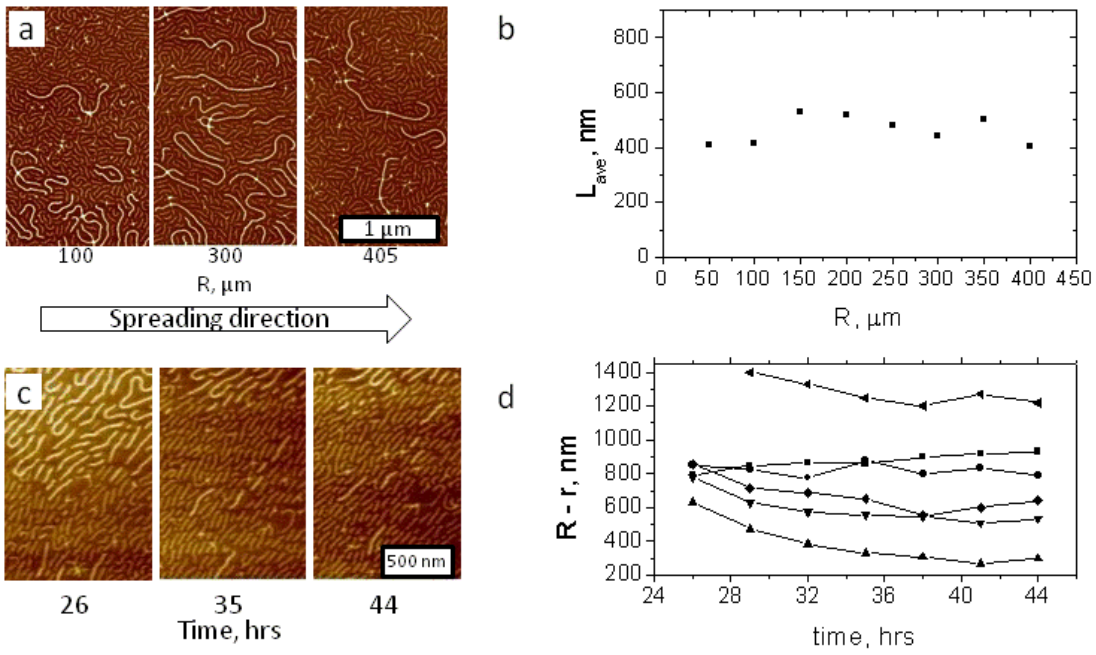

Figure 5.11 Spreading of long brushes in short brushes. (a) Images from various positions in the precursor film spread from a melt of system 4.The total length of the film is 405 µm. (b) Average length of the long brushes from system 4 throughout the precursor film. (c) Images of system 4 spreading on graphite at various times. (d) The distances over time of 7 separate brushes as they spread over the graphite substrate.

The plug-flow was verified by *in-situ* imaging of brush molecules as they spread on a substrate. This experiment was conducted on a graphite substrate, which allows the real-time imaging of the spreading process on the molecular

scale. The friction coefficient between the brushes and the graphite is sufficiently high for the brushes to move slow enough to be captured in motion with AFM. Images were taken every 4 minutes for a time period of 44 hours and individual brushes were tracked over that time. Figure 5.11c shows images of selected brushes moving through the film at various times and Figure 5.11d shows their motion relative to the film edge. As shown, the brushes generally have the same distance from the edge of the film directly showing that the long brushes move in a plug flow in a matrix of short brushes. The results support the assumption that the fractionation is caused by the difference in friction coefficient with the substrate between the brushes and linear chain matrix.

5.5 Computer Simulations. To further corroborate our observation of the spreading-induced separation in polymer-brush mixtures, we have performed molecular dynamics simulation of the motion of a single brush molecule within the matrix of the linear chains. We used a coarse-grained representation of linear chains and brush molecules. In this representation monomers were modeled by the Lennard-Jones particles with diameter σ. Since the brushes and linear chains exhibit different friction coefficients with the surface, we used varying values of the Lennard-Jones interaction parameter for the brush-substrate pair and the linear polymer substrate pair to obtain contrast in their friction forces. The connectivity of monomers into polymer chains and brush molecule were maintained by the FENE potential. The internal rigidity of the linear chains and brush molecules were introduced into the model through the bending potential

which restricted mutual orientation between consecutive monomers along the polymer backbone bond vectors. The flow conditions in the spreading polymeric film were modeled by the Poiseuille flow by applying a constant force to each particle belonging to linear chains and brush molecule. The explicit form of the interaction potentials, bond potentials, and simulation details are given in Section 5.5.1.

5.5.1 Simulation details. We have performed coarse grained molecular dynamics simulations of the motion of a brush molecule in the matrix of linear chains in contact with a substrate. The system configuration is shown in Figure 5.12. The simulation box had dimensions L_xxL_yxL_z and periodic boundary conditions were imposed in x and y directions. We have performed simulations of systems with the simulation box size 140x138.56 σ. The thickness of the film was controlled by imposing a localizing potential

$$U_{conf}(z) = 4\varepsilon\left(\left(\frac{\sigma}{h_z - z}\right)^{12} - \left(\frac{\sigma}{h_z - z}\right)^{6}\right) \tag{5.13}$$

where the value of the interaction parameter ε was set to k_BT (where T is the absolute temperature and k_B is the Boltzmann constant), h_z determined the film thickness and was set to 3.2 σ to maintain an average particle density $\rho\sigma^3 = 0.68$ within the layer. The substrate surface was modeled by a periodic hexagonally packed lattice of beads with diameter σ located at z = 0. Substrate particles, monomers belonging to linear chains and brush molecules were

modeled as Lennard-Jones (LJ) particles (beads) with diameter σ interacting through the truncated-shifted Lennard-Jones (LJ) potential:

$$U_{LJ}\left(r_{ij}\right)=\begin{cases}4\varepsilon_{LJ}\left[\left(\frac{\sigma}{r_{ij}}\right)^{12}-\left(\frac{\sigma}{r_{ij}}\right)^{6}-\left(\frac{\sigma}{r_{cut}}\right)^{12}+\left(\frac{\sigma}{r_{cut}}\right)^{6}\right] & r\le r_{cut}\\ 0 & r>r_{cut}\end{cases} \tag{5.14}$$

where r_{ij} is the distance between *i-th* and *j-th* particles, and σ is the particle diameter chosen to be the same regardless of the particle type. The cutoff distance, $r_{cut}=\sqrt[6]{2}\sigma$, and the interaction parameter $\varepsilon_{LJ}=k_BT$ were selected for polymer-polymer, polymer-brush and brush-brush interactions. The value of the Lennard-Jones interaction parameter for the polymer-substrate pair was set to 0.05 k_BT and for the brush-substrate it was equal to 0.5 k_BT. The cutoff distance for these interactions was the same and equal to 2.5σ. This allowed us to have a higher friction coefficient between brush and substrate in comparison with that for polymer-substrate pair.

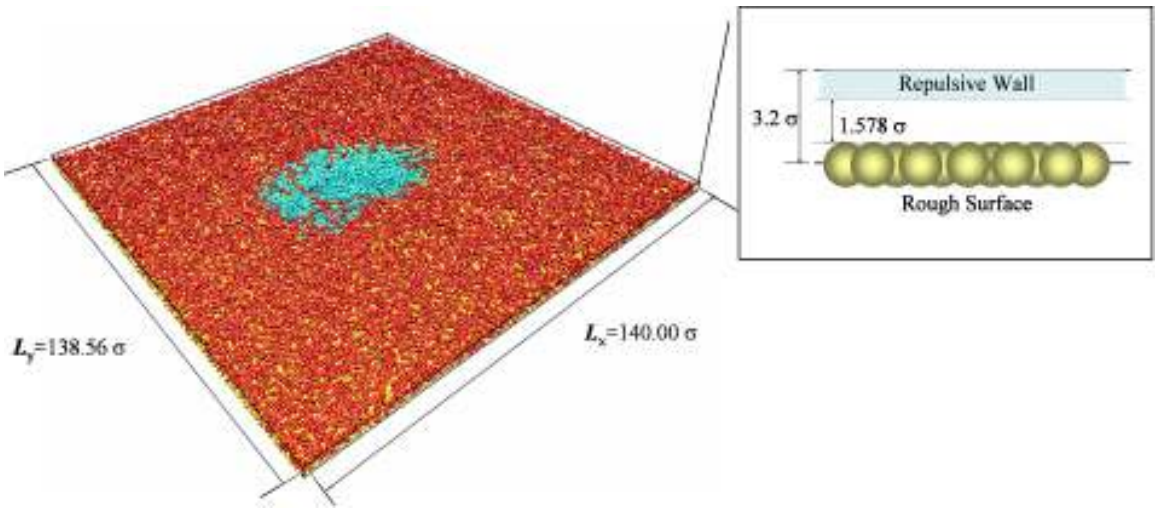

Figure 5.12 Simulation of brush on a surface. Snapshot of the simulation box with dimensions L_x, L_y and L_z. The brush molecule is shown in cyan and linear chains are colored in red. The beads forming a bottom substrate are shown in yellow. Inset shows the slice of the simulation box in *zx*-plane.

The connectivity of monomers to polymer chains and to brush molecules was maintained by the finite extension nonlinear elastic (FENE) potential:

$$U_{FENE}(r) = -\frac{1}{2} k_{spring} R_{\max}^2 \ln\left(1 - \frac{r^2}{R_{\max}^2}\right) \tag{5.15}$$

with the spring constant $k_{spring} = 30 k_B T / \sigma^2$, where $R_{\max} = 1.5\sigma$ is the maximum bond length. The repulsive part of the bond potential was modeled by the truncated shifted LJ potential with $r_{cut} = \sqrt[6]{2}\sigma$ and ε_{LJ} =1.0 $k_B T$.

The chains bending rigidity was introduced into the model through a bending potential controlling the mutual orientations between two neighboring monomers along the chain contour unit bond vectors $\vec{n}_i$ and $\vec{n}_{i+1}$

$$U_{i,i+1}^{bend} = k_B T\ K\left(1-\left(\vec{n}_i \cdot \vec{n}_{i+1}\right)\right) \tag{5.16}$$

In our simulations the value of the bending constant *K* was set to 4 for the side chains of the brush and the linear chains, and to 500 for the brush backbone. Two side chains were grafted to each monomer on the brush backbone. To maintain the orientation of the side chains with respect to the brush backbone we introduced a harmonic angle potential

$$U_{b-s}(\theta) = K_\theta\left(\theta-\theta_0\right)^2 \tag{5.17}$$

acting between backbone bonds and the first bond of the side chains with the equilibrium angle $\theta_0=\pi/2$ and the bending constant $K_\theta = 4k_BT/rad^2$.

The particle motion was described by the Newton's equations

$$m\frac{d\vec{v}_i(t)}{dt} = \vec{F}_i(t) + \vec{F}_{ext} \tag{5.18}$$

where $\vec{v}_i(t)$ is the particle velocity, and $\vec{F}_i(t)$ is the net deterministic force acting on i^{th} particle of mass *m*, and $\vec{F}_{ext}$ is a constant external force with magnitude $0.01k_BT/\sigma$ pointing along x-direction which models the effect of the constant pressure gradient across spreading film. The velocity-Verlet algorithm with a time step $\Delta t = 0.001\tau_{LJ}$ ($\tau_{LJ} = \sigma\sqrt{m/\varepsilon_{LJ}}$ is the standard LJ-time) was used for integration of the equations of motion (Eq. 5.18). To preserve hydrodynamic modes and maintain a constant temperature during simulation run we have implemented the velocity rescaling algorithm by rescaling the y and z-components of the particle velocity every 5 integration steps. The short integration step and frequent velocity rescaling allowed us to keep the system

temperature with 0.5% accuracy. All simulations were performed by using LAMMPS. All simulation runs lasted 2 10^5 τ_{LJ} with the finial 10^5 τ_{LJ} used for the data collection.

5.5.2 Simulation results. We first studied the effect of the side chain length on the velocity of the brush molecule. In Figure 5.13 we plot the dependence of the reduced brush velocity V/V_0 defined as the ratio of the velocity of the brush molecule *V* and velocity of the matrix chains V_0. The reduced brush velocity first decreases when increasing the degree of the polymerization of the brush backbone, then it reaches saturatation. Thus, there is a finite window of the brush backbone degree of polymerization where it is possible to achieve a separation of the brush molecules according to their length.

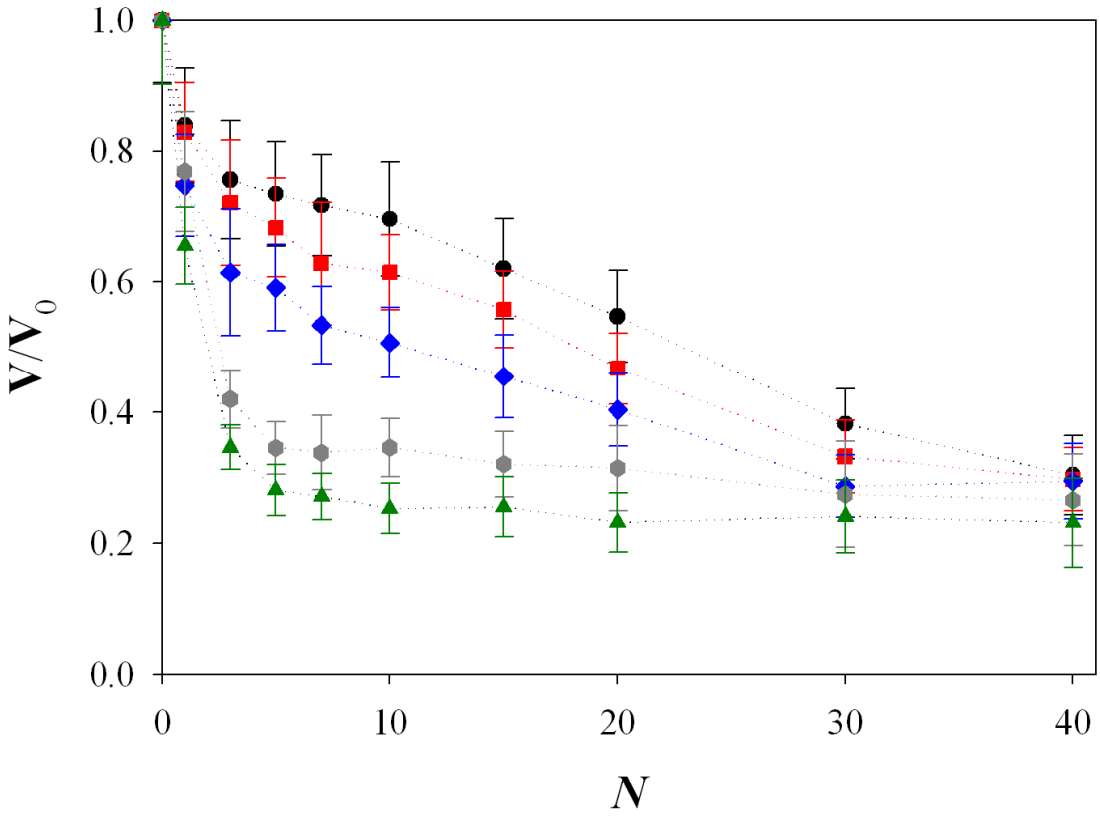

Figure 5.13 Degree of polymerization of backbone versus velocity. Dependence of the brush normalized velocity V/V_0 on the degree of polymerization of the brush backbone, N for brush molecules with side chain degree of polymerization n = 5 (●), n = 7 (■), n = 10 (♦), n = 20 (⬣), and n = 30 (▲) in a matrix of linear chains with the degree of polymerization m=30.

Another interesting feature that can be seen in this plot is the dependence of the reduced velocity on the degree of polymerization of the side chains, *n*. The reduced brush velocity decreases with increasing the length of the side chains. This could indicate that the reduced brush velocity is a function of the total chain molecular weight which is proportional to $2Nn$, however this strong dependence

on n is reduced at high aspect ratios. To test this hypothesis in Figure 5.14 we plot dependence of the reduced brush velocity on the parameter $2Nn$.

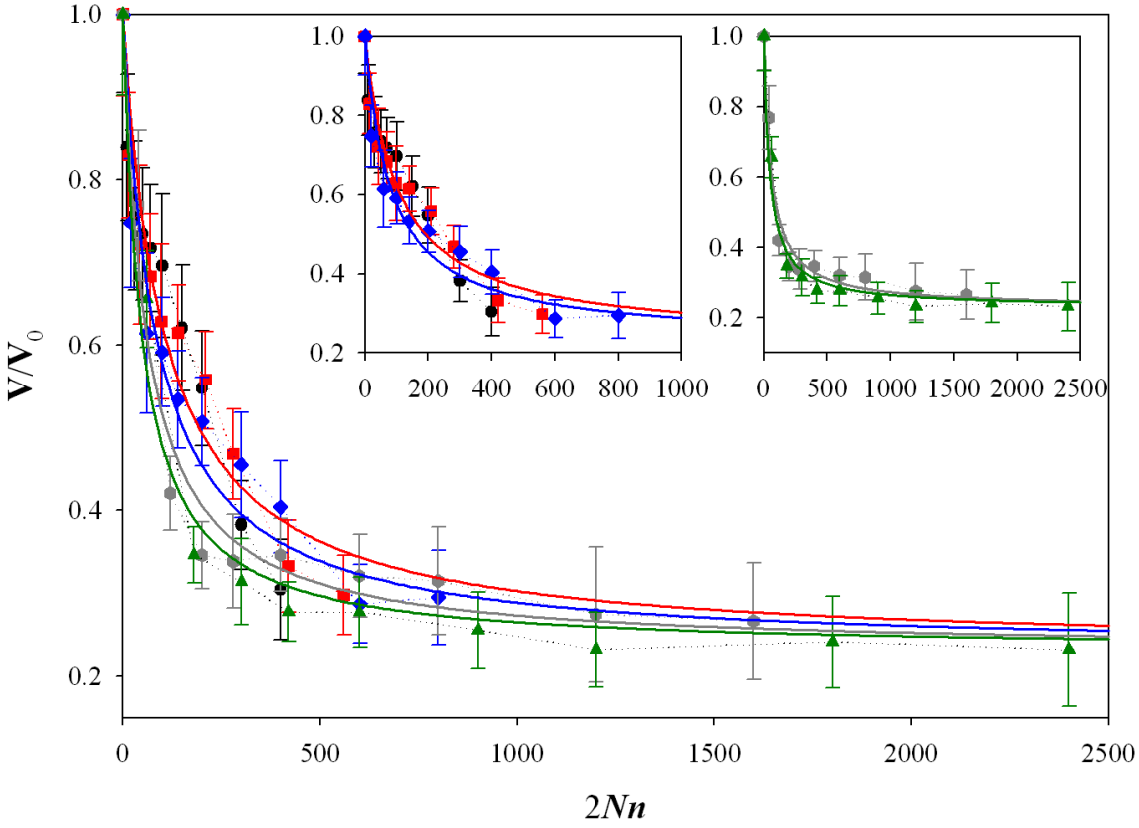

Figure 5.14 Normalized velocity versus brush area. Dependence of the normalized brush velocity V/V_0 on the total number of monomers in a brush $2Nn$ for brush molecules with the side chain degree of polymerization n = 5 (●), n = 7 (■), n = 10 (♦), n = 20 (●), and n = 30 (▲) in a matrix of linear chains with the degree of polymerization m = 30. The lines are best fit to the equation $\frac{V}{V_o} = \frac{2\beta(2nN)+\gamma}{(1+\beta)(2nN)+\gamma}$ where β = 0.13, γ = 117.3 (red line, n = 7), γ = 92.8 (blue line, n = 10), γ = 66.8 (grey line, n = 20) and γ = 53.4 (green line, n = 30).

One can identify two different groups of curves corresponding to the systems with n=7, 10 and n=20, 30 respectively. However, all sets of curves are approaching the same saturation limit. We can use eq A.8 to fit our simulation

data. The fitting parameters are within reasonable range. The value of the parameter β=0.13 for all systems. This value is close to the ratio of the values of the Lennard-Jones interaction parameters for brush-substrate and linear chain-substrate interactions (where β=0.1). The difference in the values of the parameter γ could be explained by the difference in the brush conformations (see Figure 5.150). For short side chains, the brush conformation is close to the ribbon, while the longer side chains show brush molecules with disk-like conformations (see Figure 5.15). Thus, the observed trend could be explained by the difference in the molecular conformations.

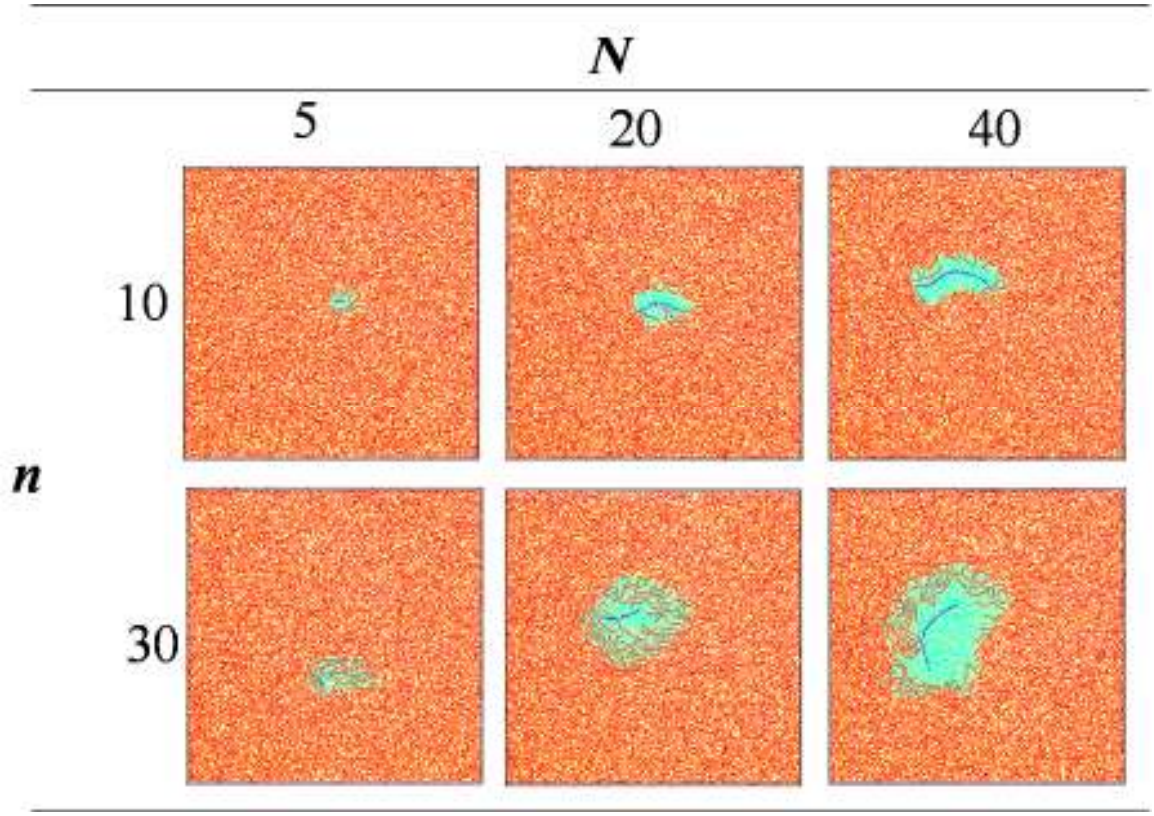

Figure 5.15 Polymer brushes under flow. Snapshots of the brush molecules with the backbone degree of polymerization, ***N*** = 5, ***N*** = 20 and ***N*** = 40, side chain degree of polymerization, ***n*** = 10 and ***n*** = 20 in a matrix of linear chains with the degree of polymerization ***m*** = 30.

To verify the applicability of the no-slip model to describe our simulation data in Figure 5.16, we show the average velocity profile relative to the frame of the moving brush molecule with the center of the coordinate system located at the brush center of mass. The flow stream lines around the brush are similar to those for a liquid flow around a fixed object. This flow exerts a drag force on the brush molecule coupling its motion with the motion of the surrounding fluid, suggesting there are components of model 1 in the analysis of the flow behavior of these brushes.

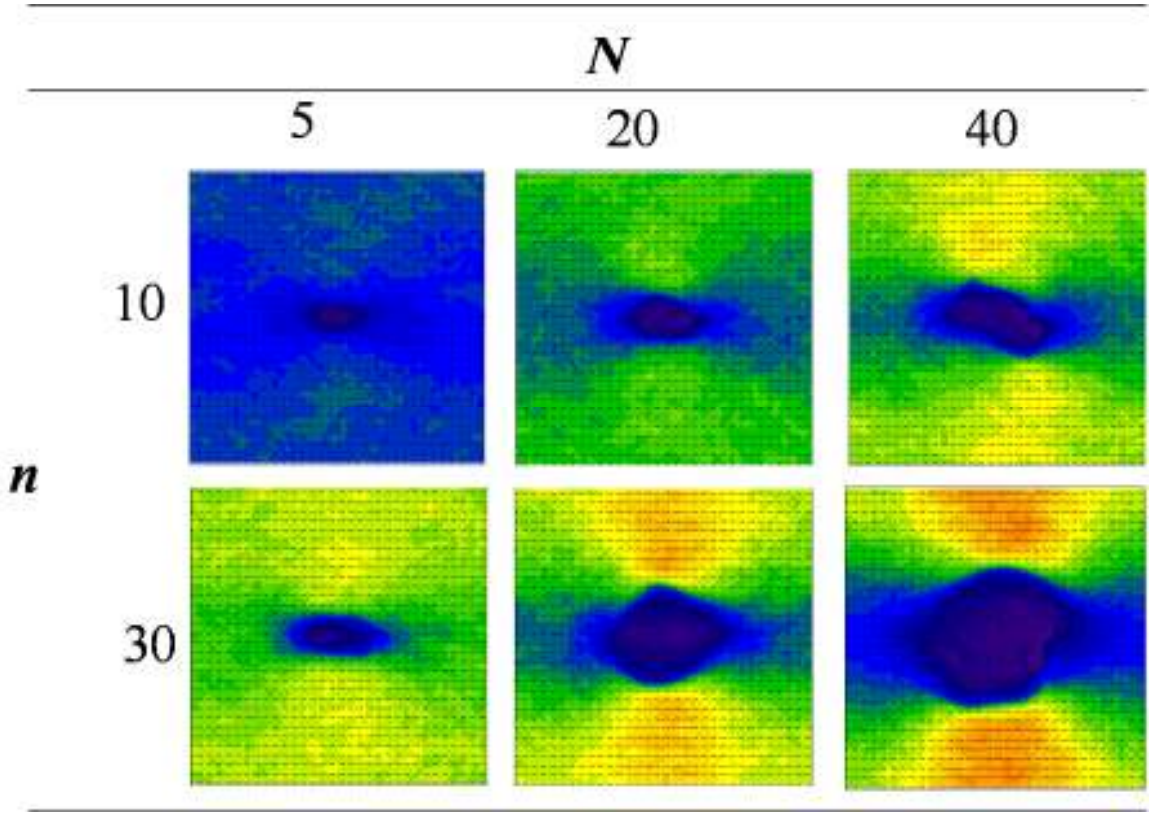

Figure 5.16 Velocity of matrix relative to brush. Velocity distribution around brush molecules with the backbone degree of polymerization, N = 5, N = 20 and N = 40, side chain degree of polymerization, n = 10 and n = 20 in a matrix of linear chains with the degree of polymerization m = 30.

5.6 Conclusions. We have shown that large polymer brushes tend to fractionate when they are spread in a linear matrix of polymers. Understanding the control of multiple component spreading films can lead to a better understanding for fields such as microfluidics and coatings, where spreading is an integral part of the technology. We have shown that the degree of the fractionation is related to both the frictions of the molecules and the linear matrix. This fractionation was controlled and the two different polymer brushes were separated from one another. In addition to the experiments conducted, computer simulations were used to verify this fractionation. The velocities of the molecular brushes were then related to that of the linear matrix through viscosity effects and from these relationships can be used to extract various physical properties of the films. The model was then tested by a system of longer brushes in a matrix of shorter brushes thus validating the model.

References

[1] Ginger, D. S.; Zhang, H.; Mirkin, C. A. *Angewandte Chemie International Edition* **2004***, 43*, 30-45.

[2] Hawker, C. J.; Russell, T. P. *MRS Bull* **2005***, 30*, 952-966.

[3] Bietsch, A.; Michel, B. *J. Appl. Phys.* **2000***, 88*, 4310-4318.

[4] McLellan, J. M.; Geissler, M.; Xia, Y. *J. Am. Chem. Soc.* **2004***, 126*, 10830-10831.

[5] Kleinbach, E.; Riede, T. *Chem. Eng. Process* **1995***, 34*, 329-337.

[6] Khan, H.; Fell, J. T.; Macleod, G. S. *Int. J. Pharm.* **2001***, 227*, 113-119.

[7] Pfohl, T.; Mugele, F.; Seemann, R.; Herminghaus, S. *ChemPhysChem* **2003***, 4*, 1291-1298.

[8] T.M., S.; S.R., Q. *Reviews of Modern Physics* **2005***, 77*, 977-1026.

[9] Zhang, H.; Mitsuya, Y.; Yamada, M. *J. Tribol.* **2002***, 124*, 575-583.

[10] Gans, B. -. d.; Duineveld, P. C.; Schubert, U. S. *Adv Mater* **2004***, 16*, 203-213.

[11] Xu, H.; Sun, F. C.; Shirvanyants, D. G.; Rubinstein, M.; Shabratov, D.; Beers, K. L.; Matyjaszewski, K.; Sheiko, S. S. *Adv Mater* **2007***, 19*, 2930-2934.

[12] Sun, F.; Sheiko, S. S.; Moeller, M.; Beers, K.; Matyjaszewski, K. *Journal of Physical Chemistry A* **2004***, 108*, 9682-9686.

[13] Sheiko, S. S.; Prokhorova, S. A.; Beers, K. L.; Matyjaszewski, K.; Potemkin, I. I.; Khokhlov, A. R.; Moeller, M. *Macromolecules* **2001***, 34*, 8354-8360.

[14] Xu, H.; Sheiko, S. S.; Shirvanyants, D.; Rubinstein, M.; Beers, K. L.; Matyjaszewski, K. *Langmuir* **2006***, 22*, 1254-1259.

[15] Sheiko, S.S.; Sun, F.; Randal, A.; Shirvaniants, D.; Rubinstein, M.: Lee, H.I.; Matyjaszewski, K. Nature, 2006. 440, 191-194.

[16] Xu, H.; Shirvanyants, D.; Beers, K.; Matyjaszewski, K.; Rubinstein, M.; Sheiko, S. S. *Phys. Rev. Lett.* **2004***, 93*, 206103/1-206103/4.

[17] Xu, H.; Shirvanyants, D.; Beers, K. L.; Matyjaszewski, K.; Dobrynin, A. V.; Rubinstein, M.; Sheiko, S. S. *Phys. Rev. Lett.* **2005***, 94*, 237801/1-237801/4.

[18] P. G. de Gennes, *Rev. Mod. Phys.* **1985**, 57, 827-863.

[19] Valignat, M. P.; Oshanin, G.; Villette, S.; Cazabat, A. M.; Moreau, M. *Phys. Rev. Lett.* **1998***, 80*, 5377.

[20] Matyjaszewski, K.; Xia, J. *Chem. Rev.* **2001**, *101*, 2921-2990.

[21] Sheiko, S.S.; Sumerlin, B.S.; Matyjaszewski, K. *Progress in Polymer Science* **2008,** 33, 759-785

[22] Matyjaszewski, K.; Tsarevsky, N.V. *Nature Chem.* **2009**, 1, 276-288

[23] Sun, F. C.; Dobrynin, A. V.; Shirvanyants, D.; Lee, H.; Matyjaszewski, K.; Rubinstein, G.; Rubinstein, M.; and Sheiko, S.S. *Phys. Rev. Lett.* **2007,** 99, 137801.

[24] Kim, C., Esker, A. R., Runge, F. E. and Yu, H.; *Macromolecules* **2006,** *39,* 4889-4893

[25] Persson, B. N. J.; *Sliding Friction:Physical Principles and Applications,* 2nd ed.; Springer: 2000; pp 261-262.

[26] Richards, S.; Fluid mechanics

Chapter 6

In Situ Studies of Flowing Polymer Chains: A Collection of Observations

6.1 Introduction. The spreading of polymer films on molecular length scales is a complex process. In addition to the displacement of the center of mass, long and flexible macromolecules change their conformation and orientation. They can also undergo segregation, disentanglement, and scission of covalent bonds. The spreading rate[1] may depend on the molecular weight,[2] conformation, and the density of surface defects.[3] To study these spreading processes on the molecular level, scientist have conducted molecular dynamics simulations.[4-6] However, these studies were all conducted in the theoretical realm and the results are based on assumptions of true 2D, where there are no crossings, and no surface defects. To verify and compliment these studies, it is important to conduct experiments which explicitly show molecules interacting with each other dynamically and in real time. There is no better way to do this then to capture movies of these molecules flowing and document their behavior as they proceed along a substrate.

In previous chapters, we investigated individual molecules in thin films that were in the stationary state, either prepared by the LB method or a stationary film after spreading (*ex-situ*). This chapter investigates spreading films while they are

in the process of flowing (*in-situ*). We image individual molecules as they flow and move in relation to one another, how they interact, and how they mix. We monitor and study a variety of phenomena only evident when molecular resolution is attained such as slip between molecules, flow mechanics of different brush conformations, dissociation of crosses, and scission of molecular brushes.

6.2 Experimental. To conduct *in situ* (real-time) imaging of individual molecules during a spreading process, several experimental parameters should be adjusted. First, one should use model molecules that allow clear resolution of the molecular contour. Second, the spreading rate should be slower than the scanning rate (the molecules most not move further then their size in consecutive frames). The AFM has a maximum capture rate of approximately 0.5 frames per minute, and to obtain a real time movie of the spreading process, the film must move slow enough to distinguish the movement of individual brushes from one frame to the next. In this case, this brush velocity is less than 100 nm/min. The former issue is resolved with our model polymer systems consisting of molecular brushes with a long backbone (N=7280, L≅2000 nm) and short side chains (n=10-30, d=10-30 nm). These model molecules are longer than their persistence length, i.e. relatively flexible, while stiff enough to allow fine resolution of the contour curvature, i.e. persistence length is larger that the tip diameter.

The second issue, was resolved by (i) using highly ordered pyrolytic graphite (HOPG) as a substrate which has a relatively high friction coefficient and

(ii) capturing images at later stages of spreading when films move slower (R^2=Dt), i.e. dL/dt~1/L~1/√t (velocity decrease with R and t).

A substrate must be chosen that has a friction coefficient high enough that the spreading process will be very slow, while maintaining a positive spreading coefficient. In using HOPG as a substrate, the spreading of polymer brushes, with PBA side chains, produces film velocities of up to 5 μm/min at short times, and much less at longer times. For the film to reach a velocity of 100 nm/min, the drop is deposited onto the substrate and imaging commences after a wait of approximately 8-12 hours. This allows for a sufficiently slow film to image, while capturing each individual image at a reasonable rate. For these experiments we collected images at times anywhere from 8 hours to 46 hours after the start of spreading.

The sample spread on HOPG is a two component system consisting of polymer brushes with different dimensions (Figure 6.1). The first brush, selected to model polymer chains, is a long brush with a back bone DP of 7280 and side chains with a DP of 50 (we call these the “long” brushes). The second brush was added to facilitate the spreading and has N = 500 and n = 35 (known as the “short” brushes). The differences in side chains allow for different height contrasts between the two brushes giving us the ability to distinguish them in our images.

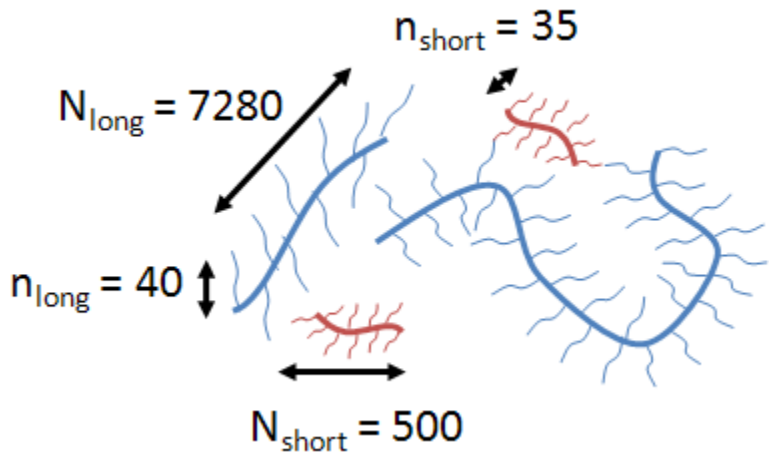

Figure 6.1 Schematic of brushes used for *in situ* experiments. There are two brushes present, known as the long (N=7280, n=40) and short (N=500, n =35) brushes. Their dimensions give them different properties and contrasts in the monolayer films.

6.3 Slip. Molecular slip, where fluids flow in direct contact with walls or surfaces, is an important phenomenon in applications. It is the reason we must rub our hands together to properly wash them and it is a very important component to the physics of lubricants. When a fluid flows past a surface it creates either a slip, non-slip, or a partial slip boundary.[7-9] If a surface is infinitely smooth, the velocity of the fluid will remain constant at all distances from the surface. However, when we introduce roughness to the surface, the velocity begins to slow close to the surface (Figure 6.2). This makes it easy for air to blow large objects off surfaces because they extend into the high velocity region of the flow, while small objects whose profiles are close to the surface only experience a slow moving fluid and thus low drag force. This effect prevents flowing water alone to take away the soap and dirt on our hands, creating a need to rub them together while washing them.

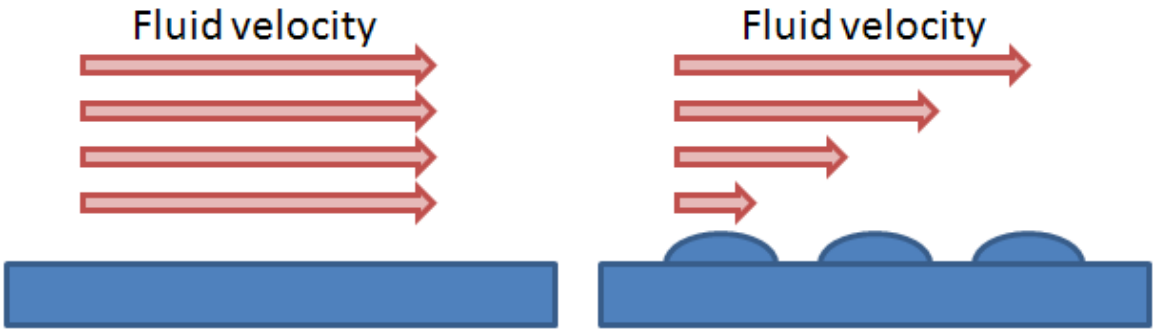

Figure 6.2 Fluids flowing over smooth and rough surfaces. Fluid velocity profiles for a smooth surface (left) and a rough surface (right). The smooth surface exhibits slip while the rough surface has a non-slip surface.

The velocity of a fluid at the surface interface is known as the slip velocity (V_{slip}). If the V_{slip} = 0 (slip length = zero), it is said that the fluid is non-slip, while the other extreme occurs when V_{slip} is equal to the velocity of the bulk fluid far from the surface (slip length = infinity). This is known as the complete slip case. In reality, most fluids possess a partial slip which can be quantified by both the slip velocity and the Navier slip length (Figure 6.3). The slip length is described as the length needed past the surface to extrapolate the velocity profile of the fluid to zero. The two extreme cases would have V_{slip} = 0 and a zero slip length and where V_{slip} is equal to that of the film there would be an infinite slip length.

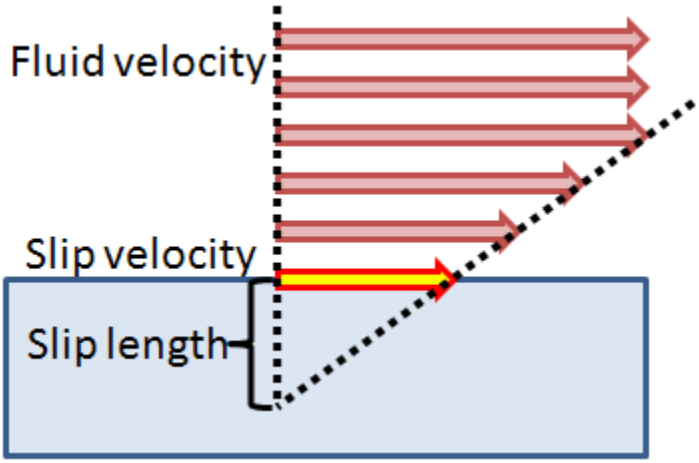

Figure 6.3 Slip parameters. Velocity profile for a fluid exhibiting partial slip. The velocity far from the surface is the bulk fluid velocity, the velocity at the surface is known as the slip velocity and the depth in the surface where the velocity extrapolates to zero is the slip length.

We have touched on the concept of slip in chapter 5 when we developed models of flow-induced fractionation. In that chapter, we made assumptions about a finite slip between the linear matrix and the individual brush molecules. However, the limited capabilities of our experimental set up prevented us from verifying our conclusions. However, by visualizing each of the individual molecules as they flow along a surface, we can directly measure the slip that occurs when these molecules flow past molecules of different types which move at different speeds. The slip exhibited by these flows is quantified below.

When we spread our brushes, the long brushes travel at a higher velocity then the short brushes (to be discussed in Section 6.4). This difference in velocities causes the brushes to flow past each other as if there were two separate surfaces. Since we can image individual molecules, this is a good opportunity to directly observe the slip phenomenon between the two types of

brushes. Figure 6.4 (top) shows the longer brushes flowing past a group of marked shorter brushes. These brushes were selected because they are stacked in an arrangement perpendicular to the faster moving brush. As time progresses the small brushes position doesn't change relative to one another, i.e. all short molecules move with the same velocity (non-slip). This is shown in Figure 6.4 (bottom). However, the short molecules move faster relative to longer molecules (finite slip). The relative difference in velocities between the short and long brushes decreases over time. This effect is simply due to the long brush catching up with the edge of the film and thus slowing to the velocity of the film front (which the short brushes move with). The effect of the brushes flowing at different velocities is discussed in section 6.4.

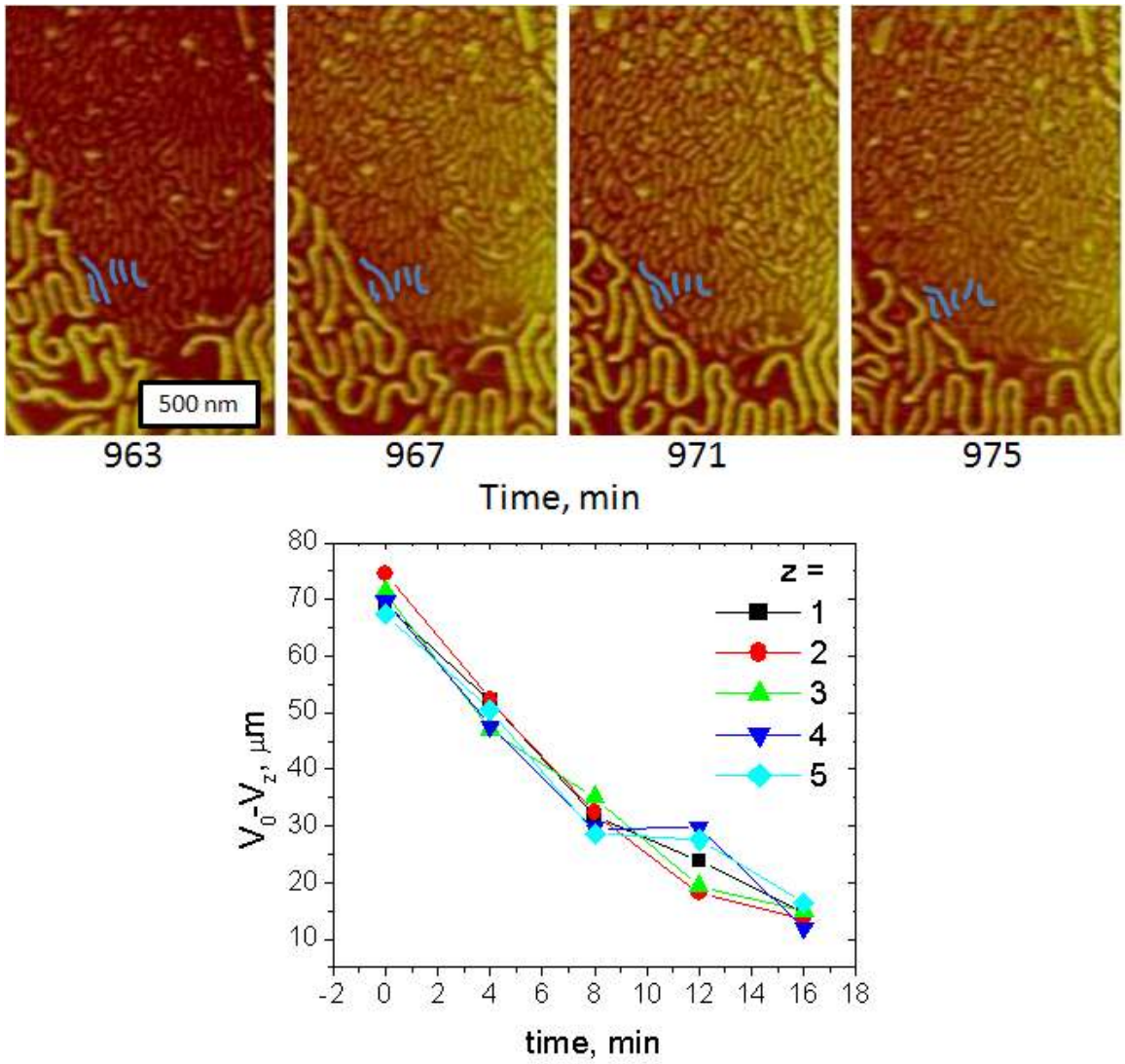

Figure 6.4 Molecular slip. Top. Long brushes flow past short brushes (labeled in blue). Bottom. The velocities of the different short brushes relative to the velocity of the long brushes. The brushes flow from top to bottom of the images.

This result is of great consequence when we consider the architecture of a microfluidic chip. As the feature size on the chips become increasingly small, slip on macromolecular length scales (10-100 nm) will become more and more

important. At these length scales, the slip length can be on the order of the size of the channel, meaning the flow of the fluid will be directly impacted by the slip. The verification and direct visual observation of the slip of these polymer brushes[10] can have a direct impact in the field of microfluidics as technology pushes the size of microfluidic chips to become smaller.[11]

6.4 Effects of conformation and brush size. As mentioned above, one of the unique features of polymer molecules is that they can change conformation. They also can change conformation during flow due to the variation in the film pressure. In their turn, conformational changes may lead to the corresponding variations of the friction coefficient. In other words, the same molecule adopting different conformations may flow (or spread) with different velocities. In previous studies,[12] we have shown that flow-induced conformational changes (cylinder-ribbon transition) cause fingering instability. These studies have been conducted with one-component polymer melts. Here, we study the spreading of mixtures of two different molecular brushes (N_1=7280 n_1=40 N_2=500 n_2=35 in a ratio of 1:9 by weight of brush numbers one to two respectively). Studying the spreading of mixtures is important to the field of microfluidics, where channels are routinely used to separate and combine mixtures of particles.[13] We observed a unique phenomenon: individual molecules of type 1 got extracted from the mixture as they undergo the conformational transition.

As shown in Figure 6.5, we see two separate regimes emerge inside the film within our spreading film. At high pressures (i.e. closer to the drop), molecules adopt a cylindrical shape which makes molecular resolution nearly impossible. As such, one usually observes a dense film since individual molecules cannot be resolved. At lower pressures (with increasing distance from the drop), the side chains of the brushes adsorb onto the surface leading to a ribbon-like conformation. In this conformation, molecules move faster causing the so-called fingering instability.

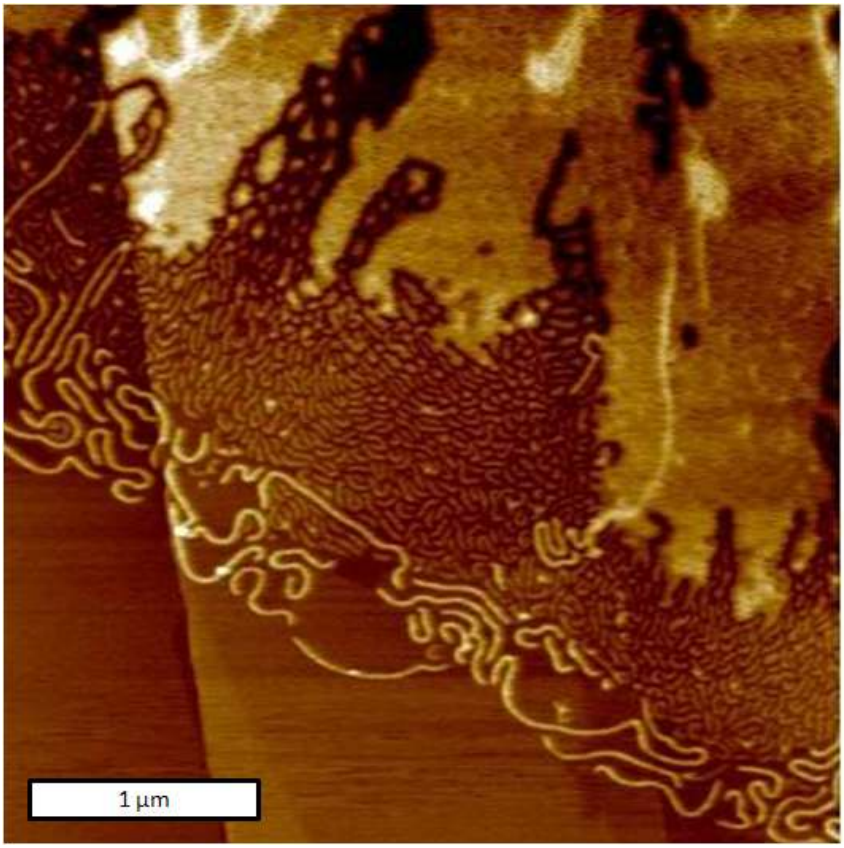

Figure 6.5 Polymer film snapshot. Image of a polymer film spreading on graphite. A high pressure conformation of the film is on the top of the image while a low pressure conformation is near the bottom.

As we spread the two component system, we see some unusual and unexpected features emerge. The most obvious is the ejection of the long brushes from the high pressure area of the film (Figure 6.6 top). We are able to track the speeds and positions of these ejected long brushes (Figure 6.6 Bottom) and we see as the 'blob' of brushes approaches the font of the film it begins to slow until it reaches its position in the front of the film. As seen from the images, there is an exclusive population of long brushes at the lead edge of the film, indicating that this phenomenon has been repeating itself many times during the course of the spreading.

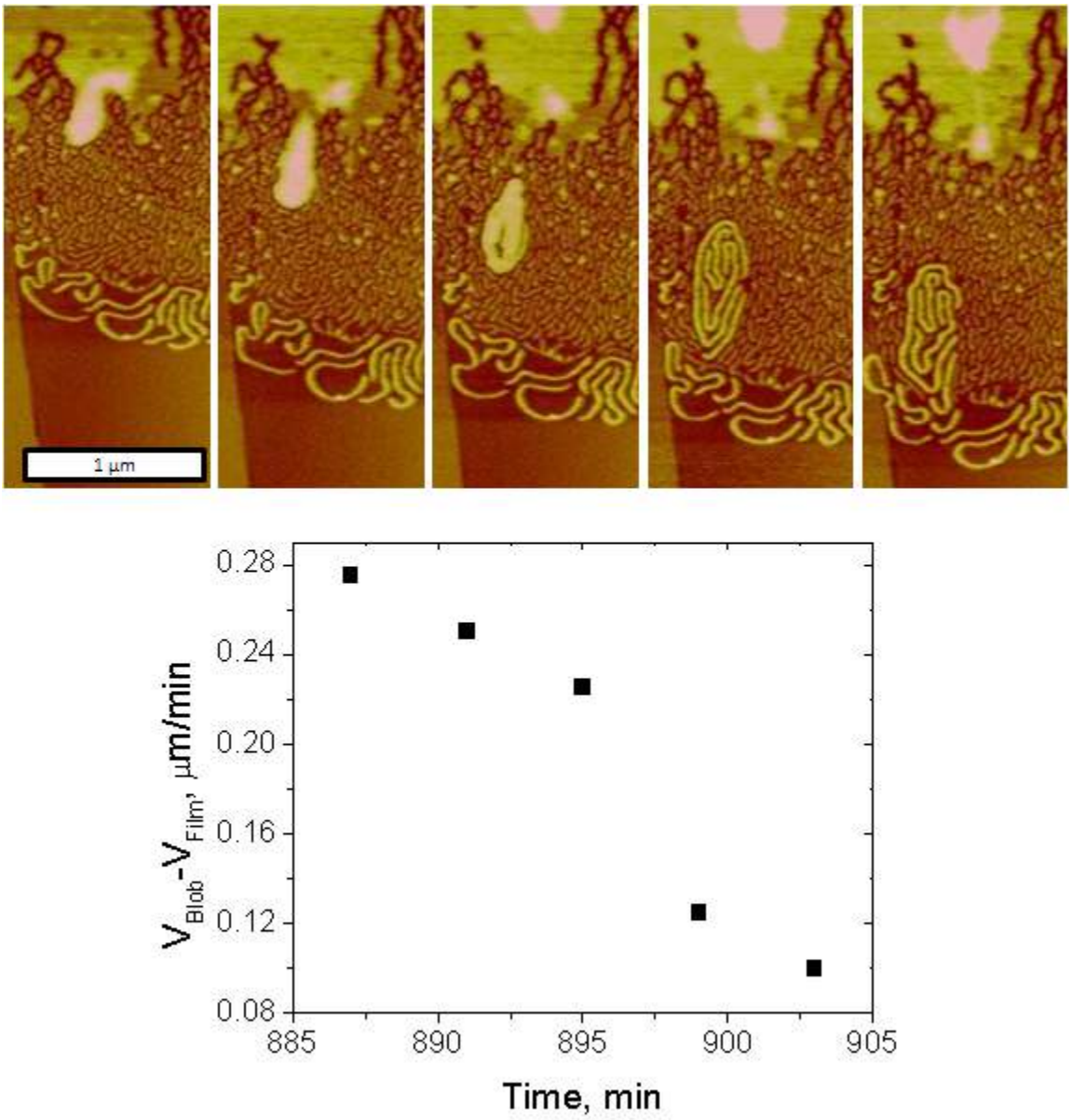

Figure 6.6 Long brushes leaving high pressure film. Top**.** A faster moving collection of long brushes being expelled from the high pressure region of the film. Bottom. The velocity of the expelled molecules relative to the edge of the film.

We now focus on the mechanism that causes these brushes to move at different rates. Is there a fundamental difference between the two brushes that cause them to slide with different velocities? To check this, we first measure the spreading rate, D, for each individual brush. We have found that D = 4 and 6 +/- 2 μm^2/min for the short and long brushes, respectively. Although this shows the longer brushes spread faster, it does not compare to the spreading rates in the mixture, which were found to be 40 and 4 μm^2/min for the blobs and the film, respectively. We double check the spreading of adsorbed brushes by spreading the melts at long time periods. This allows for enough time after the transition for the brushes to reach an equilibrium conformation. Figure 6.7 (top) shows the progression of a film moving very slowly at long times (24 - 48 hours of spreading). The longer brushes in the film move with the short brushes surrounding them. This is verified in Figure 6.9 (bottom) where we monitor the position of select brushes in relation to the film edge. At long times, these distances remain constant indicating that short and long brushes have the same friction and thus the differences in friction of the blobs leaving the high pressure region is not due the brush architecture.

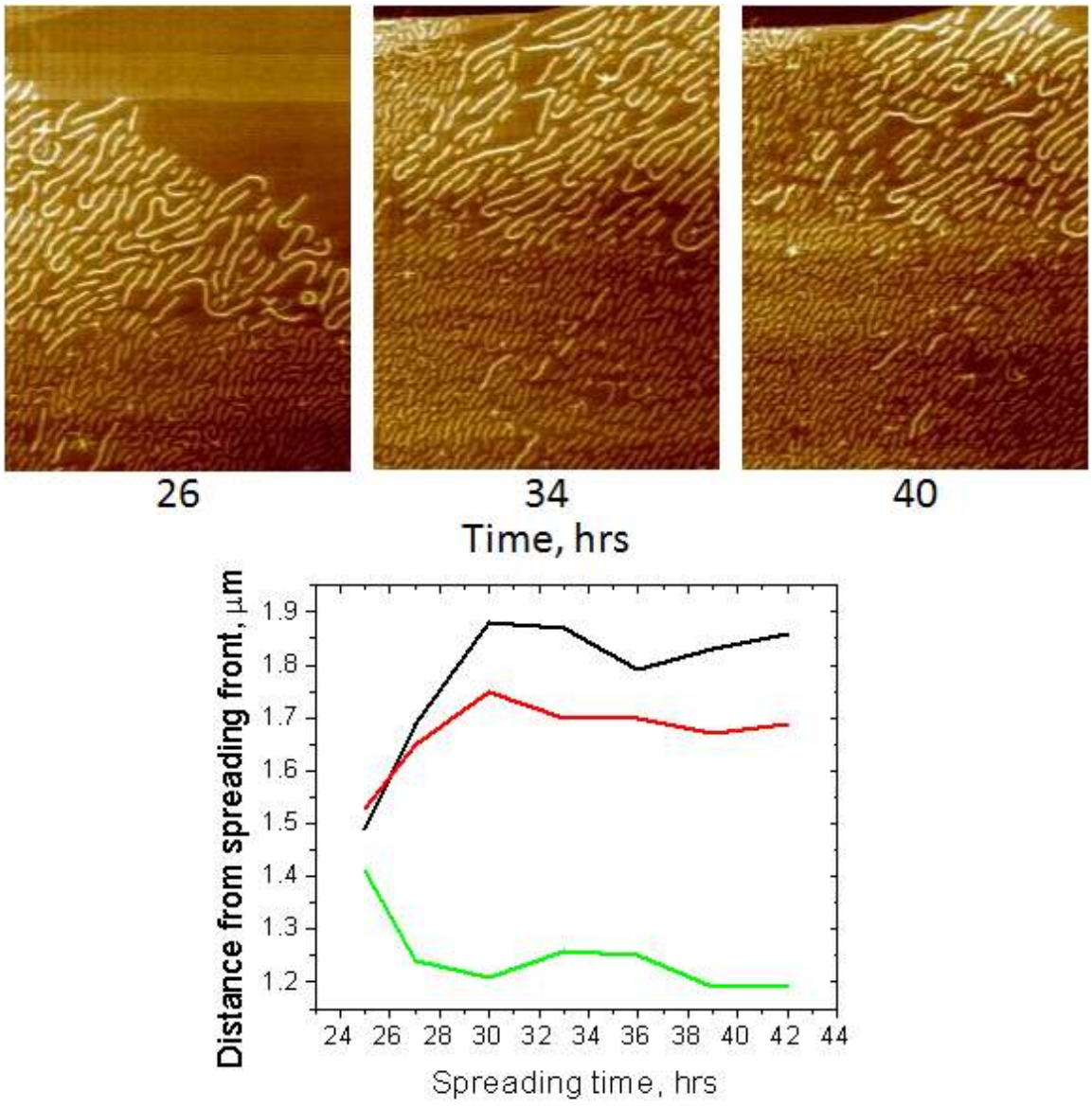

Figure 6.7 Long and short brushes flowing with the same velocities. Top. A flowing film of brushes which was adsorbed to the surface of HOPG for an extended period of time. Bottom. The distance of selected brushes from the edge of the film at various times.

We now analyze the nature of these films in each region. We have studied the low pressure region extensively and have determined that it consists of brushes adsorbed to the surface. The high pressure region is not as

straightforward. Upon first examination, it is reasonable to hypothesize that this film could either consist of a multilayer film or just a dense layer of compressed brushes. The multilayer structure implies that longer brushes are ”riding” on top of the monolayer of shorter brushes. To separate the two structures, we must determine what happens as the brushes make the transition from the high to low pressure regime: do they slide off the underlying layer, or do the side chains adsorb onto the surface and spread out?

Figure 6.8 (bottom row) shows the progression of the high pressure layer moving into the low pressure region. If the transition is a top layer of brushes sliding off its bottom layer, it is reasonable to assume that the top layer should be able to slide independently on top of the brushes, that is, it is riding on top of at least one more layer of brushes. However, we can see the dense film is physically moving with the same velocity as the adsorbed brushes. This observation suggests that the dense film does not slide on top of the adsorbed film. We then turn to an observation made where we see a single lone brush leave the dense film (Figure 6.7 top row). These images show a brush confined to both states in the dense layers of cylindrical and ribbon-like brushes. Again the brush fails to glide on top of the absorbed layer suggesting that it only undergoes a conformation change.

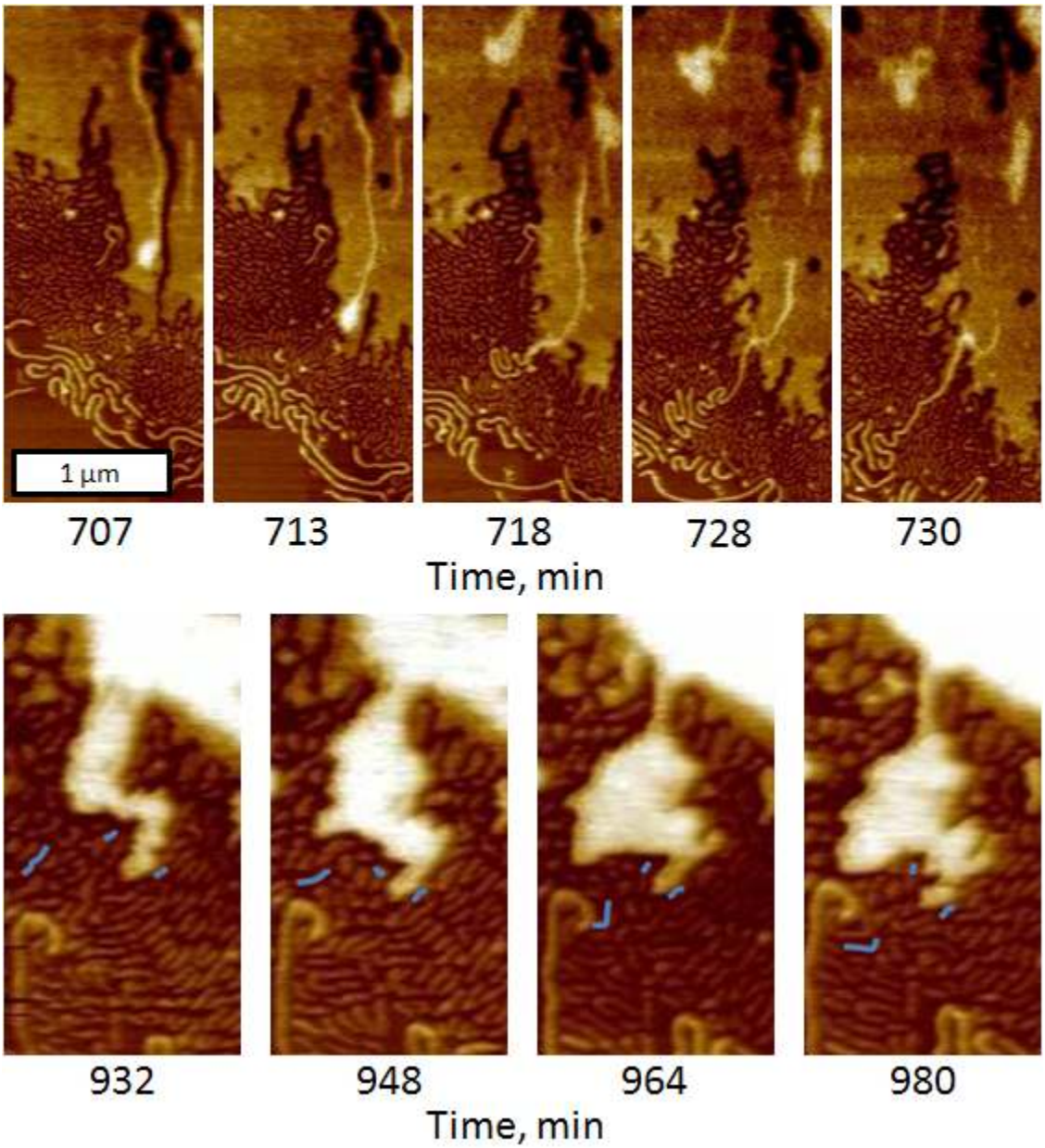

Figure 6.8 Brush transitions. Top. A lone brush being expelled from the high pressure region to the low pressure region. Bottom. Part of the high pressure region pushing around the brushes in the low pressure region.

The strongest evidence of the nature of these films is found by analyzing the heights of all the film layers in the film. Inside the high pressure region of the film, we observe terraces within the film (Figure 6.9 top left), and including the

long and short brushes, we observe four separate structures in the film: short (1) and long (2) brushes adsorbed to the surface in the low pressure region along with low (3) and high (4) terraces in the high pressure region. Upon completion of the height measurements of the four structures, we find that the heights of the low (4.1 nm) and high (5.5 nm) terraces are roughly double the heights of the short (2.2 nm) and long (2.8 nm) brushes respectively. When we factor in the previous measurement that when brushes are in the adsorbed state only about half the side chains are absorbed to the surface,[14] these results begin to suggest that the transition is simply brushes in a monolayer undergoing a conformational change. Figure 6.9 (bottom) shows a cartoon of the various conformations of the brushes in the film and their heights. It documents both the adsorbed conformation (on the left side) and the cylindrical high pressure conformation (right side). The adsorbed conformation is the same conformation discussed in earlier text while the cylindrical conformation can be viewed as a 'pipe cleaner' resting on the surface. We verify these conformations by imaging a high resolution image of the high pressure layer (Figure 6.9top right) and observe the individual chains with much smaller spacing in between them.

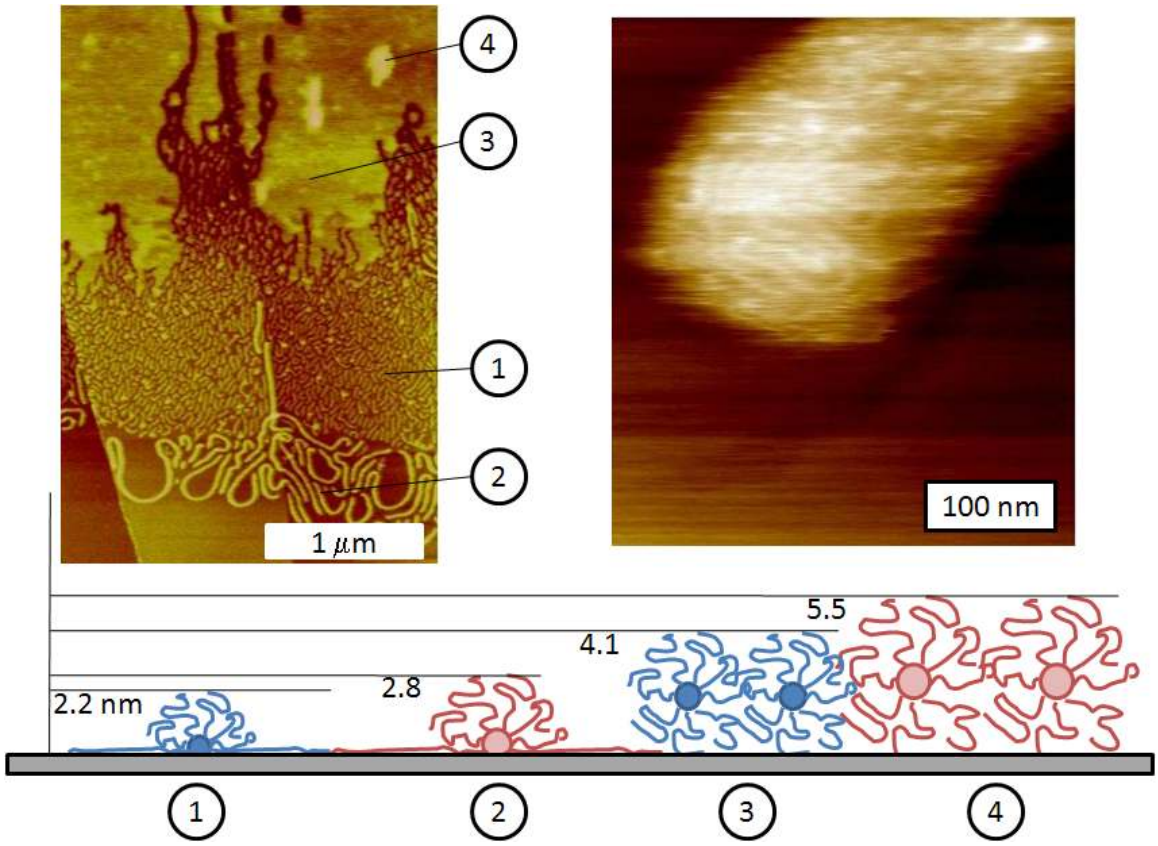

Figure 6.9 Brush conformations in film. Top left. An image from the film showing the two architectures of brushes (N=7280, n=50 and N=500, n=35) along with the two heights of terraces in the high pressure region. Top right. A close up of a terrace in the high pressure region. Upon close inspection the individual molecules that make up that terrace are visible. Bottom. A cartoon of the various conformations of the molecules in the different regions of the film. The heights given are the heights of each molecule from the surface to the top of the brush.

We conclude that the ejection of the longer brushes followed by their difference in velocities through the film is related to the conformation. As we learned in chapter 5, the brushes have friction coefficient two orders of magnitude greater than the linear polymer when spreading on mica (ξ=2.1x10^8 N·s/m^3 for the brush and ξ=2.5x10^6 N·s/m^3 for the linear). In this HOPG system, we measure the frictions of the brushes to be .041 and .41 Ns/m^3 for the cylindrical

and absorbed (ribbon-like) brushes, respectively. The cause of this difference is currently unknown but there are two potential reasons for the higher friction coefficient in ribbon-like brushes: (i) a chemically different backbone is in contact to the substrate (rather than the side chains) in the case of the ribbon and (ii) the side chains change their orientation with respect to the substrate exposing different chemical groups. Both these sources are directly affected by the conformation of molecular brushes on the surface. As the longer brush leaves the high pressure region of the film, it must undergo a conformation change, which takes time. In this time the brush is still in a transient conformation, and thus will be moving with a different friction as the fully adsorbed (ribbon-like) brushes. The longer brushes may also undergo the conformational transition at lower pressures compared to shorter brushes.

6.5 Dissociation of crossed molecules. As stated in earlier chapters, the presences of crossed topologies in films can affect optical[15] and surface properties[16] of monolayer films. We have observed spreading of crossed molecules on mica and have not observed a measurable amount of dissociation for any type of brushes while flowing. The opposite is true when spreading these molecules on graphite in the presence of many surface defects (terraces, disclinations, and holes). Figure 6.10 shows the dissociation of brushes during flow on a HOPG substrate. As observed, the brushes move together and one can see the overlaps sliding around until they become disentangled.

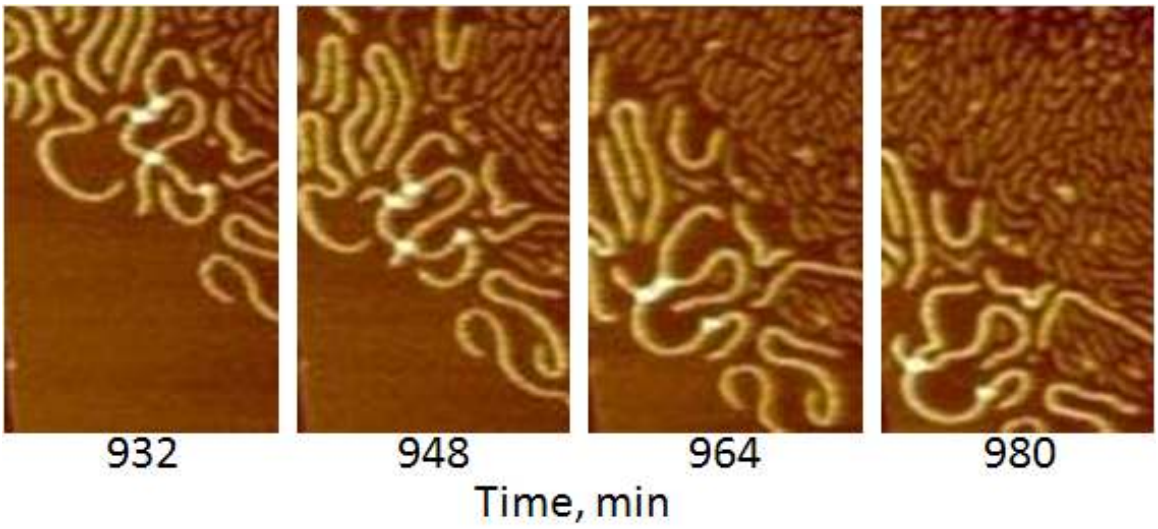

Figure 6.10 Cross dissociation. Crossed brushes dissociating during flow.

This dissociation on HOPG leaves a bit of a mystery. We observe crossed brushes dissociating very readily when they spread on graphite but we don't see any evidence of the phenomenon during the spreading on mica. This can be attributed to the differences of friction the brushes have on the different substrates. The friction coefficients were determined to be $\xi=1x10^{8}$ and $\xi=1x10^{13}$ Ns/m^3 on mica and HOPG respectively where as the friction between the brushes was determined to be $\xi=1x10^{9}$ Ns/m^3. This leaves us with two separate conditions when we examine crosses: the brush-brush friction is greater than the brush substrate friction or the brush-brush friction is less than the brush substrate friction. Small variations in friction, combined with the spreading induced diffusion[17] allow for the brushes to dissociate more readily when they spread on a HOPG substrate. In other words, we expect dissociation to occur when the variations in the friction force between the brush and the substrate overwhelm the brush on brush friction force. Although we cannot directly measure the

microscopic variations in this friction, it is not unreasonable to assume that they are greater than 0.01% (the value needed for the brush-HOPG friction variations to overtake the brush-brush friction. For the dissociation to occur on mica it would be necessary for the variations in the brush-substrate friction to be 10 times the value of the friction value.

We have also observed a crossing of molecules, an event we believe to be rarer than the dissociation of crossed molecules. Defects in the surface cause molecules to become pinned and when a molecule approaches this pinned molecule in a perpendicular orientation it can be forced onto the molecule and create a crossing (Figure 6.11 top). There is a force associated with the crossing of the brushes. When we plot the brush length during the time period when it becomes crossed, we see an extension of the brush. This extension puts an added tension on the brush and under the right conditions could possibly cause it to break. In this case, the friction with substrate is infinite (pinned molecule) or much larger compared to brush-brush friction causing formation and dissociation of crosses. If the brush-substrate friction much lower (mica + RH), then all molecules including crosses move with the same velocity (plug flow) hindering dissociation.

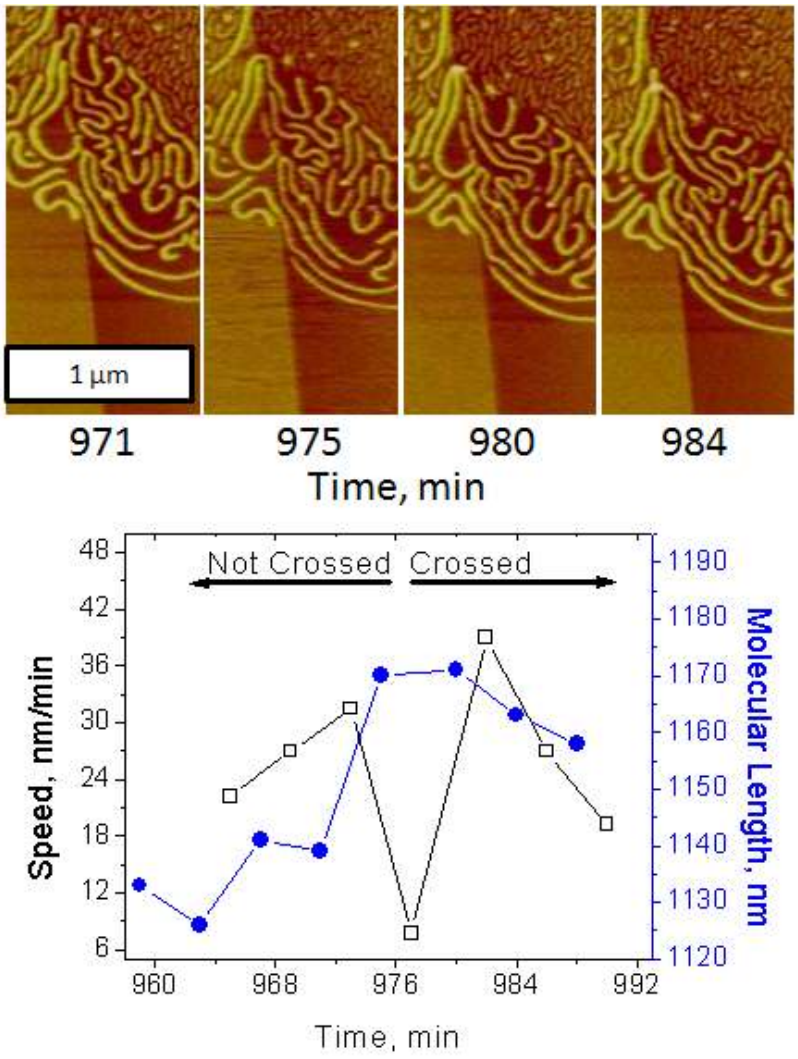

Figure 6.11 Brushes becoming crossed. Top. Two brushes becoming associated during flow. Bottom. The velocity (—□—) and molecular length (—●—) of the brush as it flows. The time where the brush becomes crossed is labeled with the arrows.

6.6 Scission. The architecture of these polymer brushes causes a tension on the backbone of these brushes. In our group, it has been previously observed that molecules with long side chains break when they are adsorbed onto a surface.[18-20] Figure 6.12 demonstrates the scission of these molecules when they are adsorbed onto a 0.2 weight % propanol in water solution. The brushes

slowly break (Figure 6.12 top) with a reaction rate of 2.3 x 10^{-5} s^{-1}. Over time, both their length and PDI decrease to the point where they reach equilibrium values (Figure 6.12 bottom). These molecules continue to break until they reach a minimum length where they adopt a star-like conformation and exert little tension on the backbone. The result is a film of molecules all below a critical length, $L_{\infty,}$ where the tension from spreading is not enough to break the backbone. Since the molecules are simply breaking, and not degrading, the total length is conserved in the film and the number average contour length can be found, $L = \frac{1}{\frac{1}{L_\infty} + \left(\frac{1}{L_0} + \frac{1}{L_\infty}\right)e^{-kt}}$, where L_0 is the initial contour length measured by AFM. For the data below L_0 = 496 nm and L_∞ = 40 nm. The breaking of the molecules can be induced by flow. Since the length of the side chains determine the reaction rate with the longest side chain breaking very quickly while brushes with very short side chains (n < 60) have not been observed to break at all.

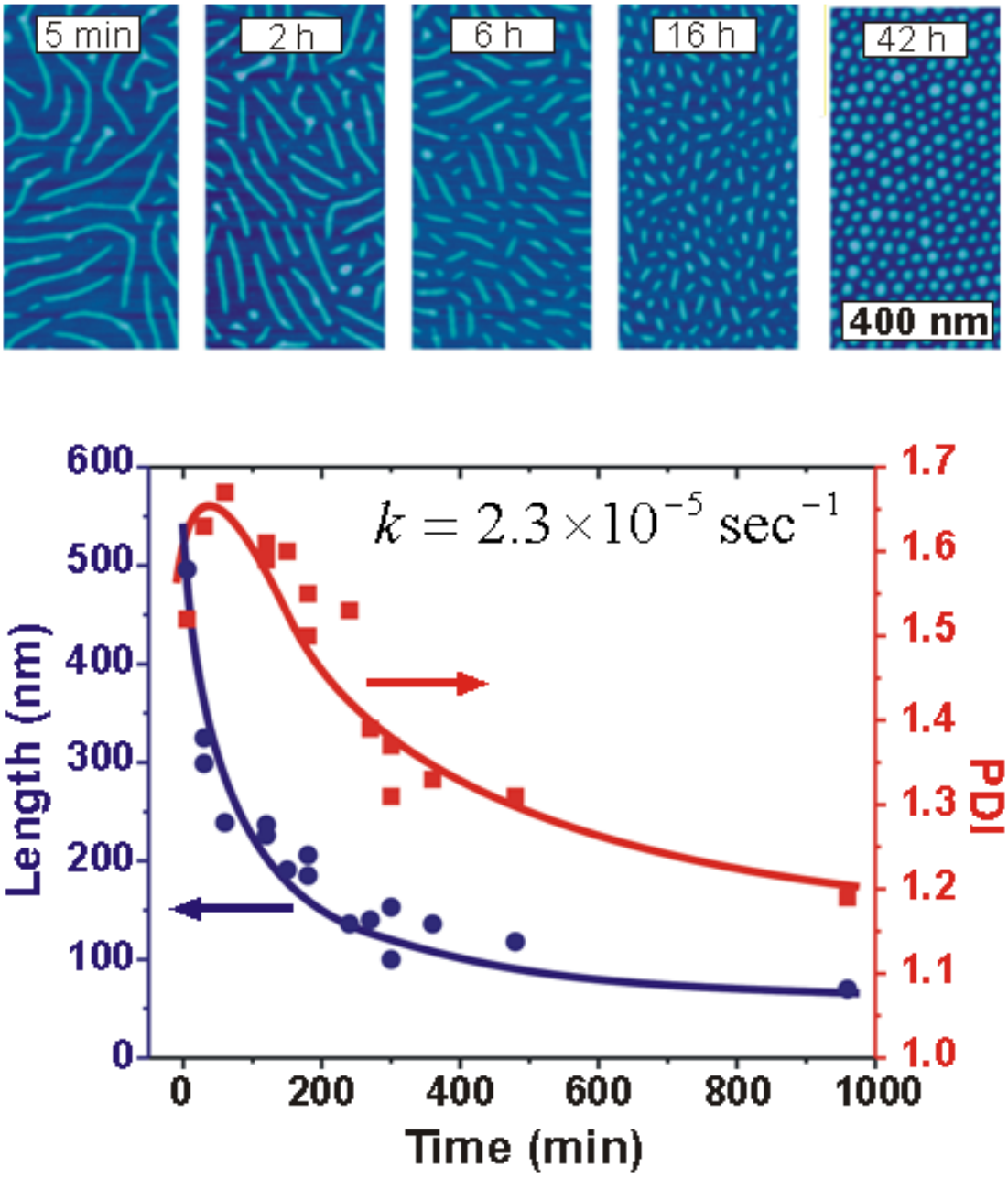

Figure 6.12 Scission of polymer brushes. Top. Images of brushes with long side chains n=140 that were allowed to sit on a 0.2 % w/w propanol water substrate for various times. Bottom The average lengths (●) and PDI (■) of those molecules as a function of time spent on the substrate. The solid lines are fits of the data.

Due to the lack of scission in the brushes with short side chains we were surprised to observe a flow induced scission when spreading the brushes with n = 50 (Figure 6.13 top). The brush is clearly pinned on a defect and then breaks as it flows. One interesting addition this observation makes to previous research is there is little apparent chain extension occurring before the breaking of the chain. Previously we have seen brushes with n = 35 extend up to 50 % of their size without breaking. However the brush observed here (n=50) becomes extended by less than a 2 % increase in length (Figure 6.13 bottom). This lack of extension could point to stong variations in the localized tension. For brushes with side chains of n=50 the average backbone tension is 1 nN while the force necessary for the backbone to break is 2.2 nN. This indicates that the single molecular spreading force can vary with some of the surface conditions. It is also worthwhile to note that some of the additional tension may have been added due to the fact that this particular brush has become pinned and the slip of the brushes has added friction and thus tension on the backbone.

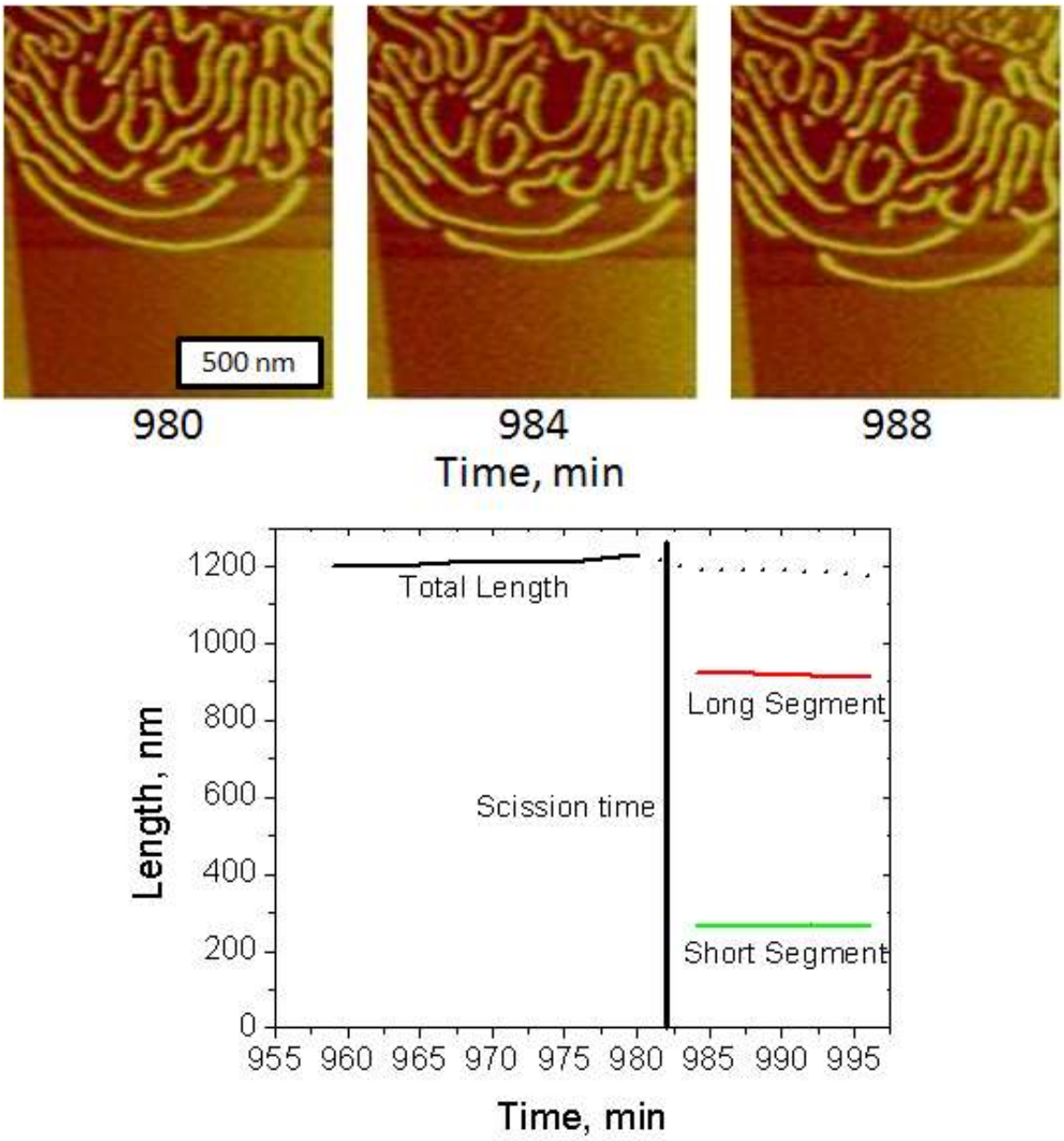

Figure 6.13 Real time scission. Top. Images of a brush undergoing scission. Bottom. The length of the breaking brush over time before and after it breaks.

6.7 Conclusions. In this chapter we have imaged the spreading of polymer films *in situ*. The movies obtained revealed many complex aspects of a spreading polymer film. Understanding these issues and phenomena lead to a more

complete understanding of how these thin films flow creating the opportunity to improve on their theory and applications. The following observations have been made:

1) The ability to visualize individual molecules during flow provides an opportunity to measure the degree of slip they undergo. We visualize a fast moving large molecule move past some slowly moving small molecules and there is no change in the velocity of those molecules, which indicates an infinite slip length.

2) The individual molecules transition from a high pressure region of the film to a low pressure region. The differences in friction between the conformations cause the longest molecules to travel out of the film faster than the shorter molecules as the spreading progresses. We have established that both the high and low pressure regions of the films consist of monolayers and we can visualize individual molecules transferring from one to the other. We conclude that the molecules move at a faster pace due to their cylindrical conformation and they gradually adsorb to the surface, causing a higher friction thus slowing down.

3) Contrary to the results discussed in Chapter 4, we have directly observed a dissociation of crossed chains. In addition to the dissociation of the chains we see them slide relative to one another as they flow. This is caused by the variations in friction between the brush-brush and the brush-surface interfaces. In addition to the dissociation of the crosses, we have also seen a creation of the crosses during certain circumstances. The creation of these crosses has a large energy barrier which is evident in the extension of the brush just before crossing.

4) For the first time we have directly observed individual molecules breaking as they flow. This is caused by the adsorption of the brushes side chains onto the surface causing a tension on the backbone. This occurrence happens more readily when the side chains of the brush are long. However we have also observed this scission event with brushes having short side chains where we have been previously unable to detect such changes. We also note that there is not a significant increase in the molecular length before scission, suggesting that the net tension on the backbone does not increase significantly.

The real-time *in situ* imaging of flowing polymer brushes clearly shows some of the complex dynamics that flowing thin films exhibit. The study of the individual processes that these films undergo can lead to a better understanding of physical properties, such as slip and molecular scission and also yield information about the equilibrium processes that progress during flow (cross dissociation).

References

[1] Cazabat, A.-M., S. Gerdes, M. P. Valignat, and S. Villette, *Interface Sci.* **1997,** 5, 129.

[2] Valignat, M.P.; Oshanin, G.; Villette, S.; Cazabat, A.M.; Moreau, M. *Phys. Rev. Lett.* **1998,** 80, 5377 – 5380.

[3] Prevost, A.; Rolley, E.; Guthmann, C. *Phys. Rev. B.* **2002,** 65, 064517.

[4] Cho, J.-H. J.; Law, B.M.; Rieutord, F. *Phys. Rev. Lett*. **2004,** 92, 166102.

[5] Qian, T.; Wang, X.-P.; Sheng, P. *Phys. Rev. E* **2003,** 68, 016306.

[6] Ren, W., W. E. Phys. Fluids **2007,** 19, 022101.

[7] Schowalter,W. R. *J.Non-Newton. Fluid* **1988,** 29, 25–36.

[8] Denn, M. M. *Annu. Rev. Fluid Mech.* **2001,** 33, 265–287.

[9] Léger, L.; Raphael, E.; Hervet, H. *Adv. Polym. Sci.* **1999,** 138, 185–225.

[10] Leger, L.; Hervet, H.; Massey G.; Durliat ,E. *J. Phys.: Condens. Matter* **1997,** 9, 7719–7740.

[11] Riehn, R.; Lu, M.; Wang, Y.-M.; Lim, S.M.; Cox, E.C.; Austin, R.H. *PNAS* **2005,** 102, 29, 10013.

[12] Xu, H.; Shirvaniants, D.; Beers, K.L.; Matyjaszewski, K.; Dobrynin, A.V.; Rubinstein, M.; Sheiko, S.S. *Phys.Rev. Lett*. **2005,** 94, 237801/1-4.

[13] Wang, M.M.; Tu, E.; Raymond, D.E.; Yang, J.M.; Zhang, H.; Hagen, N.; Dees, B.; Mercer, E.M.; Forster, A.H.; Kariv, I.; Marchand, P.J.; Butler, W.F. *Nature Biotechnology* **2004**, 23, 83.

[14] Sheiko, S. S.; Prokhorova, S. A.; Beers, K. L.; Matyjaszewski, K.; Potemkin, I. I.; Khokhlov, A. R.; Moller, M. *Macromolecules***2001**, *34*, 8354.

[15] Vroege, G.J.; Lekkerkerker, H.N.W. *Rep. Prog. Phys.* **1992,** 55 1241-1309.

[16] Matsudomi, M.; Kato, A.; Kobayashi, K. *Agric. Biol. Chem*, **1982,** 46 (6), 1583-1586.

[17] Xu, H.; Shirvaniants, D.; Beers, K.; Matyjaszewski, K.; Rubinstein, M.; Sheiko, S.S. *Phys. Rev. Lett*. **2004,** 93, 206103/1-4.

[18] Sheiko, S.S.; Sun, F.; Randal, A.; Shirvaniants, D.; Matyjaszewski, K.; Rubinstein, M. *Nature*, **2006,** 440, 191-194.

[19] Lebedeva, N.V., Sun, F.C.; Lee, H.-il, Matyjaszewski, K., and Sheiko, S.S.

J. Am. Chem. Soc. **2008,** 130, 4228-4229.

[20] Park, I.; Nese, A.; Matyjaszewski, K.; Sheiko, S.S. *Macromolecules* **2009,** 42, 1805-1807.

Chapter 7

Future Work: Control of Spreading Films

7.1 Introduction. The work presented thus far has focused on the study of individual molecules in thin films and their conformational and topological properties as they spread on a substrate. We have discussed how the film structure varies with preparation method, and how spreading affects the conformation of flowing macromolecules. However, in additional to the understanding of the spontaneous spreading process and equilibrium structure of thin films, it is equally important to study the control and manipulation of the flow rate, direction of flow, and molecular structure.

In microfluidics, researches use channels to confine, move and mix very small amounts of fluids.[1,2] Reactions on this nanoliter scale can be slowed, accelerated, or even altered by the presence of the channel walls and the mixing patterns present within the microfluidic channel. To understand this behavior it is necessary to understand how molecules mix and how they interact with each other in the presence of the channels. In the case of polymers, the size of these channels is reaching the size of the polymers themselves. These polymers undergo specific conformations in their melts with characteristic sizes. When they are forced into domains smaller than those sizes the properties are altered.

The control of the conformations and geometries of individual molecules in these films confined within narrow channels is also important. In order to properly exploit their properties such as alignment and surface tension, we must first study the effects of external fields (such as electric fields) and confinements have on molecular conformations, order, and topologies. The use of electric fields is a technique that is reversible, tunable, and switchable, making it an ideal method to explore in relation to the control of these molecular properties. In this chapter we begin to manipulate the molecules that make up thin films using electric fields. We show three possible approaches to the electric field manipulation of individual molecules in thin films: movement of the bulk drop, phase transition of a thin film, and alignment of individual molecules during flow.

To study the control of these thin films on the molecular level, we again turn to our model polymer system. The brush we use for these preliminary studies is one of our must durable samples. The geometry of this brush includes n = 35 and N = 500 and is shown in Figure 7.1.

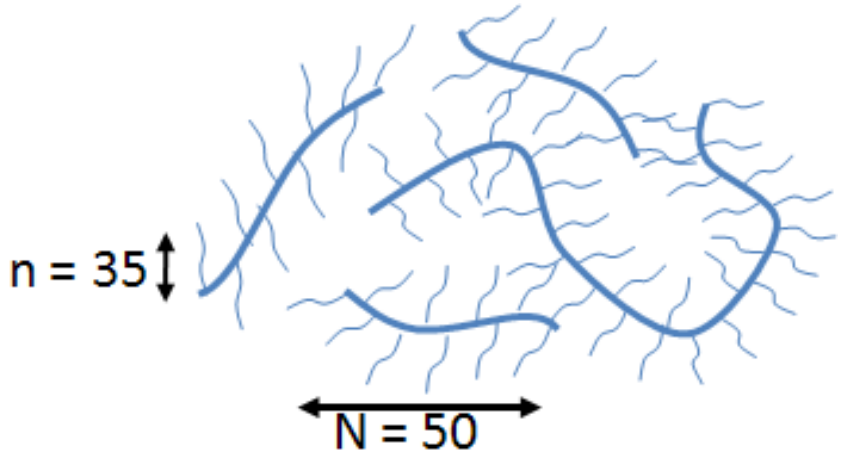

Figure 7.1 Diagram of polymer brushes. A cartoon depicting the polymer brushes whose dimensions are N=500 and n=35.

7.2 Spreading in channels. In the field of microfluidics, the forces existing between the fluid and channel walls are critical to the flow behavior. For example the degree of slip between the molecules and the channel walls can drastically alter the velocity profile of the fluid inside the channel. The confinement of polymers to spaces smaller than their molecular size begins to affect their bulk properties. For example, it is known that the confinement of polymer blends to films induces their miscibility.[3] Also, molecular dynamics simulations of polymers confined in spaces smaller than their radius of gyration slows the movement of the molecules,[4] and the dielectric properties of these thin films have been studied.[5] However, all of these techniques and experiments lack the ability to study the conformations and dynamics of the individual molecules as they relate to their flow inside small channels. It is our goal to study the conformation and orientation of model polymer systems confined to channels.

To confine brush polymers during their flow we create 2 dimensional channels using microcontact printing. This technique uses poly(dimethylsiloxane) (PDMS) stamps that are formed to molds to stamp patterns of self-assembled monolayers (SAM).[6] In our case, a PDMS stamp is used with 300 μm wide channels (Figure 7.2 left). A solution of dodecyltrichlorosilane in hexane (0.1 w/w%) is applied to the stamp drop-wise. The solution is allowed to evaporate leaving only the silane molecules behind. This stamp is then pressed to a clean sheet of mica and the silane is transferred to the mica surface (Figure 7.2). The stamp is then removed leaving behind periodically spaced regions of bare mica

and the silane SAM. The dodecyltrichlorosilane SAM has a lower surface energy than that of the mica and the resulting spreading coefficient, S, (the drop will not spread). This leaves a substrate with a series of well defined channels that will confine the flowing molecules.

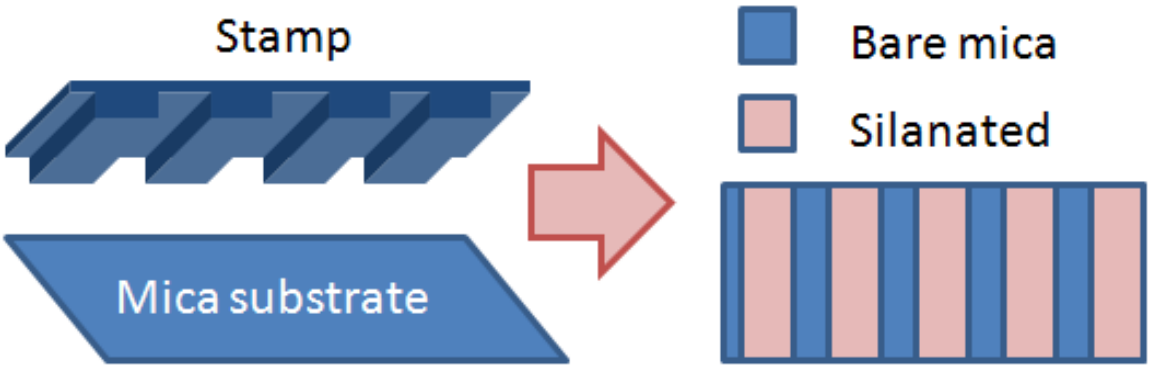

Figure 7.2 Schematic of microcontact printing. The PMDS stamp coated with dodecyltrichlorosilane (left) is pressed onto the mica substrate leaving a pattern of bare mica and silanated substrate. This effectively yields channels that are 300 μm wide for our polymer brushes to spread through.

We print the channels on cleaved mica and let PBA brushes spread on the patterned substrate (Figure 7.3 top). Figure 7.3 (bottom) shows the edge of the channel after spreading. One clearly sees the boundary between the silanated stamped area, and the region of the mica where brushes were able to spread. We can see that the defects in the channel edge are greater than the size of the molecules thus inhibiting our ability to scale the size of the channel down to the size of the molecules. To properly study the effects confinement has on these molecules as they flow, they must be able to freely flow through the channel, uninhibited by the defects along the walls. Considering that these defects are an order of magnitude larger then our molecules, this is not the case. We are

currently investigating methods to sharpen this edge. These include using a lower molecular weight PDMS to increase feature resolution on the stamp and building an ultra stable, force controlled platform to press the PDMS stamp to the mica.

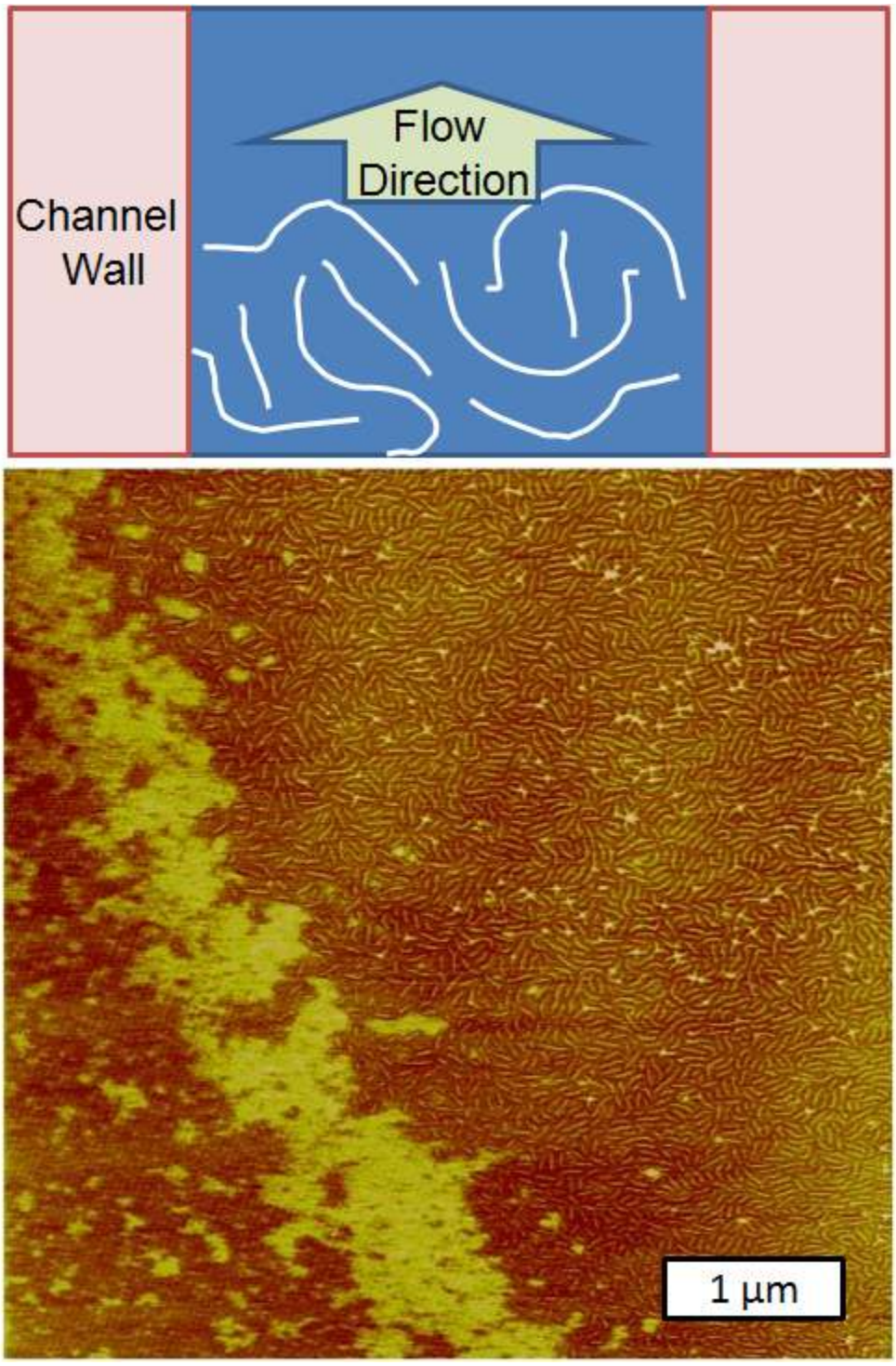

Figure 7.3 Images of the edge of a channel. Schematic of brushes flowing through a channel (top). Image of the channel (bottom). The right side of the image has brushes which have spread over bare mica while the left side of the image is the channel. Due to an accumulation of silane at the corners of the stamp, there is an excess amount of silane at the edge of the channel.

We print approximately 300 μm wide channels on our mica substrate and subsequently spread a 1 mm line of a polymer brush (N=500, n=35) melt in 97% relative humidity for 1 hr. Optical microscopy images are clearly able to see where the drop spread and where it did not: the bulk drop progressed in the areas where no silane was stamped (Figure 7.4). We have taken images at various positions at the edge of the film to determine the structure of the precursor film. In the images we see a clearly defined wall of silane which the brushes do not penetrate. The precursor film spread approximately 300 μm along the channel with the film spreading furthest at the center of the channel. Along the channel wall a sharp abrupt edge to the precursor film is visible. Unexpectedly we have also observed spreading over short distances (40 μm) in the areas where the silane was stamped. In this area, the precursor film appears to have pushed the silane causing it to build up at the precursor film silane interface. We suspect this is caused by a lack of binding sites on the mica, preventing a cross linked silane film from binding to it. This weakly bound film may be 'pushed' by the spreading brushes causing its edge to shift. This may also be a reason why there is a buildup of the silane at the channels edges. In attempts to correct this we have exposed the film to water vapor to induce a better cross linking and allowed the SAM more time to react and bind to the surface and itself. At this time, none of these attempts have proved successful.

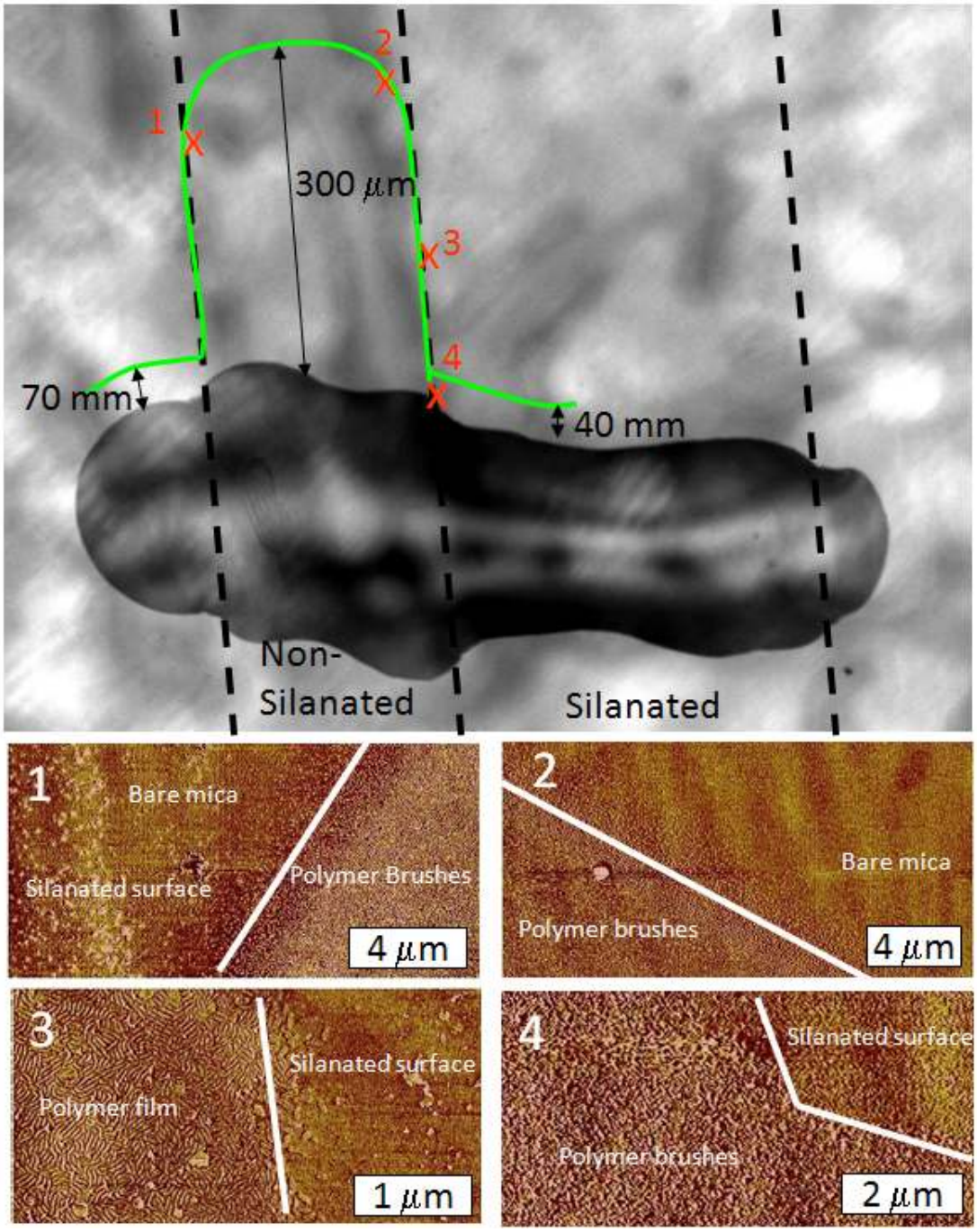

Figure 7.4 A linear drop spreading in a channel. The top picture is an optical microscopy image that shows a drop spreading in the bare mica channels along with the silanated area. The outline of the approximate location of the precursor film is traced in green. Images were taken at different locations in the film and are labeled in red. The corresponding AFM images are on the bottom half with the boundary of the polymer films outlined in white.

At this point in time we have not yet completed our goal to image these molecules in their thin films confined to channels. Technical problems prohibit the creation of channels which are on the same length scale as the molecules flowing through them as well as creating a strongly bound silane film to the mica. Each of these technical problems will be dealt with separately as this work progresses. First, the for mica we intend on using an agent, 1,1-diisopropylethylamine, to promote the chlorosilane binding to the mica.[7,8] Second, we intend on using a stamp made from a lower molecular weight PDMS. This will allow for higher resolution and sharper channel edges. We are confident that these steps will improve the quality of the channels that we create to confine our films.

7.3 Electric field manipulation of films and flow. Physically confining films to channels to direct their flow and conformation is only one method of molecular control. Another would be to control the molecular conformation and kinetics with external fields, such as electric fields. The manipulation of the wetting and spreading properties is a focus in the areas of dielectrophoresis,[9] electrowetting,[10] and electroosmosis.[11] When considering the movement of fluids, dielectrophoresis and electrowetting are closely related phenomena. They both rearrange fluids to maximize the stored electrical energy of the system.

The differences between electrowetting and dielectrophoresis are electrowetting manipulates conductive fluids (Figure 7.5 top) while dielectrophoresis manipulates dielectric fluids or particles (Figure 7.5 bottom).

We first consider the electrowetting scenario where we have a system that comprises of one fluid and one solid electrode, separated by a solid dielectric, thus forming a capacitor. This results in an energy minimization problem, balancing the electrical energy of the capacitor, $E_C = \frac{A_{sl}\kappa\varepsilon_0 U^2}{2d}$, where A_{sl} is the area of the electrode, U is the electric potential applied, κ is the dielectric constant of the material, d is the distance between the electrodes, and ε_0 is the permittivity of free space, with the change in surface energy $E_s = \Delta A_{sl}\sigma_{sl} + \Delta A_{sv}\sigma_{sv} + \Delta A_{vl}\sigma_{vl}$ where A indicates the area of the drop and σ indicates the energy per area of the interface with the subscripts sl, sv, and vl standing for the solid-liquid, solid-vapor, and vapor–liquid interfaces respectively. By balancing the energy gained by the spreading with the energy supplied by the electric potential, $\frac{A_{sl}\kappa\varepsilon_0 U^2}{2d} = \Delta A_{sl}\sigma_{sl} + \Delta A_{sv}\sigma_{sv} + \Delta A_{vl}\sigma_{vl}$, it then becomes possible to predict the final configuration of the drop. This approach assumes that the surface energies are voltage independent of electric potential and there is a negligible fringe electric field.

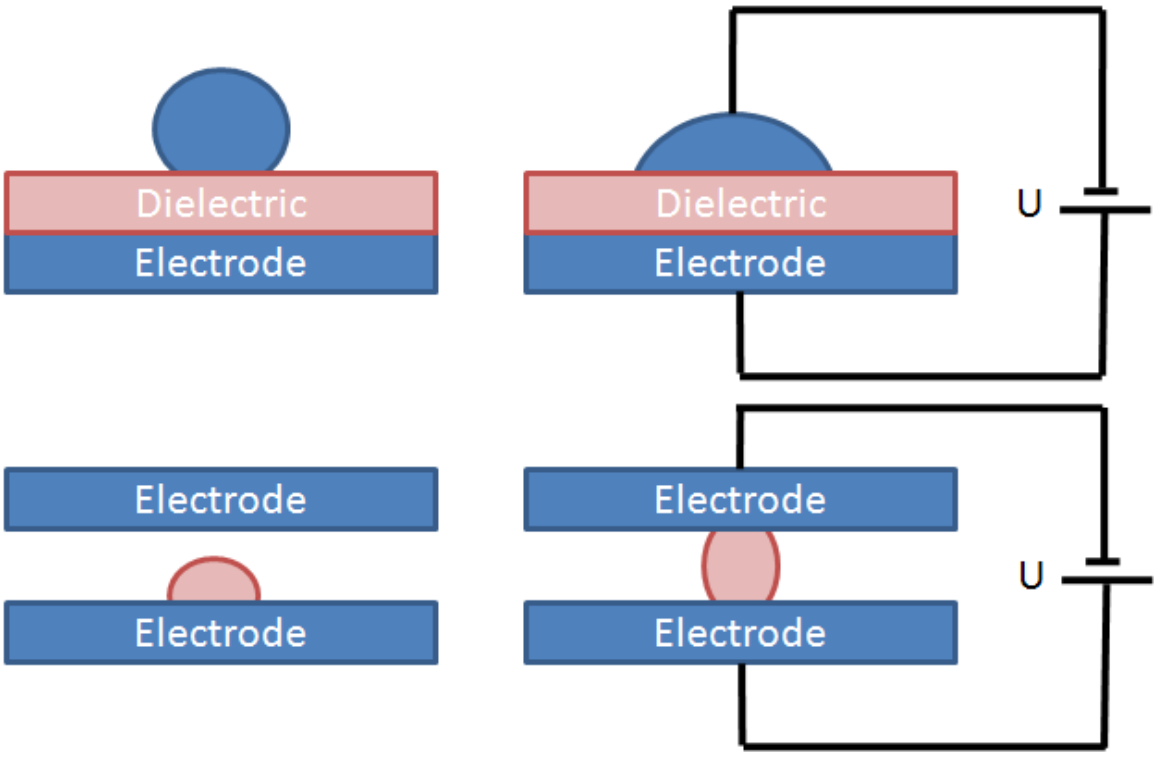

Figure 7.5 Schematics of electrowetting and dielectrophoresis. Electrowetting (top) consists of a solid bottom electrode, solid dielectric and a liquid top electrode. When the potential is off (left) the drop is in its native spreading configuration, however, when a potential is applied the drop spreads on the surface. Dielectrophoresis (bottom) uses two solid electrodes while the geometry of the dielectric changes when a potential is applied.

In our experiments, we use a polymer fluid that is non-conductive so we focus on the manipulation of the fluid using dielectrophoresis. In this case the electrical energy is dependent on the geometry of the dielectric medium between the electrodes. This energy must be balanced with the energy gained from either gravity, surface energy, or both. In order to qualitatively understand the process, we present the preferred configuration of the dielectric medium, in the absence of surface and gravitational forces, to explain the results below. To do this we compare the electrical energy of the two extremes of the dielectric geometry:

stacked dielectric with air parallel to the electrodes and side by side dielectric where air is perpendicular to the electrodes (Figure 7.6). The former behaves as capacitors in series with areas, A, each with a separation, d/2, the capacitance being $C = \left(\frac{\kappa}{1+\kappa} \right) \frac{2\varepsilon_0 A}{d}$, where κ is the dielectric constant. The latter however behaves as parallel capacitors with areas, A/2, separations, d, making the capacitance $C = (1+\kappa) \frac{\varepsilon_0 A}{2d}$. The electrical energy of a capacitor is $E=CU^2$ and since all dielectric medium have κ>1, the energy of the 'parallel' state will always be higher than that of the 'series' state. In other words a greater amount of energy can be stored helping drive the energy of the system to a minimum. For a typical polymer, where κ is between 2 and 3, this would mean that the change in dielectric energy between the two geometries would be anywhere from 11 to 25%. Electrically the material between the capacitors prefers to be aligned perpendicular to the electrodes and elongated with the electric field (Figure 7.6 right) however this must be balanced by the surface energy of the dielectric medium.

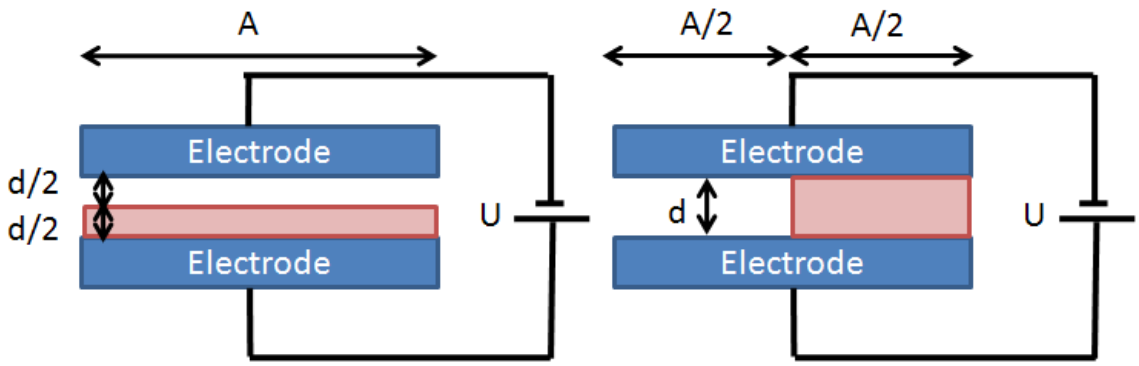

Figure 7.6 Two configurations of the dielectric medium between electrodes. A slab in between the electrodes acts (left) as capacitors in series, while the columns between the electrodes (right) act as parallel capacitors. The dimensions of the electrodes are shown while the volume of the dielectric is held constant.

First we use this concept to manipulate the bulk drop of the film. We do so by depositing a drop of linear poly(n-butyl acrylate) (PBA) onto the surface of a graphite electrode and position a needle electrode off to the side of the drop (Figure 7.7). The needle is positioned approximately 100 μm above the surface. A bias of 1 kV is applied between the graphite and the needle. The drop will then flow to the area of the highest electric field to increase the stored electrical energy in the system.

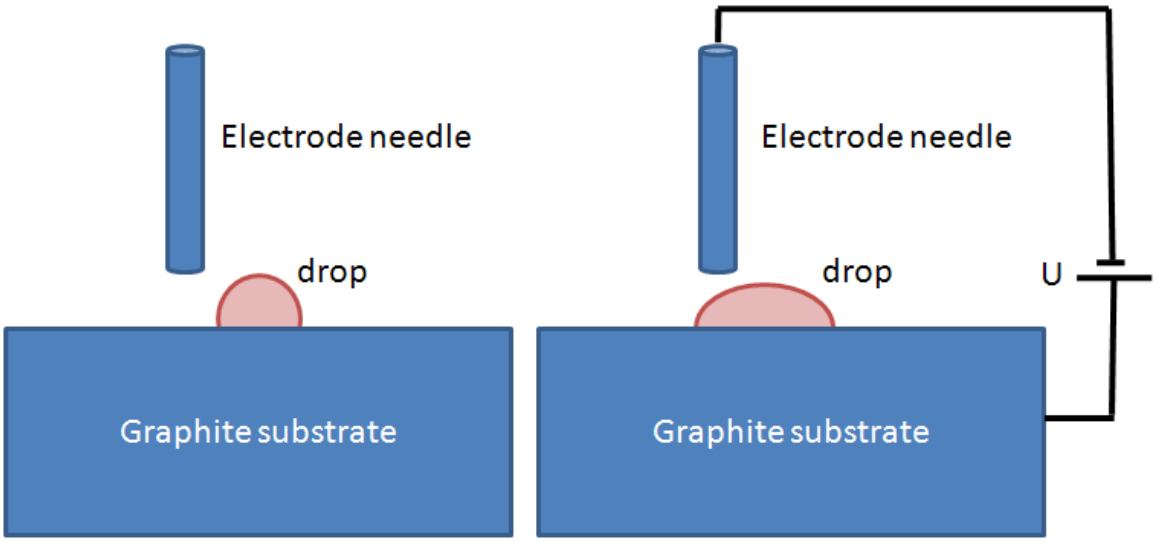

Figure 7.7 Schematic for the manipulation of the bulk drop. A bias is placed across graphite and a metal needle electrode which is offset from a drop. This directs the drop to flow underneath the needle.

When the drop is placed on the surface images were taken and it was allowed to spread for 24 hours under 2 conditions: with an applied electric field (U=1 kV) and a control experiment without the applied electric field (U=0 kV). These results are presented in Figure 7.8. The top two images represent the spreading of the control drop. The blue circles show the position of the original drop in both the before and after images. As expected, a slight radial spreading was observed in the control drop. The bottom images in Figure 7.8 show the spreading of the drop in an electric field. The left image shows the drop before it is spread while the second shows the drop after it is spread. It is clearly visible with the aid of the outlines of the starting position of the drop (blue circle) and the position of the electrodes (red circle) that there is a tendency for the bulk melt to flow into the electric field. This is because the electrical energy a capacitor can hold is greatly increased when a dielectric medium is present. This energy

change is enough to counter the energy needed to spread the drop from its original configuration.

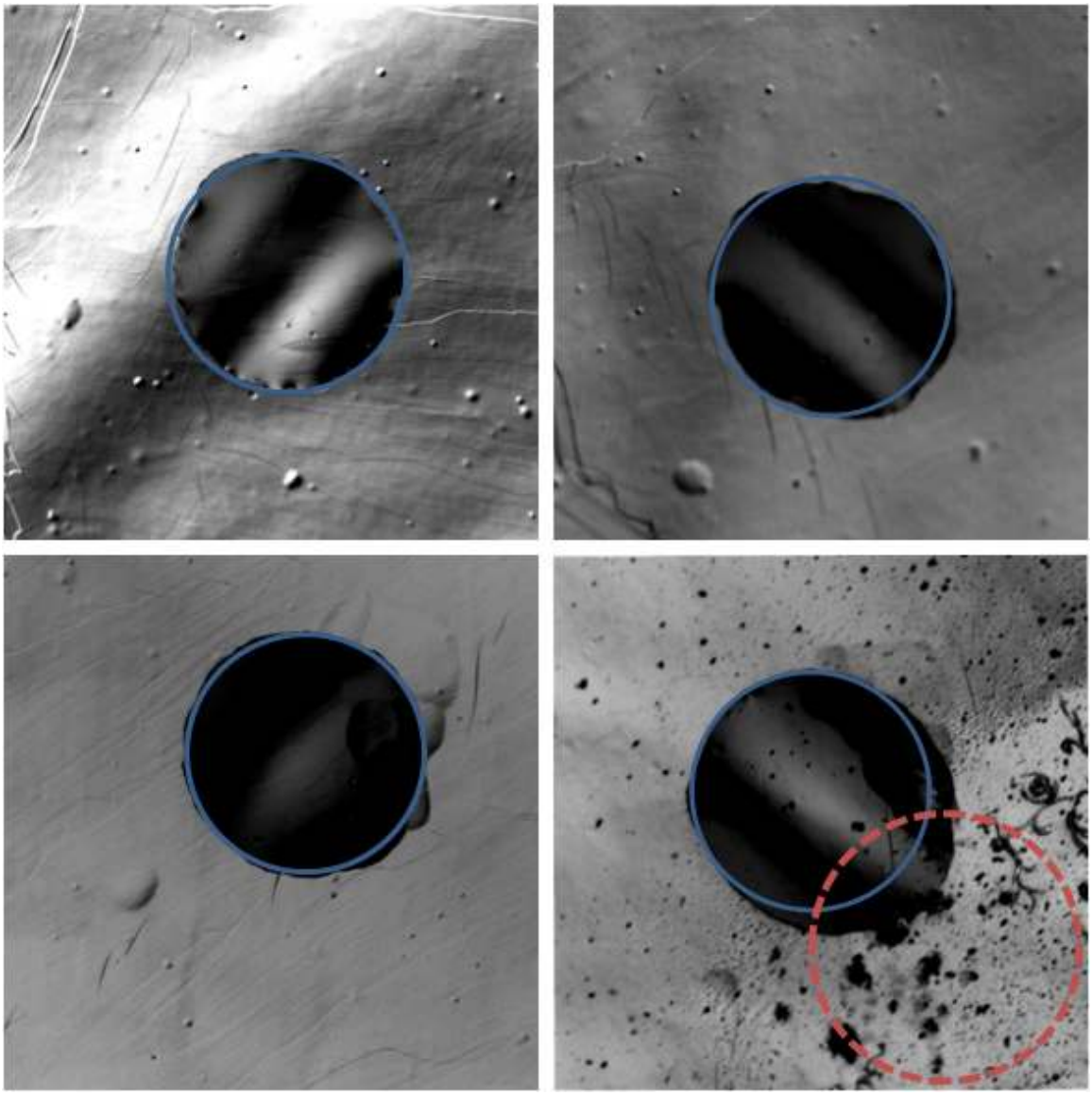

Figure 7.8 Optical micrographs of a under an electric field. The top half shows a drop before (left) and after (right) spreading for 24 hours in the absence of an electric field. The bottom half shows a similar drop spreading for 24 hours in the presence of the needle electrode. The blue circles indicate the position of the original drop while the red dashed circle indicates the position of the needle electrode.

We then explore how electric fields affect static thin films. To do so we deposit a monolayer of brushes (N=500, n=35) onto a sheet of mica using a Langmuir-Blodgett trough. The insulating mica is then place in direct contact with an electrode and a second electrode is suspended above the sample (Figure 7.9 top). The electrodes are suspended 500 μm apart and an electric potential of 1 kV is applied. To assist with this conformational change the film is exposed to a relative humidity of 97 %. The polymer films before and after the applications of the electric field are shown (Figure 7.9 left and right respectively). A transformation of the film is clearly visible. Currently, there are two hypotheses that have yet to be explored to determine the nature of this film: The brushes are changing from their adsorbed state to their cylindrical state or the electric field is degrading the brushes. Current evidence seems to back up both hypotheses. By simple observation of the film the images seem to be consistent with a partially broken down brush where some of the leftover brushes are seen as the bumps in the film. This however is inconclusive. We do know that the applied electric field of 2 V/μm is well below the electric field need to break down typical polymers (20 – 30 V/μm).[12] Also, if these polymers were breaking, then at a particular electric field we should observe behavior similar to the scission of the brushes[13] which is not the case. It must be noted however that it takes far less energy to break a brush then to degrade a linear polymer. The second hypothesis is that the brushes are undergoing a phase transition; however, this cannot be corroborated with the current data. There is evidence that suggests this mechanism is plausible. If the brushes were undergoing a simple phase transition they would

need to shift around on the surface. This is because a brush in the adsorbed conformation has a greater surface area then that of the cylindrical conformation. This makes it necessary for the brushes to spread to achieve this conformation. We know that for these brushes to spread and slide over the surface, a layer of water must be present to provide lubrication. In our experiments there must be humidity present to see the conformational change. So it is possible that these molecules must have to have the ability to slide around on the surface to fill in the space between the electrodes in order to minimize the total energy of the system.

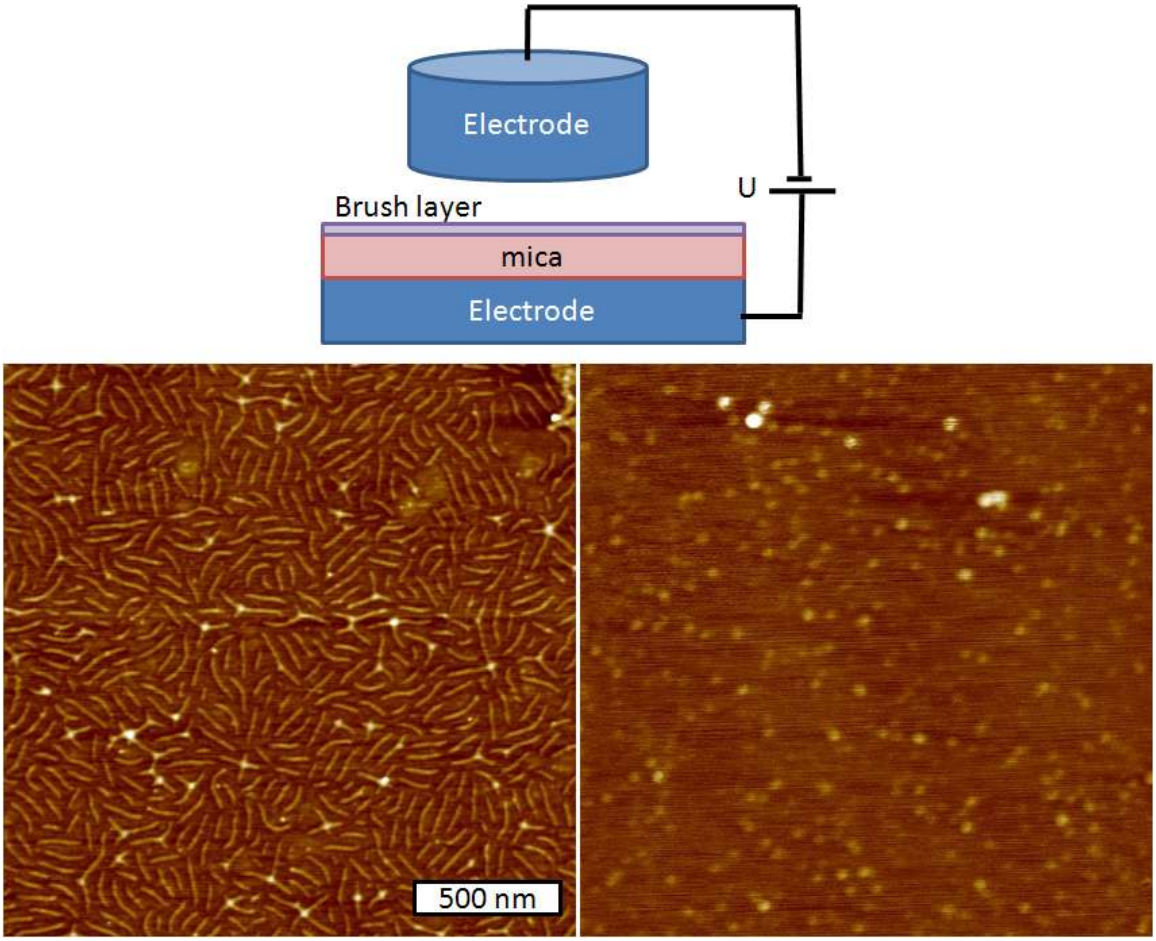

Figure 7.9 Manipulation of a static thin film in an electric field. Top. The experimental setup. Bottom. The thin film before (left) and after (right) application of an electric field.

We have repeated this experiment at 500 V, 750 V, and 1000 V, across the 500 μm gap. At 500 V we see no change in the film and at 750 V and 1000 V we see the film transform into what appears to be a dense layer. The transition between the two states occurs in a very narrow region of energy making it difficult to pin down a transition conformation of the molecules. Future experiments will focus on the threshold energy needed to cause the film to make this transformation and thus develop a mechanism to explain the results.

The dielectrophoretic forces can also be used to align particles, colloids and macromolecules.[14-16] Similar to the movement of a melt of a dielectric, the preferential orientation of a rod-like particle is for its long axis to align with the electric field. The perturbations in the electric field from the dielectric molecule produce a non-uniform electric field which allows for a torque on the molecule to allow it to reconfigure its orientation. Figure 7.10 depicts the setup we use in our first attempts to exploit this force. We lay two parallel electrodes onto a mica surface with a drop consisting of the brush melt placed between them. This setup is then placed into a chamber with a relative humidity of 97 % to induce spreading while an electric field is applied. Electric fields were applied at values of 0.5, 0.75, and 1 V/μm.

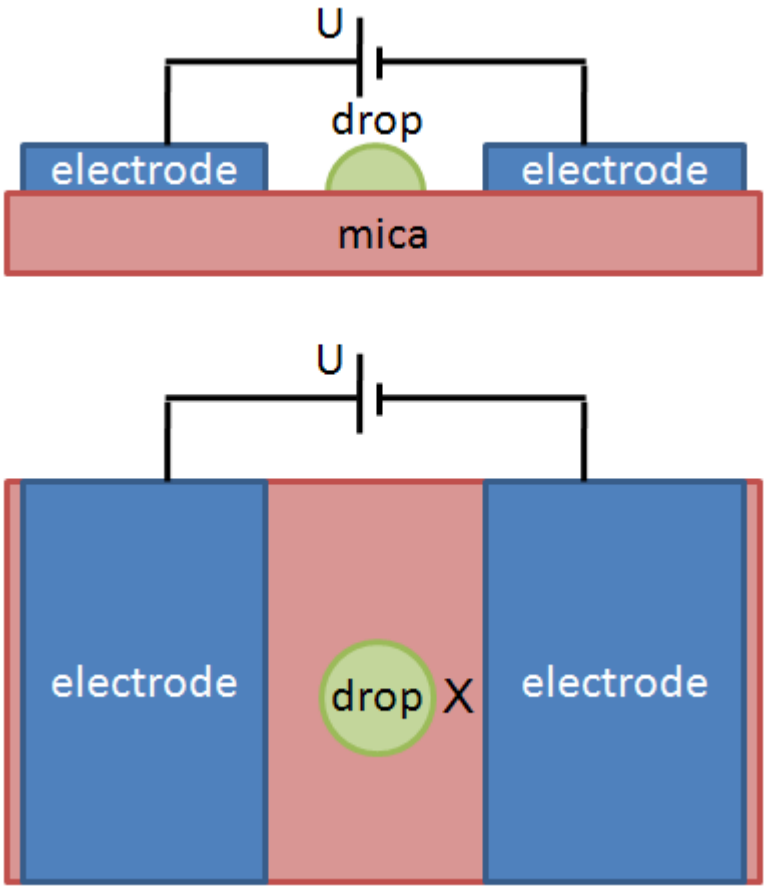

Figure 7.10 Schematic of a drop spreading in an electric field. A drop is place on mica between two electrodes and allowed to spread (side view – top and top view – bottom). The area imaged is marked with an X.

These experiments produced results similar to the manipulation of a thin film. The electric field of 0.5 V/μm seemed to retard the spreading as none or very little of the brush film was observed. At the higher electric fields, spreading was observed of the transformed film described earlier. Figure 7.11 depicts the spreading films seem in the electric fields of 0.75 and 1.0 V/μm. The area of the spreading drop that the images were obtained from is marked with an X. In the lower of the two, we were able to visualize brushes in the film however there was

no orientation present, while the 1 V/μm spreading film showed no presence of brushes. We suspect that the mechanism that creates these films while spreading is the same mechanism that creates the similar static films (described above). It is unclear what electrochemical effects are present in our experiment. It is known however that dielectrophoresis under DC electric fields can be affected by electrochemical breakdown[17] or electroosmotic currents.[18] In future work, experiments will be conducted using AC electric fields to limit these effects.

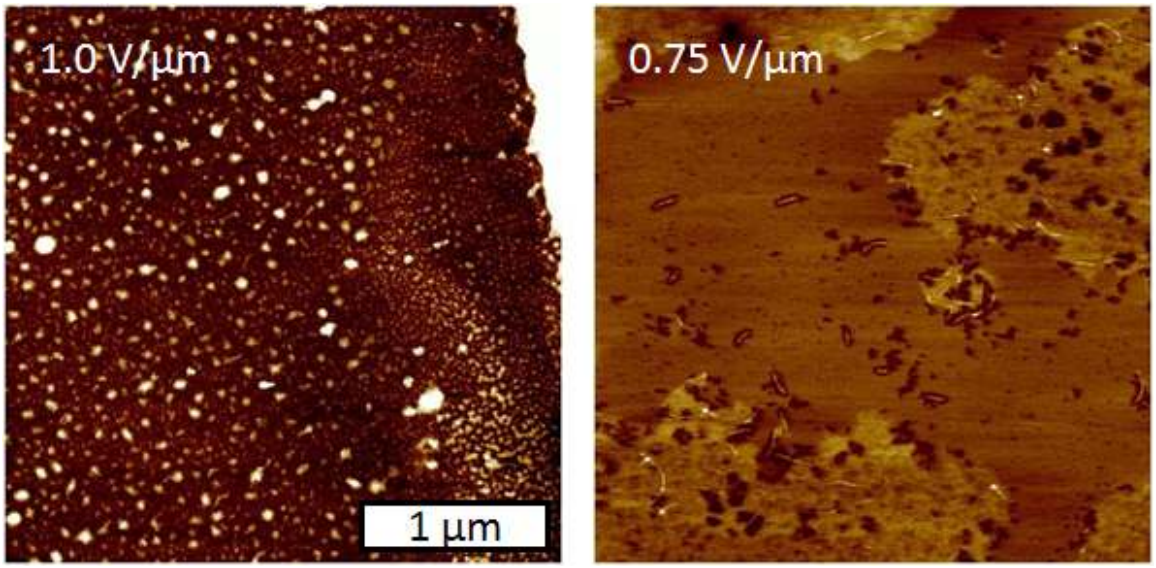

Figure 7.11 Films from the spreading of a droplet in an electric field. In both cases a thicker film forms while spreading from the drop. At lower electric field values, there are some brushes present; however, it is unknown what causes this film morphology.

7.4 Conclusions. We have come full circle by studying the formation of the polymer films, studying their flow and mixing, and ultimately manipulating the properties in those flows. Ideally, the behavior exhibited in these polymers throughout this work will be enhanced and eventually be controlled by confining

them to channels and manipulation with electric fields. The prospects made available by such control include smaller lithography methods,[19] limiting the defects in polymer films, thus improving liquid crystals,[20] and creating tunable surface properties.[21]

This Chapter outlines preliminary experiments aimed at the control of these films yielding the following conclusions:

1) Channels were patterned on a mica substrate using microcontact printing to confine spreading polymers. The ultimate goal of this process is to spread molecules through and around features comparable to their molecular size (1 – 10 μm). This however has lead to multiple complications that have yet to be worked out: I. So far we are unsuccessful at patterning stamps to that particular size, II. When we pattern channels on the surface, a residue that inhibits the spreading is left behind, III. We were unable to print the walls of the channels that are molecularly smooth, i.e. there are features on the channels walls comparable to the molecular size, and IV. The silane molecules used to create the channels did not bind to the mica effectively and the spreading molecules were able to deform the channel walls. We have also proposed possible solutions to some of these issues to be pursued in future work. However, we did have some success in creating channels and confining molecules to them. When we made large channels (widths ~300 μm) we were able to visualize the molecules spreading within the printed channel much better than the patterned surface. Using this result along with strategies to improve the process, should allow for the ability to

study these individual polymers when they are confined to channels on the order of their molecule size.

2) We have begun to use electric fields to manipulate the conformation of these molecules in the films and as they flow. First we show that the presence of an electric field caused the molecules to undergo a compressed conformation as opposed to an adsorbed one. Then we have shown the ability to spread the bulk reservoir in a manner that is inconsistent with the spreading without the field. The main mechanism that drives this additional reservoir spreading is dielectrophoresis. Finally, we show the effect the electric field has on spreading. When the spreading drops were exposed to electric fields we saw one of two effects depending on the field strength: A retardation of the spreading ($U<500$ V) or the spreading of the thicker film ($U>750$ V). Future work will use alternating electric fields to examine how the electric fields affect the films properties such as packing, folding, conformations, and topology to hopefully control these properties.

The refining and further study of these results will lead to a better control of spreading. In the future, this should allow for better development of thin films with specific properties and tunable features that will lead to better performing and cheaper devices that integrate polymer films.

References

[1] Pfohl, T.; Mugele, F.; Seemann, R.; Herminghaus, S. *ChemPhysChem.* **2003***, 4*, 1291-1298.

[2] Squires, T.M.; Quake, S.R. *Reviews of Modern Physics* **2005***, 77*, 977-1026.

[3] Zhu, S.; Liu, Y.; Rafailovich, M.H.; Sokolov, J.; Gersappe, D.; Winesett, D.A. Ade, H. *Nature.* **1999**, 400, 49.

[4] Aoyagi, T.; Takimoto, J.-I.; Doi, M. *J. Chem. Phys*. **2001,** 115.

[5] Cho, Y.-K.; Watanabe, H.; Granick, S. *J. Chem. Phys*. **1999,** 110.

[6] Mrksich, M.; George M. Whitesides, G.M. *Trends in Biotechnology. 1995, 13, 228.*

[7] Lyubchenko, Y. L.; Gall, A. A.; Shlyakhtenko, L. S.; Harrington, R. E.; Jacobs, B. L.; Oden, P. I.; Lindsay, S. M. *J. Biomol. Struct. Dyn.* **1992**, *10*, 589.

[8] Crampton, N.; Bonass, W.A.; Kirkham, J. Thomson, N.H. *Langmuir* **2005,** *21,* 7884-7891.

[9] Hughes, M.P. *Electrophoresis*. **2002,** 23, 2569-2582.

[10] Mugele, F.; Baret, J.-C. *J. Phys: Condens. Matter.* **2005,** 17, R705.

[11] Barz, D.P.J.; Ehrhard. P. *Lab on a Chip.* **2005**, 5, 949 .

[12] Olszowka, V.; Kuntermann, V.; Boker, A. *Macromolecules.* **2008**, *41*, 5515-5518.

[13] Sheiko, S.S.; Sun, F.; Randal, A.; Shirvaniants, D.; Matyjaszewski, K.; Rubinstein, M. *Nature*, **2006,** 440, 191-194.

[14] Herlihy, K.P.; Nunes, J.; DeSimone, J.M. *Langmuir* **2008,** *24,* 8421-8426.

[15] Yang, M.; Chew Lim, C.; Liao, R.; Zhang, X. *J. Microelectromech. Syst.* **2006**, *15*, 1483–1491.

[16] Yang, C. Y.; Lei, U. *J. Appl. Phys.* **2007**, *102*, 094702.

[17] Hermanson, K.D.; Lumsdon, S.O.; Williams, J.P. Kaler, E.W.; Velev, O.D. *Science.* **2001,** 294, 1082.

[18] Lumsdon, S.O.; Kaler, E.W.; Velev, O.D. *Langmuir.* **2004,** 20, 2108

[19] Cheng, J. Y.; Nelson, A.; Rettner, C. T.; Sanders, D.P.; Sutherland, A.; Pitera, J.W.; Na, Y.-H.; Kim, H.-C.; Hinsberg, W.D. *J. Photopoly. Sci. Tech.* **2009,** 22, 219-222.

[20] Vroege, G.J.; Lekkerkerker, H.N.W. *Rep. Prog. Phys.* **1992,** 55 1241-1309.

[21] Matsudomi, M.; Kato, A.; Kobayashi, K. *Agric. Biol. Chem*, **1982,** 46 (6), 1583-1586.